Self-Potential Method in Geothermal Investigations
at Saline Hot Spring, Krabi

Maytipa Phalakarn

A Thesis Submitted in Partial Fulfillment of the Requirements for the
Degree of Master of Science in Geophysics
Prince of Songkla University
2018

Self-Potential Method in Geothermal Investigations
at Saline Hot Spring, Krabi

Maytipa Phalakarn

A Thesis Submitted in Partial Fulfillment of the Requirements for the
Degree of Master of Science in Geophysics
Prince of Songkla University
2018

Thesis Tile   Self-Potential Method in Geothermal Investigations at Saline
Hot Spring, Krabi

Author   Miss Maytipa Phalakarn

Major Programs   Geophysics

_____

Major Advisor   **Examining Committee**:

……………………………..   …………………….......Chairperson
(Asst. Prof. Dr. Helmut Dürrast)   (Assoc. Prof. Dr. Tripob Bhongsuwan)

                                …………………….........Committee
                                (Assoc. Prof. Wan Ismail Wan Yusoff)

                                …………………….........Committee
                                (Asst. Prof. Dr. Helmut Dürrast)

      The Graduate School, Prince of Songkla University, has approved this thesis as partial fulfillment of the requirements for the Master of Science Degree in Geophysics

                               ………….………………………….
                                (Prof. Dr. Damrongsak Faroongsarng)
                                    Dean of Graduate School

This is to certify that the work here submitted is the result of the candidate's own investigations. Due acknowledgement has been made of any assistance received

.....................................Signature

(Asst. Prof. Dr. Helmut Dürast)

Major Advisor

.....................................Signature

(Miss Maytipa Phalakarn)

Candidate

I hereby certify that this work has not been accepted in substance for any degree, and is not being currently submitted in candidature for any degree

......................................Signature

(Miss Maytipa Phalakarn)

Candidate

ชื่อวิทยานิพนธ์	การสำรวจด้านศักย์ไฟฟ้าธรรมชาติสำหรับการสำรวจแหล่งพลังงานความร้อนใต้พิภพในพื้นที่แหล่งน้ำพุร้อนเค็มจังหวัดกระบี่
ผู้เขียน	นางสาวเมธิภา ผลาการ
สาขาวิชา	ธรณีฟิสิกส์
ปีการศึกษา	2560

บทคัดย่อ

แหล่งพลังงานความร้อนใต้พิภพเป็นระบบกักเก็บพลังงานที่เกิดขึ้นใต้ผิวโลก ปัจจุบันมีการสำรวจแหล่งความร้อนใต้พิภพเพื่อนำมาใช้ประโยชน์ในด้านต่างๆ เช่นผลิตกระแสไฟฟ้า หรือพัฒนาเพื่อส่งเสริมการท่องเที่ยว ตัวกลางหลักที่ทำหน้าที่พาพลังงานความร้อนในระบบนี้ก็คือของไหลซึ่งถูกถ่ายเทจากชั้นหินกักเก็บในระดับลึกขึ้นสู่พื้นผิวผ่านทางรอยแตกหรือรอยเลื่อนของหิน จึงถือได้ว่ารูปแบบการไหลของนี้เป็นพารามิเตอร์สำคัญนำไปสู่ข้อมูลของแหล่งกักเก็บในระดับลึกได้ วิธีการสำรวจทางด้านธรณีฟิสิกส์มักถูกนำมาใช้เพื่อศึกษารูปแบบและเส้นทางการไหลในชั้นใต้ดินเพื่อที่จะตีความข้อมูลเหล่านี้ไปสู่ลักษณะและระบุตำแหน่งของแหล่งกักเก็บในระดับลึกได้ในกรณีที่ระบบเหล่านั้นไม่สามารถตรวจพบได้บนผิวดิน งานวิจัยนี้มุ่งเน้นไปที่วิธีการสำรวจด้านศักย์ไฟฟ้าธรรมชาติ เนื่องจากวิธีนี้เกี่ยวข้องโดยตรงกับรูปแบบการไหลของของไหลในชั้นใต้ดิน เพื่อให้การตีความข้อมูลมีความถูกต้องแม่นยำงานนี้จึงได้นำวิธีการสำรวจสภาพต้านทานไฟฟ้า การวัดอุณหภูมิของผิวดิน และการสำรวจทางธรณีวิทยา มาประยุกต์ใช้ร่วมด้วย การสำรวจนี้มีเป้าหมายเพื่อศึกษาและทำความเข้าใจโครงสร้างทางธรณีวิทยาในระดับตื้นของแหล่งน้ำพุร้อนเค็มคลองท่อม จังหวัดกระบี่ ผลจากการสำรวจด้านศักย์ไฟฟ้าธรรมชาติแสดงให้เห็นว่าค่าความผิดปกติที่เป็นลบเกิดจากน้ำร้อนเค็มที่ไหลขึ้นในแนวดิ่ง ขณะเดียวกันค่าความผิดปกติที่เป็นบวกนั้นเกิดขึ้นจากน้ำที่ไหลลงในสภาวะแวดล้อมที่มีความเค็ม ลักษณะของสัญญาณศักย์ไฟฟ้าธรรมชาติที่เกิดขึ้นนี้เป็นผลจากการรวมกันของสัญญาณที่เกิดขึ้นจากศักย์ไฟฟ้าแบบต่อเนื่องและศักย์ไฟฟ้าจากการแพร่ ผลจากการสำรวจในงานนี้ชี้ให้เห็นว่าน้ำเค็มและน้ำร้อนเค็มในพื้นที่ศึกษามีความเกี่ยวข้องกับชั้นดินในระดับตื้นมากๆ ดังนั้นการปลูกสร้างสิ่งก่อสร้างหรือการขุดเจาะต่างๆที่จะเกิดขึ้นในอนาคตควรคำนึงถึงผลกระทบที่จะเกิดขึ้นซึ่งอาจจะไปทำลายระบบการเกิดน้ำพุร้อนเค็มนี้ได้

Thesis Title   Self-Potential Method in Geothermal Investigations at Saline Hot Spring, Krabi

Author   Maytipa Phalakarn

Major Program   Geophysics

Academic year   2017

Abstract

Geothermal system formed deep inside the earth, but often show surface manifestations in form of hot springs, which are often tourist attractions and their water can be used for recreational or medical spa. Energy from these geothermal systems can be used for electricity generation or direct uses. The main medium which transfers the energy in the system is the geothermal fluid, which carries the heat from deeper reservoirs to the surface through open fractures and faults, which act as higher permeability pathways. Thus, the pattern of fluid flow is a key parameter to obtain details of the deeper parts of the reservoirs. Geophysical surveys were often performed to study and identify these fluid flow pathways and the water circulation in the subsurface in order to estimate the reservoirs characteristic and potential and also provide evidence of geothermal systems that have no surface expressions. This study focusses on self-potential (SP) surveys used to infer permeable pathway at depth as the self-potential response is directly linked to subsurface fluid movements. Moreover, electrical resistivity surveys, ground surface temperature measurements, and geological surveys are integrated in order to provide better interpretation and based on that drawing a hydrogeological model of the study area. The exploration was conducted at Khlongthom Saline Hot Spring, located in Krabi, Southern Thailand. The combination of the quantitative results from all survey methods revealed a pattern of fluid flow in the relative shallow subsurface of the area. Additionally, self-potential data showing that negative SP anomalies correlated well with hot saline water flowing up, and positive SP anomalies can be associated with water flowing down in an overall higher saline environment. The SP response is a result from the sum of streaming potential and diffusion potential. It can be concluded that the saline hot spring water in the area is often very shallow and separated by shallow fractures, and additional hidden hot springs could be identified; locations where the saline water flow upwards but not reaching the surface. Understanding of this unique hot spring system is vital for further development in this area as the results from this study should be considered when designing buildings or other infrastructure projects in this area.

ACKNOWLEDGEMENT

CONTENTS

CONTENTS (CONTINUED)

LIST OF TABLE

LIST OF FIGURES

LIST OF FIGURES (CONTINUED)

LIST OF FIGURES (CONTINUED)

LIST OF FIGURES (CONTINUED)

LIST OF FIGURES (CONTINUED)

LIST OF FIGURES (CONTINUED)

LIST OF FIGURES (CONTINUED)

LIST OF FIGURES (CONTINUED)

LIST OF FIGURES (CONTINUED)

CHAPTER 1

INTRODUCTION

1.1 Introduction
1.1.1 Importance and benefit
Hot springs are natural phenomena, the surface expression of a geothermal system, where hot water flows up from depths to the surface. The occurrence of hot springs can be utilized for the benefit of people, such as geothermal power plant for electricity generation used for industry or agriculture, and the direct use for tourism, like spa. Hot springs in Thailand are found in several parts, including northern part, central Thailand, western part, and southern part. In Southern Thailand hot springs are distributed in many provinces, especially in Krabi province, which is one of the famous tourism destinations in Thailand due to the rich and diverse nature. Examples of hot springs in Krabi are Khlong Nam Ron, Ban Nam Ron, Nam Tok Ron Saphanyoong and Saline Hot Spring Khlongthom, which were developed for eco- and health tourism.

Saline Hot Spring Khlongthom is one of the most popular tourist destinations in Krabi province and it is an important area for many people including local and foreign tourists as well as local people. They use the hot spring as a natural spa because of the belief that hot springs there have natural healing properties; such as the water can improve blood circulation, help to relax and to release stress. Moreover, the importance of the Saline Hot Spring Khlongthom is the fact that it is a unique geothermal area different from general hot springs in Thailand, as the water contains high sodium chloride so that the water itself tastes salty. The hot spring occurs from hot water in a deeper reservoir flowing through fractures into groundwater layers that are saline water, then there is a mixing between hot water and saline water in that shallow layer before the hot water reaches the surface, thus resulting into a saline hot spring. Basic information about this hot spring is obtained from surveys of geology, geochemistry and geophysics. However, the complex system in the subsurface of this area is not yet really determined, and recently the area attracted the larger scale tourism resulting in many new buildings that can have an impact on the shallow subsurface. More understanding about the area is important for conservation and sustainable development. Therefore geophysical surveys of self-potential method, ground surface temperature, and resistivity method were applied for obtained the characteristic of shallow subsurface water flow in this area.

1.1.2 Objective of the study
Saline hot spring Khlongthom is the surface expression of a geothermal system of unconventional characteristics, as it is saline, and therefore needs to be better understood. The distribution and occurrence of hot spring waters at depth can be imaged with electrical resistivity methods, whereas for the flow patterns of hot waters upwards the self-potential method can be applied. Therefore, the objective of this work is to obtain patterns of fluids flow in the shallow subsurface, delineate the anomaly zones, as well as the location and size of hot springs in the study area by using a combination of geophysical methods, mainly self-potential, but also ground surface temperature measurements, vertical electrical sounding and resistivity tomography, or 2D resistivity.

The self-potential method is the central part of this work because of its sensitive to water flow related to hydrothermal systems.

1.1.3 Expected Outcome

This research is expected to provide more understanding about the fluid flow of the hot water in the shallow subsurface of the saline hot Spring Khlongthom, Krabi, Southern Thailand, which might lead to a better and sustainable utilization and conservation during future development.

1.2 Literature Review

This part defines the review of literature related to the aim of this work including six main topics as following: geothermal system and investigation of them by using geophysical methods, intrusive zone cause saline or brackish water, the detail of self-potential mechanisms and methods, ground surface temperature measurements, vertical electrical soundings and resistivity methods, and finally a brief history of surveys at the Saline Hot Spring Khlongthom.

1.2.1   Geothermal System

Geothermal energy refers to heat energy which generated and stored inside the earth. Normally it is related with an area of higher heat flow or higher geothermal gradient, with a general geothermal gradient of 25°-30° C/km as an average (Dickson and Feneli, 2002). The general geothermal gradient is the result of increasing temperature with depth in the earth, whereas regions which a higher geothermal gradient represent geothermal systems at depth. The main source of geothermal energy in the earth is the decay of radioactive elements and heat flow from the core and mantle to the cooler surface.

The basic concept of geothermal systems comprises three main parts shown in Figure 1.1. When focusing from the bottom to the top in the schematic diagram the first main part of the system is the heat source that drives the system, normally it is a magmatic intrusions with higher temperature additionally to the normal temperature increase as a function of depth (Marechal et al., 2012). The second component is a larger reservoir (Bowen, 1989); this refers to hot permeable rocks where fluid circulation extract heat and these permeable rocks were covered by impermeable cap rocks. In general a reservoir requires a fluid pathway that has a connection between the reservoir and the recharge area, and a way where the fluids can flow through up to the surface and exiting in form of geysers, mud pools, and hot springs. The main fluid pathways are faults and fractures in the subsurface. The final component is a fluid that is carrying the heat energy; geothermal fluids can be liquid or vapor depending on temperature and/or pressure, but the main working fluid in geothermal systems is water.
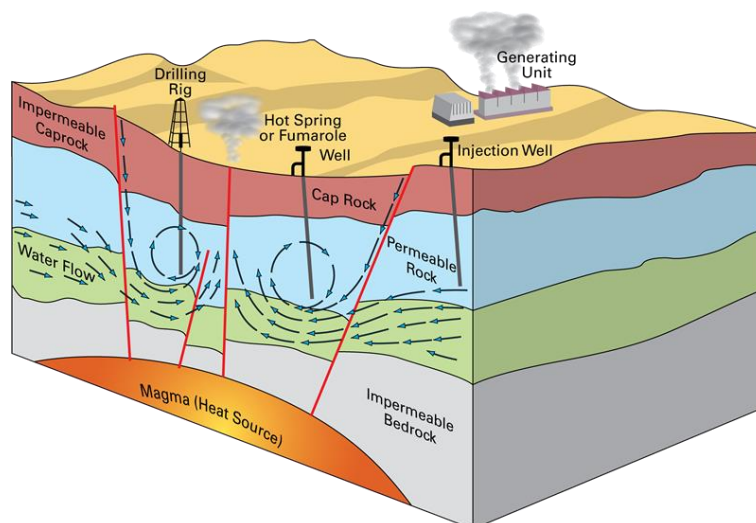
Figure 1.1 Schematic diagram of a geothermal system (Natural Environment Research Council, 2018).

The main mechanisms of geothermal systems are that fluids in the reservoir were heated up by a heat source, and this then is causing the fluid convection because of gravity and buoyancy force, because when the fluids were heated up the density decreases. Then the hot fluids were replaced by cold fluids which have a higher density. The hot fluids finally find a pathway upwards to an outflow at the surface.

Use of geothermal energy

Recently, geothermal energy was used in many applications that require heat. The basic is that geothermal energy technology taps into subsurface areas where a suitable temperature exists, whereas the use of this energy depends on the requirements. The most common use of geothermal energy in the world is electricity generation because there are many benefits, such as renewable energy, produces of no waste or pollution, reliable method to create electricity and overall sustainable. However, electricity generation from geothermal energy cannot be available everywhere because of it requires higher installation costs and higher temperatures, but there are many ways for uses of energy in case of low temperatures. There are many direct applications of geothermal energy, such as heating propose, heating industries and home, greenhouses serviced by combined space and hotbed heating, swimming pools and bathing propose (Bowen, 1989). There are many ways for utilization of geothermal resources, as the correct use of that depends on the classification of them (Mburu, 2012).

Classification of geothermal systems

Understanding geothermal resources are the main key to a successful exploration and utilization of them, thus a clear definition of the nature and characteristics of geothermal system is required (Axelsson, 2013). As mentioned in previous parts, geothermal systems requires three main components that can vary, so there are in various ways of classification based on heat source, heat transfer, their reservoir temperature, nature of fluid, physical state, enthalpy, utilization and geological setting (Saemundsson et al., 2009; Masum, 2015). All geothermal fields are individual, but also can broadly be classified by certain common characteristics and different aspects. The first three most

common classifications of that comprise reservoir temperature, enthalpy, and physical state (Gupta and Roy, 2007; Bodvarsson, 1964; Axelsson and Gunnlaugsson, 2000). Additionally, geothermal systems also classified based on a regional perspective and this work also focusing on the question of what is the geological settings of the study area.

Geothermal systems are easy to be found when there are manifestations on the surface, like hot springs, but in case of hidden geothermal resources the physical properties of the system have to be utilized using geophysical methods. The geophysical properties or the characterizations of possible geothermal resources can be investigated by geophysical methods that have been performed in many studies. The geophysical characterizations can estimate the heat source and the pathways of the hot water to the surface, e.g. hot springs as surface exit; detailed explanations of investigation methods are provided in the section of geophysical methods.

1.2.2 Natural occurrence of seawater intrusion

Seawater intrusion is the displacement of seawater into freshwater aquifers. Normally, this occurs in coastal freshwater aquifers when there are the different densities between seawater and freshwater, which seawater slightly heavier than freshwater, thus it can intrude into aquifer forming a saline wedge below the freshwater. The encroaching seawater will encounter an area known as the zone of dispersion, where the freshwater is mixing with seawater at an interface. This interface is the boundary which is in a dynamic equilibrium; it can move with seasonal variations of the water table and daily tidal fluctuations. These movements along the interface are actually a transition zone of mixed salinity.
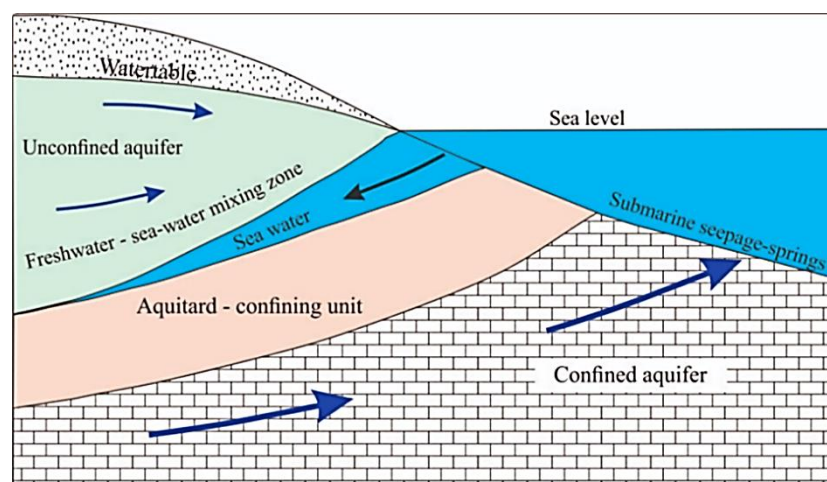
Figure 1.2 Seawater intrusions into a coastal aquifer environment. This represents an unconfined aquifer extending seawards and a water table merging with the shoreline. Seawater intrudes the aquifer and it is higher density then freshwater, thus it extends landward below the freshwater. Confined aquifers also extend seawards. In both aquifer types, the degree to which sea water enters the aquifers largely depends on the overall energy, or hydraulic drive of groundwater flow towards the coast. Some of this freshwater can seep through the sea floor (http://www.geological-digressions.com).

1.2.3 Self-potential mechanisms and methods
Introduction
Self-potential (SP) refers to the natural occurring electrical potential difference that can be found everywhere in the earth ground (Bérubé, 2004). Anomalies of self-potential can be generated by subsurface fluid flow, heat flow, or occurrence of ore bodies; in geophysical investigations self-potential method is therefore applied for detect these sources. Self-potential method has been used widely for several applications, such as delineate conductive ore deposit, seepage analysis, investigations of groundwater flow and geothermal exploration (Bérubé, 2004; Erchul, 1988; Corwin, 1989; Ravil and Jardan, 2013). Recently, even really small self-potential signals are possible to be measured. This part of the work is providing a detail description of self-potential mechanisms and methods, and also provides a literature review of self-potential surveys on geothermal areas and laboratory experiments on the effect of salinity self-potential signals.

Governing equations of self-potential
Fundamental equations used to explain the generated and interpreted SP signals are based on the quasi-static regime of Maxwell equations. When focusing on thermodynamics, the existence of a possible measured electrical field at the ground surface is related to the existence of a driving source current density in the ground (J_s). The total electrical current density (J) in a porous material is the sum of the conduction current explained by Ohm's Law and the driving source current density (J_s) associated with the pore fluid pressure field (Revil and Cathles, 1999),

$$J = \sigma_0 E + J_s \quad\text{.. (1)}$$

where E is the electric field (V m^{-1}) (in the quasi-static limit of the Maxwell equations written as E = $-\nabla\psi$, where ψ is the electric potential expressed in V), σ_0 is the electrical conductivity of the porous material (S m^{-1}), and J_S is a source current density (A m^{-2}) associated with any disturbance that can affect the movement of charge carriers. The general equation for coupled flows can be written as following

$$J_i = L_{ii}X_i \quad\text{.. (2)}$$

where J_i is flow per unit area of type i, X_i is the gradient or driving force of type i, and L_{ii} is the conductivity coefficient for type i flow. In the nature if these flows occur at the same time, they will interfere with each other. The gradient of one type can drive a flow of another; this is called couple flows, such as an electrical flow can be driven by hydraulic gradient and the absorption of heat in the metal. So, the total flow can be written in following form

$$J_i = \sum_{j=1}^{n} L_{ij}X_j \quad\text{.. (3)}$$

where i = 1, 2… n and L_{ij} is the couple coefficient relating flow of type i to force of type j, and X_i is the gradient or driving force of type j. If in the measured area is no external electrical field, thus an electrical current density in the porous media will be driven by a hydraulic, thermal, or chemical gradient that can be written in following form

$$J = L_{EH}i_h + L_{ET}i_t + L_{EC}i_c \text{ ....(4)}$$

This equation indicates that SP at the surface is not only the result from electrical current density of fluid flow, but also the result from thermal or chemical flows (Friborg, 1996).

Source of self-potential anomalies
For being major sources of self-potential there are several different electrochemical mechanisms that can generate the natural potential difference in the earth subsurface (Friborg, 1996). This multiplicity of sources can cause difficulties in interpretation, because when several sources are contributing to the electrical potential and all of them can be superposed, then there is no really a way to separate a self-potential anomaly by their origin. Self-potential anomalies related with mechanisms of charge polarization occurred in the deeper earth and can be divided into four main mechanisms. A description of each mechanism follows, especially streaming potential because it is important for this work.

Streaming potential
Streaming potentials are related with fluid flow in charged porous media as in case of water flows through a rock and soil. This potential occurs whenever an electrolyte moves with respect to a stationary slid that it is in contact with (Friborg, 1996). The contribution of the self-potential signal resulting from streaming potentials is most important for investigations of fluid flow in subsurface due to fact that it directly provides information associated with subsurface fluid flow (Friborg, 1996).

Further, streaming potentials are related to the occurrence of electrical double layers that can be found at pore water mineral interface, which refer to the coupling of fluid flow with electric conduction within porous media that is known as electro-filtration. This is one of several electrokinetic phenomena. Others include electro-osmosis, electrophoresis and sedimentation potential (Overbeek, 1952). Electrokinetic phenomena were first observed in capillary tubes in 1859 by Quincke and later in 1879 as formulated by a theoretical model developed by Helmholtz. This model is still in use today and can represent to be almost true in case of electrolyte flowing through a porous medium, thus the phenomena can be explained by the Helmholtz-Smoluchowski equation and the electrical double layer.
Streaming potential requires two-phase systems to produce these effects, and the concept behind that is based on electrical double layers. That occurs when a liquid is moving with respect to a solid surface, the solid surface becomes charged and ions that generally exhibit negative charges depending on the pH value of the mineral in the solid phase, thus the opposite charge from the liquid will accumulate near the solid surface. The accumulated charges result in a diffuse layer characterized by an excess of positive charges and lack of negative charges with respect to the free pore water in the central part of the pores. The excess positive charged ions in the diffuse layer are also dragged along with when there is fluid flowing, which refers to pressure gradient forces, thus causing an electric convection current (I_{conv}). Therefore, this convection current will cause an imbalance of mobile charges, which a lack in the upstream (low pressure) and accumulation in the downstream (high pressure), thus generating an electrical potential

difference. This potential difference is the streaming potential and the opposite is driving the conduction current (I_{cond}) back through the fluid. In steady state the two currents are balance each other. Additionally, the magnitude of the streaming potential is depending on the resistance of the turn back current path.

Since 1989, as presented jointly, the Poisson's equation, the Gouy-Chapman diffuse layer, and the characteristics of the parabolic velocity profile of the Poiseulle's flow express the convection and conduction of the current as following (Morgan et al., 1989):

$$I_{conv} = -\pi\varepsilon\frac{\xi}{\eta}G\Delta P \dots\dots\dots (5)$$

$$I_{cond} = -\pi\sigma_w G\Delta V \dots\dots\dots (6)$$

where ΔP is the pressure difference driving the flow, ΔV is the potential difference, ε is the dielectric permittivity of fluid, $\boldsymbol{\xi}$ is the zeta potential, $\boldsymbol{\eta}$ is the viscosity of the fluid, σ_w is the fluid conductivity and G is the geometric factor.
In case of steady state condition following will be obtained,

$$\Delta V = -\frac{\varepsilon\xi}{\eta\sigma_w}\Delta P \dots\dots\dots (7)$$

$$\frac{\Delta V}{\Delta P} = \frac{\varepsilon\xi}{\eta\sigma_w} \dots\dots\dots (8)$$

This is the Helmholtz-Smoluchowski equation which was discussed before, and the ratio as $\frac{\Delta V}{\Delta P}$ refers to the streaming potential coefficient, C. This coefficient involves with the dielectric permittivity, conductivity, viscosity of the fluid and the zeta potential.

Electrical double layer
The main concept describing the electrokinetic phenomena and self-potential signals is the electrical double layer theory, which is the system of electrochemical coating at the mineral surface. At a contact between two different phases, for example, between solid and liquid or between two immiscible liquids there commonly occurs charge redistribution. Generally the negative surface charge of minerals will attract positive ions (counterions) and it repels the negative ions (coions) that cause the formation of a diffuse layer. Whenever liquids or solids are moved with respect to each other, a small layer of liquid is attracted to the solid; it occurs a shear plan inside as the liquid is located at a short distance from the solid surface. This shear plan places somewhere in the diffuse layer of counterions. The movement between solids and liquids resulting in transport of charges and this is causing an electric current. Figure 1.3 shows that the electrolytes flow through and along a solid-liquid interface. This flow refers to pressure gradient and some of the counterions in the diffuse layer in the electrical double layer would be shear off and transported along with the flow. Thus, this is resulting in an excess of positive charges (counterions) at the downstream end of the flow. Lower numbers can be found at the upstream end. This separation of charges results in the

occurrence of an electrical potential difference that in turns drives back a current in opposite direction with fluid flow.
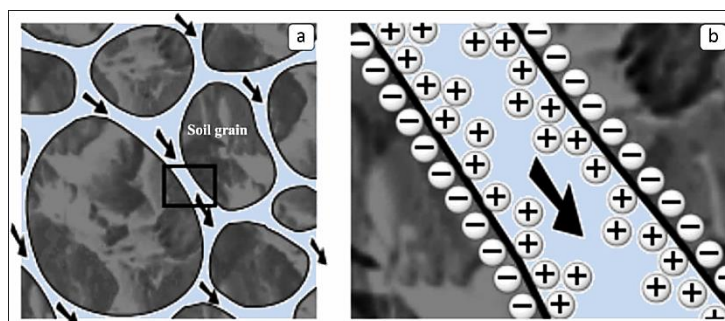
Figure 1.3 Schematic representation of the occurrence of an electrical double layer, (a) indicating electrolyte flowing through a porous medium, (b) a close-up of the electric double layer, after Bérubé (2004).

Zeta potential

A main physical property behind the electrical double layer is the zeta potential (ξ), which is the electrical potential at the shear plan within the electrolyte (Jouniaux and Ishido, 2013). Nowadays, the location of the zeta potential is unexplained by theories, but it is an indicator of their electrical potential; a higher zeta potential refers to a higher surface potential of the charged particles. In addition the zeta potential cannot be measured directly; instead it can be calculated from measurements of the surface charge or it can be estimated from electrokinetic measurements (Bérubé, 2004).
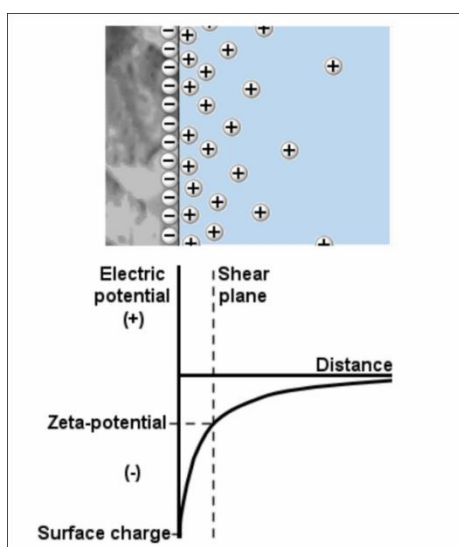
Figure 1.4 Simple model showing the distribution of charge at the solid-liquid interface that corresponds to Gouy-Chapman model. The zeta potential is the electric potential value at shear plane, which indicating by vertical dashed line (Bérubé, 2004).

Figure 1.4 presented the shear plan located at the point not far from the solid phase as where the liquid begins to flow. The electrical potential at this point is the zeta potential, and it is directly proportional to the surface charges forming on the solid. There are two main key chemical processes that can act to develop a surface charge including

adsorption of ions and the hydrolysis of surface hydroxyl group; both of these ordinary occur at the same time (Friborg, 1996).

The zeta potential is a complex function of several parameters, consisting of pH, temperature, and chemical composition of solid and liquid. However, the most importance factor is pH value of the electrolyte. It has an influence on the surface charge on the solid in both chemical processes, when the surface charge is acquired through hydrolysis of surface groups and when acquired through specific absorption (Friborg, 1996). Chemical equilibrium equations indicate that the surface charge density can decrease with increasing pH; so the influence on the zeta potential is that it will also decrease with increasing pH (Stumm, 1992).

The pH of electrolyte also has a secondary influence on the zeta potential, as very low and high pH values have an effect on the ionic strength. The ionic strength of electrolyte is another property of their chemical composition. This involves the zeta potential by its influence on the thickness of the double layer. The ionic strength is a measure of the total amount of charge in the electrolyte, it is defined as

$$I = \frac{1}{2}\sum c_i z_i^2 \quad\text{...} (9)$$

where c_i the concentration of type I and z_i^2 is its charge. Increasing ionic strength will cause a compression of the diffuse part of the double layer, which results in a decrease of the magnitude of the zeta potential even if the surface potential is not affected. (Friborg, 1996)

Temperature also is a factor that can influence the zeta potential. It is known to influence all chemical processes that are involved with the formation of surface charges; and the equilibrium constants of several materials and electrolytes depend on temperature. A change in temperature will also affect the thickness of the double layer. At higher temperatures the thermal motion of ions and the charged particles will have an increase in the mobility, so this extends the double layer and results into an increase in the zeta potential. However, the influence of temperature is really complex; an increase can simultaneously act to reduce the zeta potential by reducing the adsorption of ions. The combination of several temperature dependencies is difficult to predict; it might be positive, negative, or insignificant, depending on how the different effects cooperate (Friborg, 1996).

Diffusion potentials
Ideally, concentration differences in earth ground can create diffusion potential. Causing this potential occurs at a point where there is an excess of ions of a certain species which it will back to a homogeneous distribution by the diffusion force; this is causing an ion transport in the direction of the concentration gradient, which would increase an electrical convection current. Relocation of cation represents positive current and relocations of anions represents negative current. For one to one electrolytes, such as NaCl, the sample is monovalent, thus the net diffusion current flow density (J_D) which is driven by the concentration gradient would be

$$J_D = e^0 \nabla C (D_C - D_A) \quad\text{.....................................} (10)$$

where e^0 is the elementary electrical charge, C is the electrolyte concentration, D_C and D_a are the diffusivities of both, cations and anions, respectively. The net current flow resulting from the difference between D_C and D_a, in steady state this is balance with the conduction current in the opposite direction. In turn, the conduction current causes a potential drop causing a measured self-potential anomaly. In case of a known concentration gradient, this can be estimated by the convection current as no other sources are present; but naturally it is more complex due to the fact that there always several kinds of ion involved creating the diffusion current. In most self-potential investigations, it is believed that diffusion potentials can contribute to background values; however it is not easy to determine their influence. One problem is that it is not clear why the diffusion potential change over time; in fact all concentrations should disappear over time, except a continuous source of ion is existing. However, no continuous source has been present.

Thermoelectrical potential
In a survey associated with geothermal areas there have been several reports about SP anomalies generated by temperature gradient. Many geothermal areas represents large self-potential anomalies, assuming that they are generated from a combination of electrokinetic and thermoelectric coupling. Additionally, both positive and negative anomalies can occur in geothermal systems (Corwin and Hoover, 1979). Normally in geothermal areas, self-potential coming from thermoelectric effects is of smaller amplitudes and shorter wavelength than anomalies causing by electrokinetic effects, however in this case electrokinetic occurs because the thermal source induces convection in the groundwater. Nowadays, pure thermoelectric effects are not clear understood, but the idea is that they are caused by differential thermal diffusion of ions in the groundwater and of electrons and ions within soil and the rock matrix. Thermoelectric coupling coefficient refer to the magnitude of thermoelectric coupling; this coeeficient is the ratio of resulting gradient of electrical poptential to the applied temperature gradient $\Delta V / \Delta T$. The ratio values were presented data in many rock types in 1963 by Nourbehecht, the data shown ranging from -0.1 to 1.5 mV/°C.

Mineral potentials
The mineral potentials are often called sulphide potentials due to these potentials are generally most observed above sulphide mineralization. Almost all ore bodies that can generate SP anomalies are good electronic conductors. Electrochemical gradients in earth ground are the driving force of mineral potentials. Earlier ideas attributed these phenomena to oxidation of the part of ore bodies over the groundwater table, as this mechanism should cause positive anomalies over ore bodies. But the general observation is opposite and this theory cannot explain for graphite. After that Sato and Moony (1960) presented a review of earlier theories and they also have provided explanations about electrochemical processes in which the ore bodies do not directly take part in the chemical reaction but act only as an inert conductor of electrons. Since ore bodies (electronic conductor) extends above the water table they cause differences in electrochemical reactions at the upper and lower part of the ore body so that this produces a potential at the interface of the mineralization with electrolyte. A cathodic electrochemical form in the upper water table by the chemical reduction of the ions in

the electrolyte (electrons gain), while at depth below the water table, anodic electrochemical oxidation occurs (electrons loss). However, this hypothesis does not explain all the occurrences of SP from minerals and no hypothesis is yet able to explain for all observed mineral potentials (Parasnis, 1997; Reynolds, 2011).
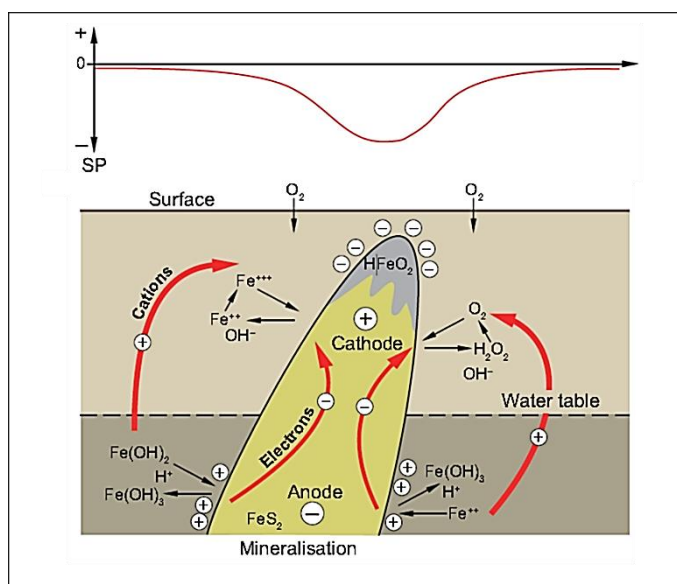
Figure 1.5 Self potential mechanisms, current and ion flow in the vicinity of an ore body later (Sato and Mooney, 1960; Dentith and Mudge, 2014).

Field procedure of self-potentials
The concept of self-potential method is measuring the natural potential difference between any two points; according to this the method is passive as it does not require the injection of any current to the ground. The basic equipment necessary to perform the survey is relatively simple. The required equipment consists of a pair of non-polarizing electrodes, high input impedance voltmeter, and cables. This survey method for determining electrical potential differences in the ground can be performed along profile lines and loop surveys or grid surveys. The details description of equipment, data acquisition and field technique are as following.

Equipment
In order to obtain self-potential values a pair of electrodes has to put into the ground and connected by cable to a voltmeter. A special requirement is that the electrodes should be non-polarizing electrode type (porous pot) because at metal electrode electrochemical interaction with the ground can occur thus generating a noise potential. A non-polarizing electrode is set by porous container containing metal electrodes submerged in its own salt, for example, copper in copper sulfate solution. The salt solution inside can seep through the porous pot thus creating electrical contact with the ground (Figure 1.6).
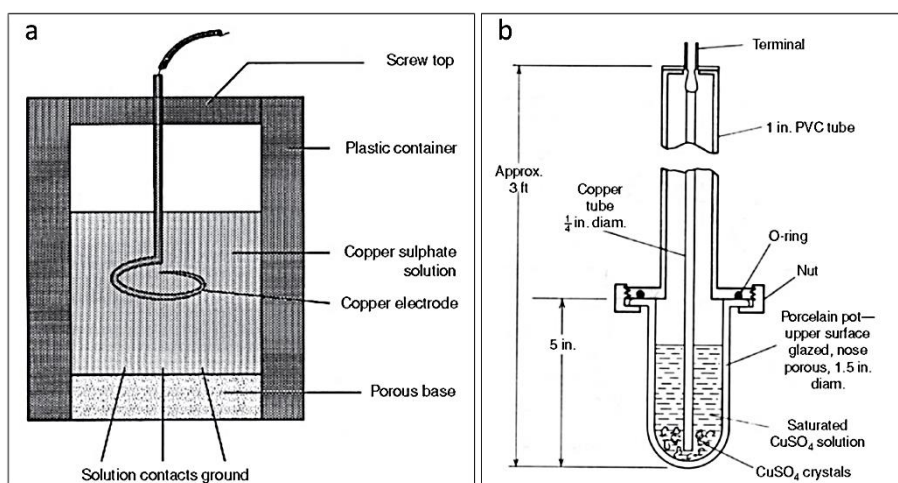
Figure 1.6 Non-polarizing electrodes (a) showing cross-section through a non-polarizing porous-pot electrode and (b) showing walking stick of the electrode. (Reynolds, 2011).

Field techniques

The field procedure of SP measurements has two alternative techniques, which can be separated due to the electrode configurations (Revil and Jadani, 2013). The first is leapfrog configuration, also called dipole or gradient configuration. This technique refers to measuring of the potential gradient [mV/V], which is performed by two electrodes fixed and generally separated 5 to 10 m apart and moves together along staked lines (Dentith and Mudge, 2014). The midpoint between the two electrodes is observed. The two electrodes are leapfrogged along the traverse, and it is required to obtain the correct polarity of the recorded potential. The electrode's trailing has to be connected with the negative pole of the voltmeter. The leading electrode should be connected with the positive pole. A disadvantage of this technique is that the error often accumulates as the transverse is moving on. An advantage here is that it requires only short lengths wires which are constantly moved along with the electrodes (Dentith and Mudge, 2014; Figure 1.7).
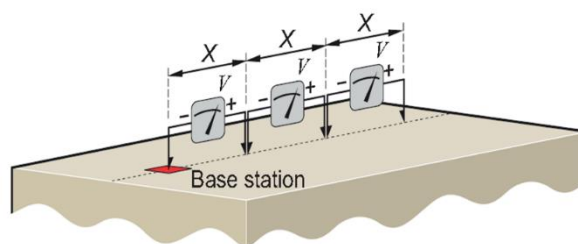
Figure 1.7 Field technique of self-potential measurement by leapfrog configuration. (Dentith and Mudge, 2014).

The second procedure is the fixed-based configuration, also called potential amplitude, performed by keeping one electrode at base point outside the survey area and other electrode moved along a traverse (Dentith and Mudge, 2014). At each station the total potential is measured directly. This method requires long wires connecting the electrodes to cover an area. In order to obtain the correct polarity of the potential

recorded, the reference electrode is connected to the negative pole of the voltmeter, and the moving electrode is connected to the positive pole of the voltmeter. The base station requires being located in an undisturbed area or a zone of low potential gradient assigned as starting point with a potential value of 0 V. A disadvantage of method is that it needs a long cable, but an advantage is that this method avoids the accumulation of electrode polarization errors. In this technique absolute SP is measured (Dentith and Mudge, 2014; Figure 1.8).
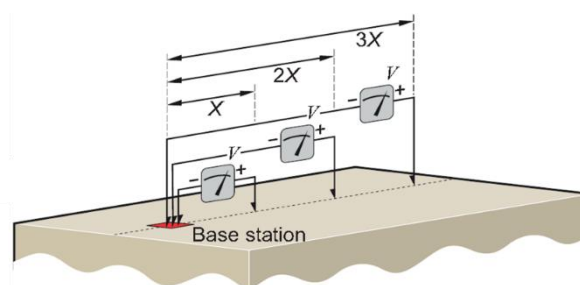
Figure 1.8 Field technique of self-potential measurement by fixed base configuration. (Dentith and Mudge, 2014).

Self-potential mapping
The objective in self-potential is to build a map of the electrical potential distribution on ground surface. In this case, fixed base configuration is used, so this map refers to the potential map as a map relative to the base station. Self-potentials like all scalar potentials in physics as defined to an additive constant. Generally, the fixed electrode is buried in hole surrounded by mud as reference station. The roving electrode is used to measure the electrical potential at a set of stations, which requires a GPS meter for recording the geographic coordinates at each measurement station. The drift of the voltage between both electrodes has to be kept as small as possible during measuring time. For large-scale mapping of SP, this can be performed by several strategies, with details discussed as following (Revial and Jadani, 2013).

The first strategy is called loop network, which has been used by numerous researchers (e.g. Revial and Jadani, 2013). The concept of loop network is performed by choosing one base station as reference and measurements are carried out with scanning electrodes at different secondary stations. For extending the measurement area, the first base station is moved and the reference electrode is then located at the position of the last measurement station; additionally, this step requires a leap frog (Revial and Jadani, 2013). Measurements have to be repeated to close a loop. The main issue when closing the loop is to need to check the closure error and this closure error is used to correct the SP measurements. The closure error is the effect from propagation of error when changing the reference electrode. Making the correction along a closed loop can be done by performing the naturally continuity of the electrical potential using the first base station data as a base station for all loops, and then correct the closure error along the loops (Revial and Jadani, 2013; Figure 1.9).
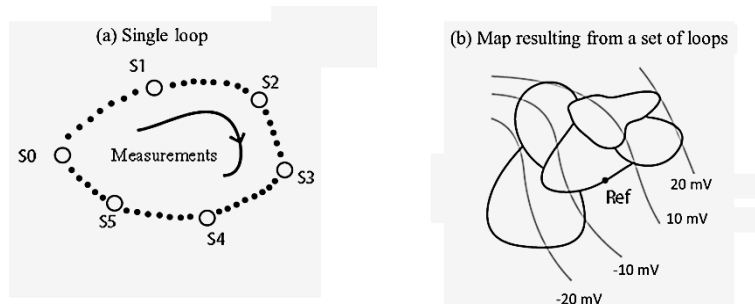
Figure 1.9 Self-potential mapping by using loop network strategies. (a) Single loop and S0 is the initial base station which the self-potential value should be close to zero (b) self-potential map is done by combining information of several loops and using one base station as reference for all loops (Revial and Jadani, 2013).

The second strategy is a star network, which is preformed when the difference of the potential between a number of base stations is several hundred meters far from other base stations, or the wires which were used between two points were not always protected which can cause induction effects. For a star network, each base station is used as the local reference of further profiles with a radially distribution more or less around the base station (Revial and Jadani, 2013; Figure 1.10).
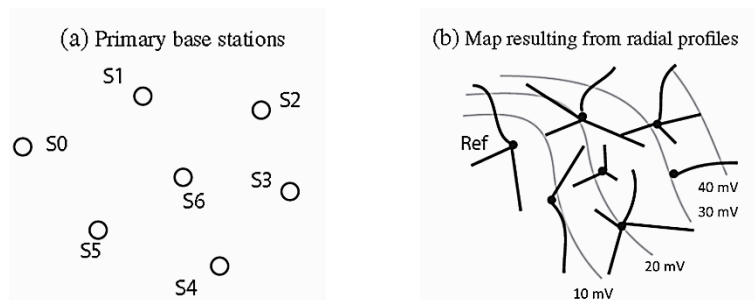
Figure 1.10 Self-potential mapping by using a star network. (a) Set of base stations is chosen and setup in the ground; then the difference in potential is measured between these stations. (b) Each station is used as a secondary reference and profiles in radial orientation from this station are measured. One of the base stations is used as a reference for the entire survey in order to make the final self-potential map (from Revial and Jadani, 2013).

The third strategy is the direct measurement of the electrical field (see Revial and Jadani, 2013). This strategy is not measuring the electrical potential but directly measure the electrical field at a set of stations. The advantage of this method is that it does not require long wires and it is easy to perform in a field survey; but it is difficult to measure the noise of the first spatial derivative. The electrical field at a station can be measured by carrying out measurements of the potential difference in two normal directions. A reliable electrical field value at this point is based on the average of the electrical field magnitudes at several points over an area (Revial and Jadani, 2013; Figure 1.11).

(a) Primary base stations   (b) Map of the electrical field
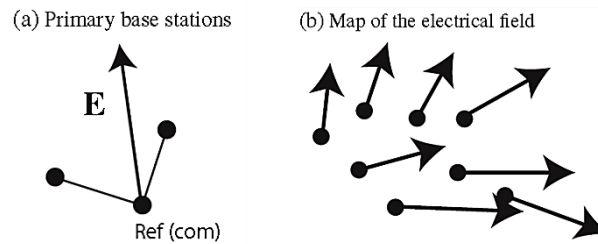
Figure 1.11 Large-scale mapping of the electrical field. (a) Each station is formed in a L shape by three using measurement points. (b) Vector map of the electrical field done from a pair of measurements repeated at various stations (from Revial and Jadani, 2013).

Correction of self-potential data
In order to evaluate and correct the drift obtained during the acquisition of the data; the raw data of the self-potentials were processed after the survey, which generally requires two corrections steps, including reference correction and closure correction. Additionally, in case a self-potential survey is affected by terrain, a topographic correction is required.

Reference correction
The first step is the reference correction that must be applied to each self-potential profile when it has changed the reference electrode positions (e.g. Revial and Jadani, 2013). This approach is to combine the different parts of a self-potential profile and to correct various changes of the reference electrode. Each section of the survey profile measured with a single reference must be shifted to the end of the previous section. By this the first section will be the same but the rest will be will be shifted along with in the direction of where the measurements were carried out.

Closure correction
In case self-potential data is taken from a closed profile, the first point is the same with the last point; therefore their self-potential value measured should theoretically be the same. Nevertheless, this usually not true in several surveys due to environmental disturbance present during the survey, such as soil temperature, soil moisture, instrumental error, thus causing drift. As the drift increases over time of measurement and accumulates it has to be corrected; this refers to closure correction.
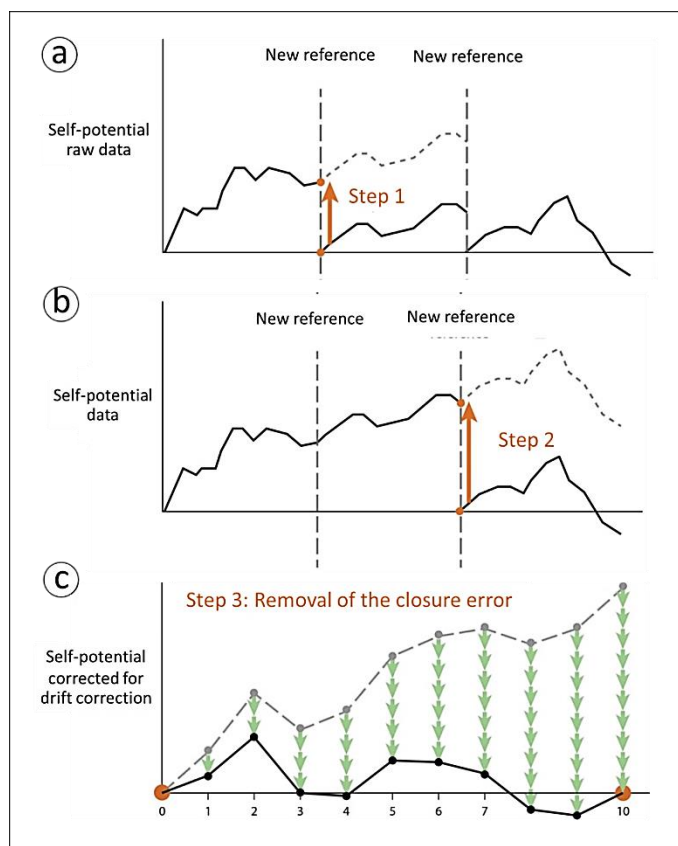
Figure 1.12 Correction steps for the raw data of a self-potential profile along a closed loop. Step 1-2: At each change of base station the potential is set continuous. Step 3: Removal of closure error (after Barde-Cabusson and Finizola, 2012, unpublished SP Processing Tutorial, provided by authors).

Figure 1.12a and b show the reference correction steps of self-potential data processing, with the second part of the profile measured shifted to the end of the first part, and the third part is also shifted to the end of the second part of profile. Figure 1.12c presents a dataset of self-potential data containing ten data points, and closure correction applies on these after steps of reference correction. The drift is accumulated along the measurement between the first and the last point; so correction of this drift is required for all data points. The initial point refers to the reference of the profile that does not require the correction. The next point after the reference will be corrected as $1/10^{th}$ of the total drift, which 10 is the number of data points that is not including in the reference. This is applied to every data point, such as for the second point will be corrected for $2/10^{th}$, etc…until the last point of profile that will be correct $10/10^{th}$ of the total drift.

Topographic effect
In general, self-potential values tend to become more negative with increasing elevation as reported from several previous investigations, e.g. Jackson and Kauahikaua (1987), Aubert and Atangana (1996) and Sasai et al. (1997). This phenomenon is called topographic effect or terrain effect, which is caused by subsurface fluid flow along a slope through a porous rock generating a electrokinetic potential. Thus, sometimes self-

potential data already corrected by closure correction must be corrected for the topographic effect; this correction can be calculated from equation

$$C_{TE} = -K\Delta h \dots\dots\dots\dots\dots\dots\dots\dots\dots (11)$$

where C_{TE} is topographic effect correction value (mV), K is the topographic correction factor (mV/m), which can be determined from relationship between self-potential values and elevation, an example of that showing in Figure 2.9 (Wanfang et al., 1999), and Δh is absolute elevation difference from base station.

In case the topographic has an effect on the self-potential values, the residual self-potential (SP_residual) can be determined by removing the topographic effect from the closure corrected self-potential (SP_ci) value as following:

$$SP_{ci} = SP_{Residual} + C_{TE} \dots\dots\dots\dots\dots\dots\dots (12)$$

Limitation of self-potential method

Self-potential surveys focusing only on the direct current field, all other electric potentials are considered as noise, which should be avoided (Corry et al., 1983). The first thing that should be avoided in a self-potential survey is the cultural noise. Changes in the natural self-potential field can result from electromagnetic communications, buildings, fences, power lines, pipelines, and others. There is a vulnerable of the surveys to such noises. In order to avoid these noises measurements should not be taken within 10 m of a cable in the ground so any offset can be avoided. The base stations also should not be within 500 m distance of such cables. Additionally, gas lines, metal pipes, fences, railroad tracks, and industry area can also result in noise of self-potential values; if possible measurement should not be conducted in such areas (Corry et al., 1983).

In choosing a field technique to employ self-potential measurements as leapfrog or fixed base, it is important to care about polarities as it will minimize errors. The reference or trailing electrode needs to be connected to the negative pole of the voltmeter, while the moving or leading electrode should always be connected to the positive voltmeter pole (Corry et al., 1983). Electrodes are one of the main things that have to be taken care of, while electrodes themselves also can have an effect on self-potential variations. This effect can be avoided by cleaning the bottom ceramic surface of the electrodes after each measurement, keeping the electrodes out of sunlight if possible, shielding the pots from diurnal temperature changes when taking any reading, and keeping them in a constant temperature bath when not making measurement (Corry et al., 1983).

Moreover, a survey should not be carried out under conditions where the soil moisture might have changed during the survey, as this can change the electrical potential of the subsurface. A survey should be stopped if there is heavy rain or should stop for at least a period of twelve hours after heavy or long rain. However, a survey might continue in case of a short rain shower where water has not penetrated into the soil more than 1 cm (Corry et al., 1983).

Analysis and interpretation of SP anomalies

After data processing, interpretation of self-potential anomalies can be used to evaluate its source. Self-potential result can be interpreted both quantitatively and qualitatively. Most of interpretation procedure depends on the target of investigation. There have been several works on quantitative interpretation; normally quantitative interpretation can be achieved through numerical techniques. Which techniques are used in the field data compared with results from forward models is based on charged geometrical structures. Self-potential anomalies are often interpreted qualitatively by profile shape, amplitude, polarity (+ or -) and contour pattern.

Self-potential methods have been wildly used in many applications, like geothermal, hydrology (Schiavone and Quarto, 1984; Rao, 1953) and environmental engineering to determine sources of geothermal flow and groundwater investigation, additionally to detect seepages at dams and embankments (Ogilvy et al., 1969). The most significant application of self-potential is its direct correspondence with subsurface water movements, and self-potential data are always analyzed as profiles which transect the study area in part that are considered representative of the area. Figure 1.13 indicates self-potential profiles related with hydrological meaning; the difference of profile patterns delineate the most possible directions of groundwater flow (Richards et al., 2010).

Normally, in case of hydrothermal zones positive self-potential anomalies are characteristics of the upward movement of hydrothermal fluids and negative anomalies are for downward movements of hydrothermal fluids. However, in several cases the topography can be represent effects, so the self-potential/elevation gradient on each side of a hydrothermal system can be asymmetric (Lénat, 2007). The interpolation of the self-potential data in that situation might be improved by an analysis of the self-potential and elevation relationship. In addition, positive and negative self-potential anomalies do not have the same meaning in hydrogeological and hydrothermal areas. Such as in case of active volcanoes, both areas are present, the hydrogeological zone is located at the lower slope and in the shallow subsurface, the hydrothermal zone is on the upper slope and at summit of the volcanic edifice; the amplitude of self-potential anomalies can vary from one system to another; however, this not always the case (Finizola et al., 2004; Aizawa et al., 2008; Lal, 2016).
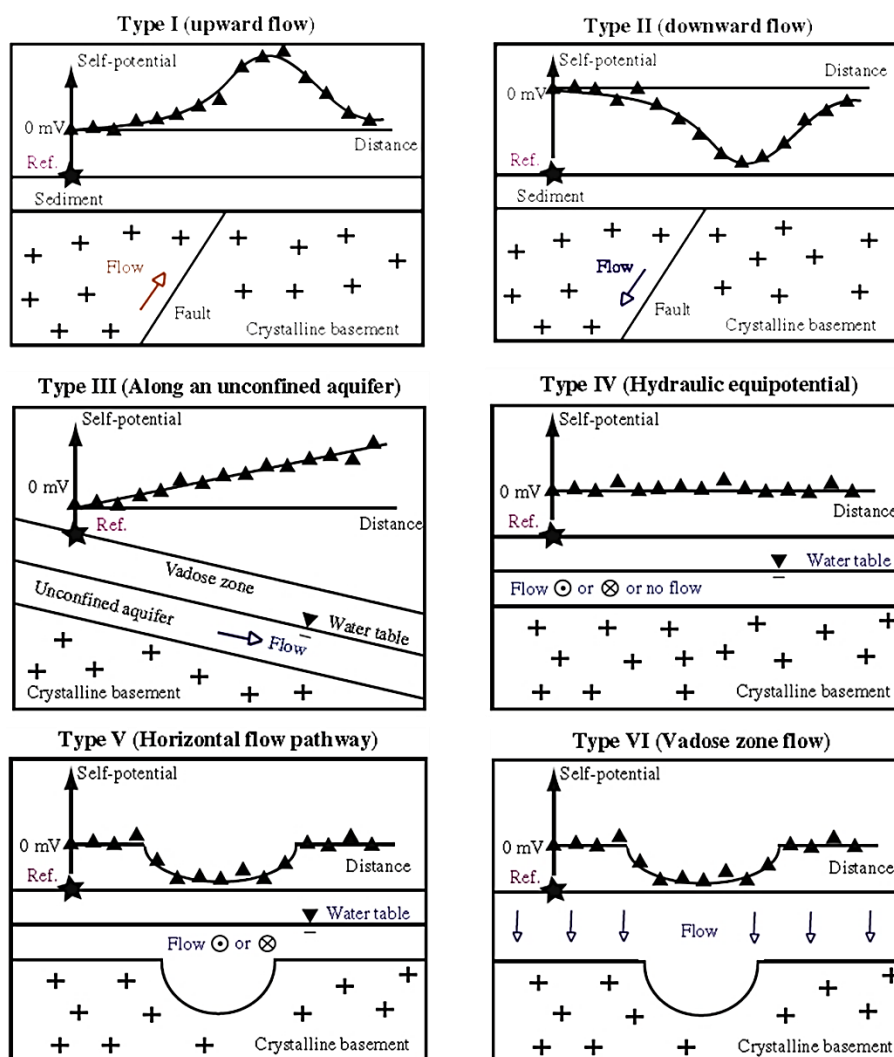
Figure 1.13 Common self-potential anomalies and their potential hydrogeological explanation. Filled-triangles is noisy self-potential measurements measured at ground surface and "Ref" is the reference electrode (zero potential) of the profiles (Richards et al., 2010).

Salinity and self-potential method
Whenever fluid flow in the subsurface is a saline groundwater, the interpretation of self-potential anomalies is often challenging and complicated. There have been several works applied for understanding the relationship between salinity and self-potential method.

Ikard et al (2012) described time-lapse self-potentials laboratory measurements performed in a sand box associated with a salt tracer injection upstream. Their study found that salt injection can be monitored with self-potential method. SP can be used to detect in heterogeneous porous materials preferential fluid flow pathways. The salt injection reduces the magnitude of the (negative) streaming potential coefficient, so that a decrease in the magnitude of the self-potential field can be linked directly with the groundwater flow. Additionally, the salt concentration gradient is responsible for a

diffusional electrical current, thus creating a second type of self-potential anomaly. Figure 1.14 shows results of their experiments indicating that at the top surface of the tank there is another contribution that generates a positive self-potential. This anomaly is related to the diffusion potential which is associated with the salinity gradient. In case of a salt plume or saline groundwater this flow can produced a self-potential signal with opposite sign compare to general cases of groundwater flow.
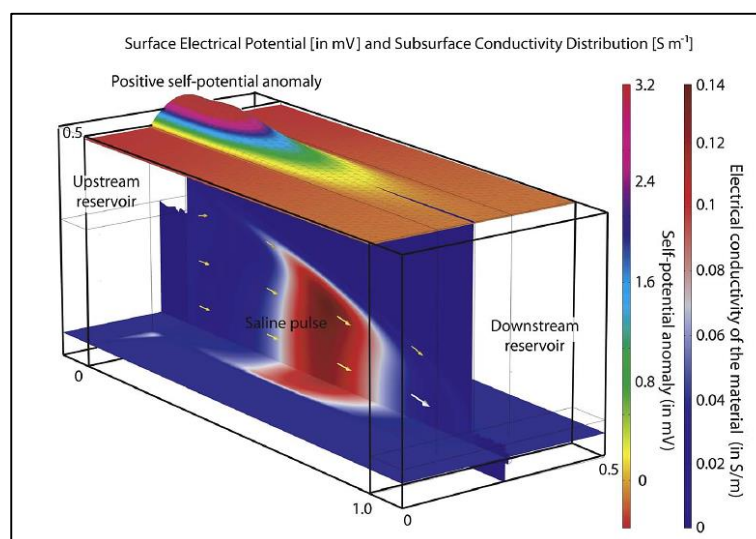
Figure 1.14 Image of the 3-D resistivity distribution of self-potential anomaly map at the top surface of the tank during a saline pulse experiment (from Ikard et al., 2012).

Martínez-Pagán et al. (2010) reported a sandbox experiment of self-potential monitoring of a salt plume. The leakage of a plume of salty water was monitored from a hole made at the bottom of a small tank which was located at the top of the main sandbox. The SP response related to the migration of the salt plume in the sandbox was measured over time. Results showed that the SP anomaly was observed with amplitudes varying from a few millivolts to a few tens of millivolts, at the start of the leak and after a few minutes, respectively. They suggested that there are two mechanisms that created these anomalies; a combination of streaming potential and diffusion potential related to pore water flow, as well as the gradient in the chemical potential of ionic species, respectively.

Vinogradov et al (2010) and Jaafar et al. (2009) measured the streaming potential coupling coefficient in sandstones saturated with NaCl that dominated artificial and natural brines up to 5.5 M, carried out on cylindrical sandstone core samples. They report that the magnitude of the coupling coefficient decreases with increasing brine salinity. According to the studies the magnitude of the zeta potential decreases with increasing brine salinity in the low salinity domain (<0.4 M). However, it reaches a constant value at higher salinity (>0.4 M). According to the authors, Vinogradov et al (2010), a constant value of zeta potential monitored at high salinity indicated a maximum packing of counterions in the electrical double layer's diffuse part.

Esmaeili et al (2016) investigated the streaming potential coupling coefficients and zeta potential at low and high salinity conditions. Streaming potential coupling coefficients of 36 sand samples were measured with salinity values from 0.0005 M to 0.025 M of NaCl solutions. They obtained the streaming potential coupling coefficients and zeta potential and much lower scattering in the data points was accomplished for different saline water injections. They also presented an empirical expression for the measured coupling coefficients which can give streaming potential coupling coefficients and zeta potential from 0.0001 M to 5.5 M salinity range.

Thus, in case of a saline groundwater environment, a positive self-potential anomaly can be related with saline water flowing down, whereas a negative self-potential anomaly can be related to saline water flowing up, opposite with anomalies of normal groundwater (see Figure 1.14). Upwards flowing saline water would be likely hot saline water due to natural hot springs in the area. There are two contributions to the total source current density that generates SP signals: first is the streaming current density associated with the flow of the pore water itself, and the second one is the diffusion current density associated with gradient of the salinity (Ikard et.al, 2012).
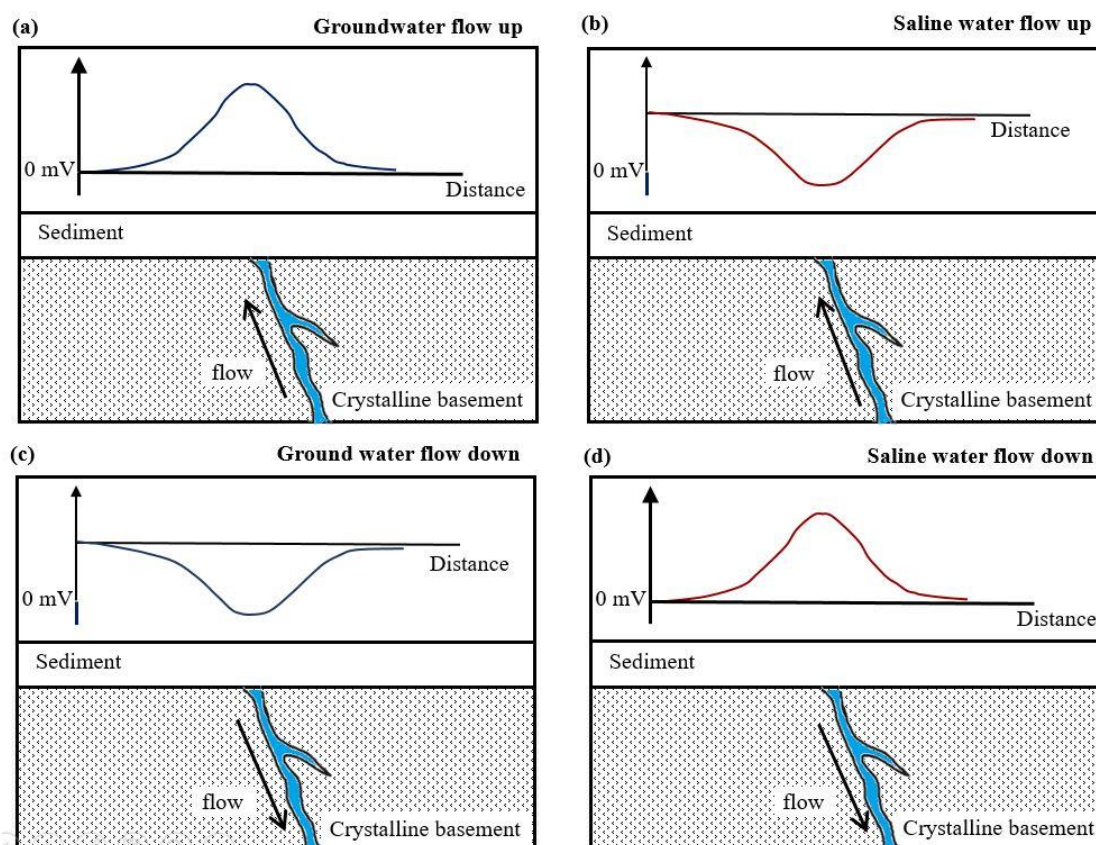
Figure 1.15 Interpretation the fluid flow, which generates self-potential signals; self-potential signal generated from, a: normal groundwater flow up; b: salty water flow up; c: normal groundwater flow down; d: salty water flow down. Scales are arbitrary.

1.2.4 Ground surface temperature measurement

The geothermal system loses the heat to the ground when the fluids flow by conduction. However, the soil temperature at 30 cm depth and deeper is protected from diurnal temperature changes due to the poor thermal conductivity of soil (Pearson et al., 2008). Surface temperature measurements can be performed by using a temperature probe at 30 cm of depth along same profiles of self-potential. The measurements have to done avoiding huge diurnal temperature variations. A surface temperature anomaly of more than 10° C above atmospheric temperature can be interpreted to geothermal activities.

1.2.5 Electrical resistivity surveys

Introduction

For the resistivity method man-made-generated electrical currents are introduced into the subsurface and then resulting differences in the potential are measured at the surface. The aim of this method is to determine subsurface resistivity distributions. Deviations of measured potential differences from expected ones of a homogeneous subsurface can provide information on the electrical resistivity of inhomogeneities in the subsurface (Kearey et al., 2002). The ground resistivity depends on several geological parameters, e.g., mineral and fluid composition, porosity, as well as the degree of water saturation. Surveys utilizing electrical resistivity have been widely used for many applications, such as in the search for potential groundwater sources, to observe types of groundwater pollution, to locate subsurface cavities, faults and fractures, in stratigraphic correlations of petroleum fields, and in prospecting conductive ore-bodies (Loke et al., 2013a; Reynolds, 2011; Parasnis, 1979).

Basic resistivity theory and geometric factor

Considering an electrical material uniform in a cylinder of side length L through which a current (I) is passing (Figure 1.15). Resistivity of this material is defined as the resistance in ohms between the two opposite faces of a geometrical shaped container of such material. As dR is the resistance of such container, dL is length, dA is the cross-sectional area, with the resistivity ρ given by (Kearey et al., 2002; Reynolds, 2011):

$$\rho_a = \frac{dRdA}{dL} \quad \text{...} (13)$$
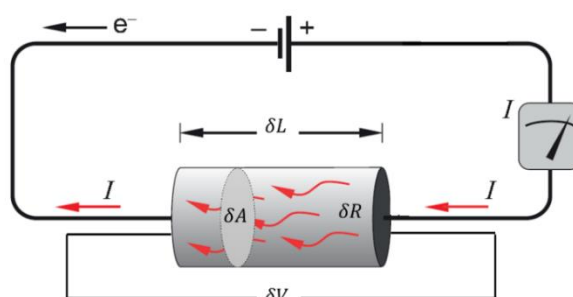
Figure 1.16 Basic parameter used in defining resistivity applied from Kearey et al. (2002).

From Figure 1.15, it can be seen that for an element of homogeneous material the current (I) is going through the geometrical shaped container causing a potential drop -dV between the ends. According to Ohm's law that the ratio of potential drop to the applied current also defines the resistance such that –dV = dRI, and from Equation 13 the potential gradient (dV/dL) can be obtained by

$$\frac{dV}{dL} = -\frac{\rho I}{dA} = -\rho J \dotfill (14)$$

where dV/dL represents the potential gradient through the element in Vm^{-1}, and J is the current density in Am^{-2}. Generally, the current density in any direction within a material is determined by the negative partial derivative of the potential in that direction divided by the resistivity (Kearey et al., 2002).

A simplest case is shown in Figure 1.16 with a homogeneous subsurface and a single point current source on the surface (e.g. Loke, 2000). For such a single current electrode input into the surface of an Earth layer of uniform resistivity the circuit is completed by a current sink at a larger distance from the electrode and with the current flowing from the electrode radially away. The current distribution is uniform over hemispherical shells centered over the source. At a given distance r from the electrode, the current density J is the current divided by the area over which the current is distributed the (a hemisphere; $\frac{1}{2}\pi R^2$), so this is given by

$$J = \frac{I}{2\pi R^2} \dotfill (15)$$
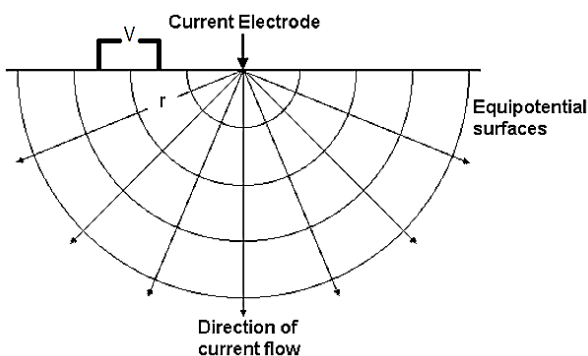
Figure 1.17 Current flows radially away from the electrode and the resulting potential distribution (Loke, 2000).

From Equation 15, the potential gradient is associated with this current density by

$$\frac{dV}{dr} = -\rho J = \frac{-\rho I}{2\pi R^2} \dotfill (16)$$

The potential V_r at point r from the current point source obtained by integration

$$V_r = \int_\infty^r dV = -\int_\infty^r \frac{\rho I}{2\pi r^2} dr = \frac{\rho I}{2\pi r} \dotfill (17)$$

From Equation 17 the potential at any point on or below the surface of a homogeneous half space can be calculated. Hemispherical shells as shown in Figure 1.17 indicate surfaces of constant voltage, called equipotential surfaces. When the current sink is at a finite distance from the source (Figure 1.17) the potential V_m at an internal electrode M is the sum of both potential contributions, V_a and V_b from the current source at A and the current sink at B (Kearey et al., 2002); then

$$V_M = V_{AM} + V_{BM} \quad \dots\dots\dots\dots\dots\dots\dots\dots\dots\dots \text{(18)}$$
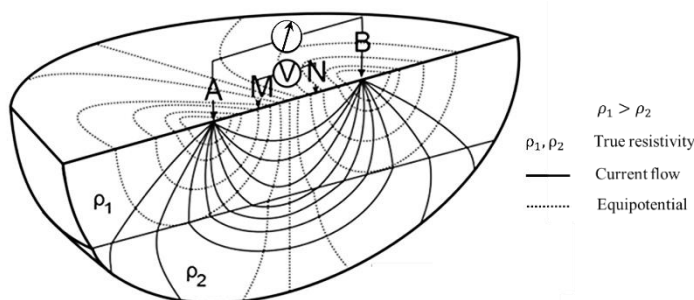
Figure 1.18 Current flow lines from electrode B to electrode A, then measuring potential between M and N, and indicating equipotential lines for a half space with two layers with different resistivity characteristics (from Knödel et al., 1997).

From Equation 2.5 it can be followed that

$$V_M = \frac{\rho I}{2\pi} \left(\frac{1}{AM} - \frac{1}{BM} \right) \quad \dots\dots\dots\dots\dots\dots\dots\dots \text{(19)}$$

Similarly

$$V_N = \frac{\rho I}{2\pi} \left(\frac{1}{AN} - \frac{1}{BN} \right) \quad \dots\dots\dots\dots\dots\dots\dots\dots \text{(20)}$$

Now ΔV (V_{MN}) can be calculated by

$$\Delta V = V_M - V_N = \frac{\rho I}{2\pi} \left(\frac{1}{AM} - \frac{1}{BM} - \frac{1}{AN} + \frac{1}{BN} \right) \dots\dots\dots\dots \text{(21)}$$

Thus

$$\rho = \frac{dV}{I} \left(\frac{2\pi}{\frac{1}{AM} - \frac{1}{BM} - \frac{1}{AN} + \frac{1}{BN}} \right) = k \frac{V}{I} \dots\dots\dots\dots\dots \text{(22)}$$

where k is the geometric factor that depends on the arrangement of the four electrodes, Figure 1.18 showing that common arrays with their geometric factors. Resistivity meters normally give a resistance value, R = V/I, so in practice the apparent resistivity value is calculated by (Kearey et al., 2002)

$$\rho_a = kR \quad \dots\dots\dots\dots\dots\dots\dots\dots\dots\dots \text{(23)}$$

(a) Wenner $k = 2\pi a$

(b) Pole−Pole $k = 2\pi a$

(d) Dipole-Dipole $k = \pi n(n+1)(n+2)a$

(d) Pole-Dipole $k = 2\pi n(n+1)a$

(e) Schlumberger

exact $k = \pi \dfrac{L^2 - l^2}{2l}$

Ideal dipole '$2l$' ; $k = \pi \dfrac{L^2}{2l}$
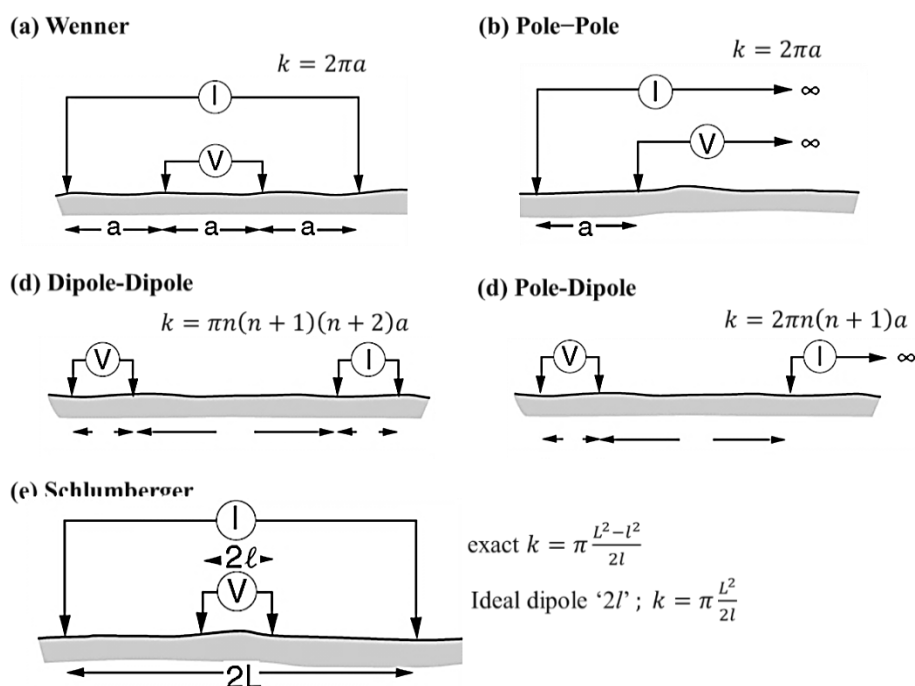
Figure 1.19 Some common arrangements of electrodes and their geometric factors applied from (Milsom, 2003).

It has to be realized that the calculated resistivity value is not the true resistivity value of the subsurface, rather an "apparent" value, which is the resistivity of a homogeneous ground that gives the same resistance values when investigated by the same array. The relationship between the "apparent" resistivity and the "true" resistivity is complex. In order to determine the true values of subsurface resistivity inversions are required (Loke, 2000).

Relationship between material and resistivity
At shallow depths the electric current flows in the earth through two main methods; electronic conduction and electrolytic conduction (Kearey et al., 2002). In electronic conduction, free electrons provide the current flow, for example in metals. In electrolytic conduction, on the other hand, free ions moving in the groundwater provide the current flow. In environmental and engineering surveys, electrolytic conduction is the more common mechanism (Kearey et al., 2002). Electronic conduction is dominant when conductive minerals are present. Resistivity values of common rocks and soils are shown in Figure 1.19. Igneous and metamorphic rocks usually have higher resistivity values, as the resistivity of these rocks considerably depends on the degree of porosity and fracturing, and the percentage of the pores and fractures filled with water. A given rock or soil type can exhibit a large range of resistivity, from about 1,000 to 10 million $\Omega \cdot m$, depending on porosity and pore fluid content. This can be applied for the detection of fracture zones and other weathering features in engineering and groundwater surveys (Milsom, 2003). Sedimentary rocks on the other side usually are more porous and have higher water contents, thus lower resistivity values compared to igneous and metamorphic rocks (Kearey et al., 2002).

Resistivity values of the rocks and sediments depend mainly on the composition, the porosity, and the salinity of the water contained in the pores and cacks. Unconsolidated sediments, like sand, and soils generally show lower resistivity values than sedimentary rocks. The resistivity value depends on their porosity as well as their clay content. Clayey soils usually have a lower resistivity value than sandy soil. However, there is an overlap in the resistivity values of different rock and soil types and classes. Because the resistivity of an individual rock or soil sample depends on several factors, e.g., porosity, degree of water saturation, concentration of dissolved salts. Seawater has a very low resistivity (about 0.2 Ω·m) because of relatively high salt content (36 ppt). Resistivity method is therefore an ideal method for mapping the areas with saline waters (Keller et al., 1966).
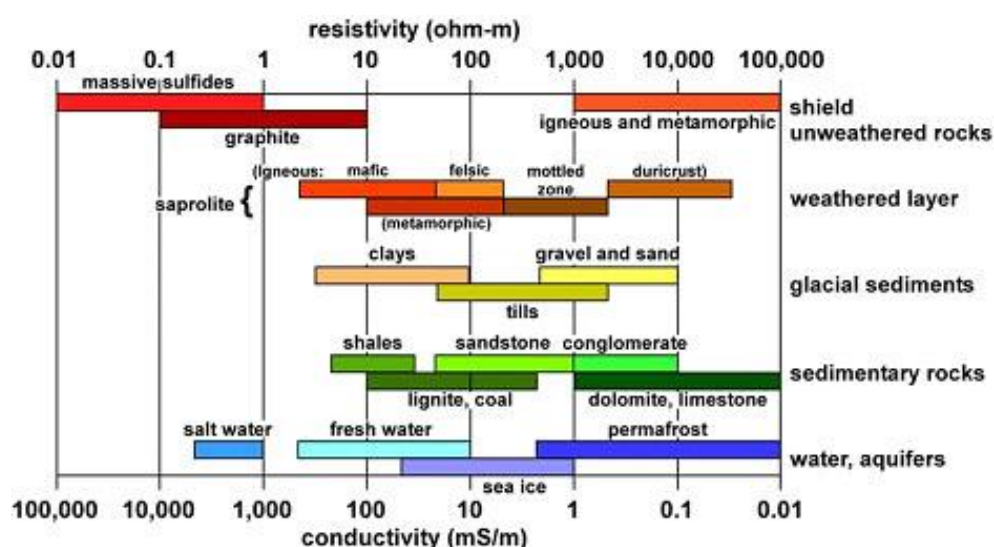
Figure 1.20 Approximate ranges of electrical resistivity values (ohm-m) or conductivity values (mS/m) for selected earth materials (based on Palacky, 1988).

1-D resistivity surveys and inversions
Since 1920's when the resistivity method was originated, the conventional sounding surveys is wildly used for quantitative interpretations (e.g. Kearey et al., 2002). For this method the center point of the electrode configuration is fixed, while the spacing between the electrodes is successively increased in order to get more information from deeper sections of the subsurface (Reynolds, 2011).

Measured apparent resistivity data are generally plotted in log-log scale. In order to interpret the obtained data it is assumed that the subsurface comprises of horizontal layers. In case of a sounding survey, the subsurface resistivity therefore changes only with depth and not in horizontal directions. A one-dimensional model of the subsurface is used to interpret the measurements as shown in Figure 1.20a. The resistivity sounding method's main limitation is that it cannot determine changes in the resistivity in horizontal directions of subsurface layers (Loke, 2015).
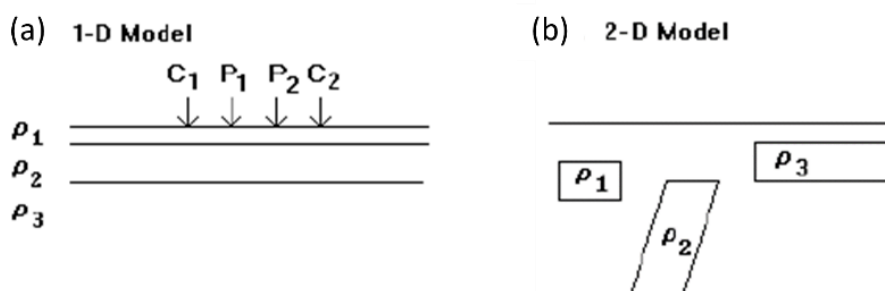
Figure 1.21 1-D (a) and 2-D (b) models used in the interpretation of resistivity measurements (Loke, 2015). C and P are current and potential electrodes, respectively; $\rho_{1,2,\ etc.}$ indicate layers or areas of different resistivity .

2-D electrical surveys
Two-dimensional (2-D) models are more accurate models of the subsurface where the resistivity changes in both the vertical direction and the horizontal direction along the survey line (Figure 1.20b). However, it is assumed that the resistivity does not change in a direction perpendicular to survey line, which is a reasonable assumption for many cases; especially for surveys over larger geological bodies. In several geological cases, this method can give useful results that are compatible with information from other geophysical methods, such as seismic, which can map undulating interfaces better, but has difficulties in mapping discrete subsurface bodies such as boulders, cavities, and groundwater pollution plumes if not applying advanced data processing techniques (Loke, 2015).

CHAPTER 2

RESEARCH METHODOLOGY

This chapter describes the details of data acquisition during field surveys and procedures of data processing used in this study. For the data acquisition, this chapter explains the study area and how data were collected. For data processing, this chapter explains about what corrections have been done for the data, how to corrected them, and steps of processing.

2.1 Study Area

Khlongthom saline hot spring is a unique geothermal system, which information provided from previous works in this area showing that the hot water from a deeper reservoir is mixing with salty water from the ocean via intrusion into the shallow groundwater layers thus representing the natural saline hot spring (Ngansom and Dürrast, 2016). For this work, geological and geophysical methods, mainly self-potential method, combined with ground surface temperature measurements and vertical electrical sounding (VES) were applied to understand patterns of fluids flow in the shallow subsurface and delineate anomaly zones in the Khlongthom saline hot spring. The saline hot spring is located in Khlongthom District, Krabi Province, which is located on Southern Thailand's east coast (Figure 2.1). It has a total area of 4,710 km^2, 800 kilometers south of Bangkok; it is an area of outstanding natural beauty, with beaches surrounded by tower limestone formations. Much of the coastline is covered by cave and limestone rock formations, tropical islands, palm fringed beaches; waterfall, and mangrove forest.

Figure 2.1 Khlongthom (red star) located in the south-eastern part of Krabi Province (from: mapsofworld, 2017).

Climate

The climate of Krabi province is influenced by the tropical monsoon; is warm all the year and there are two seasons, the hot season in January to April and the rainy season in May to December. In addition, two periods from April to May and September to October are the hottest. Generally, the temperature range is 17 °C to 37 °C.

Geography

The topography of Krabi comprises mainly of mountains and highlands alternated with plains in some parts. Additionally the Krabi provincial administration covers more than 130 islands in the Andaman Sea. There are mainly natural forests covering the area as well as mangroves and Cassia trees. Sandy clay conditions are suitable for growing agricultural products, including rubber trees, palm oil trees, mangos, coconuts, and coffee. The Krabi River flows 5 kilometers through the city and falls into the Andaman at Tambon Pak Nam. There are other several streams, such as the Khlong Pakasai and the Khlong Krabi Yai, which originate from the highest mountain range in province, Khao Phanom Bencha.

Geology

Spectacular land and seascapes of Krabi are defined by the geology. There are karst landscape and headland cliffs along its shoreline, which both has been formed from limestone. The tower karst is developed in massive Permian limestone and dolomitic limestone of the Ratburi Group, and two types of tower karst are prominent in the region, including peak forest karst and peak cluster karst.

The main study area of this work, the saline hot spring is located about 70 km southeast of Krabi City. In an area of 0.5 km^2 15 natural hot springs can be found, ten within the mangroves and five outside and nearby. Hot spring surface exit temperatures range from 41 to 47 °C, and the water salinity is about 2.1 ppt. Saline hot spring is located 5 km from the Andaman Sea, connected via the Phela river system and its mangrove rich tributaries. Figure 2.2a presents the geological map of Khlongthom saline hot spring, which indicates that the geology of the study area consists of sediments, gravel, sand, silt, marine clay and sandstone. As cross- section AA' showing that the geotectonic evolution of the area, an initial the horizontal layering of stratigraphic units according to age (see Fig. 2.2b), from the bottom to the top are getting younger. When compressional tectonics was applied almost vertical fractures resulted in different blocks with the current surface geology distribution (see Fig. 2.2c).
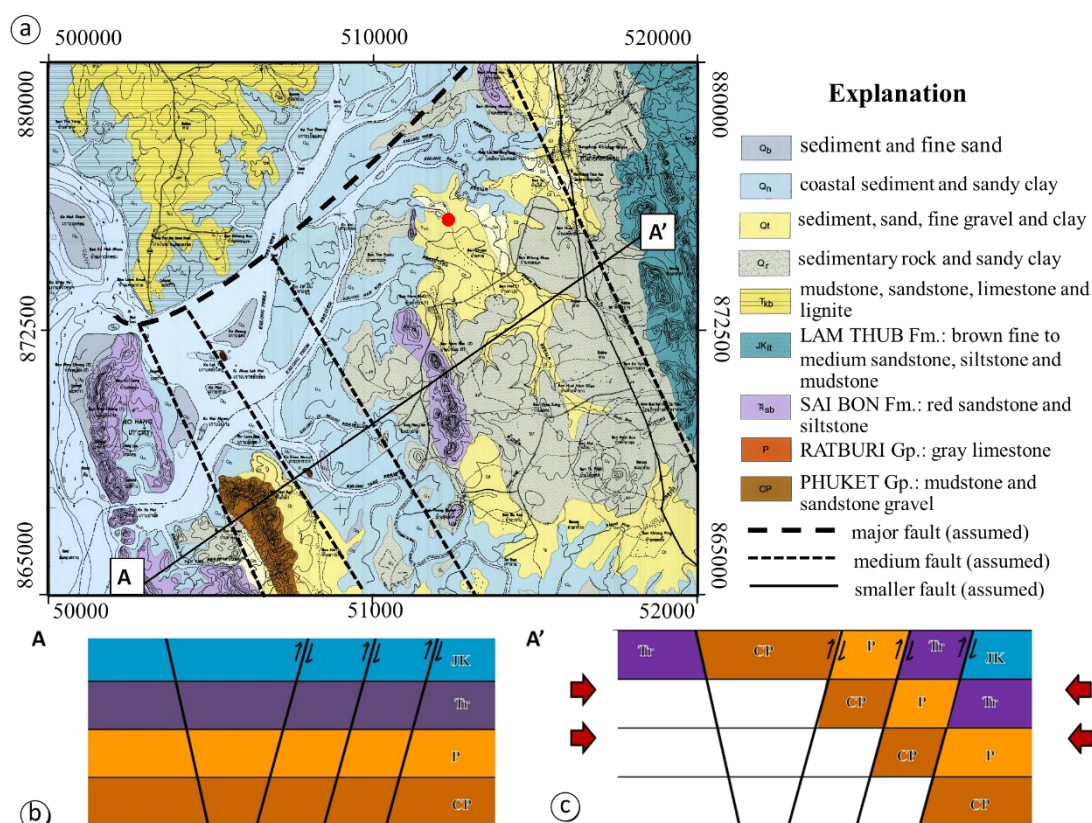
Figure 2.2 Schematic drawing of the geotectonic evolution of the area (not to scale): a) Overview geological map of Amphoe Khlong Thom, Krabi province and location of cross-section AA'. b) Initial horizontal layering of stratigraphic units according to age. c) Compressional tectonics with almost vertical fractures resulted in different blocks with the current surface geology distribution.

2.2   Previous work in study area

Ngansom and Dürrast 2016 investigated the saline hot spring Khlongthom by the integration of several methods, geological, geochemical, and geophysical. Their results show that the saline hot spring is quite unique in its occurrence. Hot spring waters from the depth flow upwards and mix with saline groundwater aquifers as the result of seawater intrusion from a nearby estuary and the existence of a salt marsh south and east of the main hot spring site. Geoelectric data show very low resistivity values in the shallow subsurface which that corresponding to black marine clay and groundwater salinity. Geochemical analysis showed that saline groundwater and hot water from deep aquifers mix while emerging along faults.

Wattanasen et al. (2015) investigated the subsurface geological structure of the saline hot spring Khlongthom. They carried out geochemical, microbiological, and geophysical methods including resistivity, seismic, and gravity, which covers an area of about one square kilometer. They reported that the subsurface model in the area is suggested to be of three main layers. The first is a top soil layer with a thickness of about <2.5 m lying on the second layer of thick marine clay (8-22m thickness), and the third layer is basement rock at deeper depth, possibly sandstone. The topographic variation of sandstone causes a basin which lies elongate in E-W direction. Geological

investigation found fault breccia with geophysical data indicated that there are three fault zones cutting through the area. The major one, its strike direction is between E081W to E-W. In addition, two minor fault zones are in N058W and N035E. Chemical analysis indicated the salinity in area has confirmed by the high content of K, Mg, Ca, and Na ions that are higher than in normal, non-saline, hot springs; especially, the Na content is more than 200 times higher.

2.3 Geological Survey

Geological surveys were carried out in study area before geophysical investigations because it is crucial to understand the geology of the area. A geological survey will be applied in this work depends on what data are needed and will be available from the survey. This method will provide the information of sediment and rock types, stratigraphic setting, and location of possible fault at shallow depth. The aim of geological studies is an understanding about geology, hydrology, and lithology of the study area in order to select the areas which should explore for obtaining more data related to hot springs by using geophysical methods. The first survey was done before geophysical investigations were done along line surveys (Figure 2.3), and the second survey was done before geophysical methods were done in loop surveys (Figure 2.3). Details of the geological surveys are as following:

- ➢ Survey the surrounding area of the study area, such as measurement of water temperature, observation of sediment and rocks, and surface manifestations of hot springs.
- ➢ Create lists of these manifestations in the study area.
- ➢ Plot the location of hot spring on geological maps.
- ➢ Estimate the boundary of hot spring area.
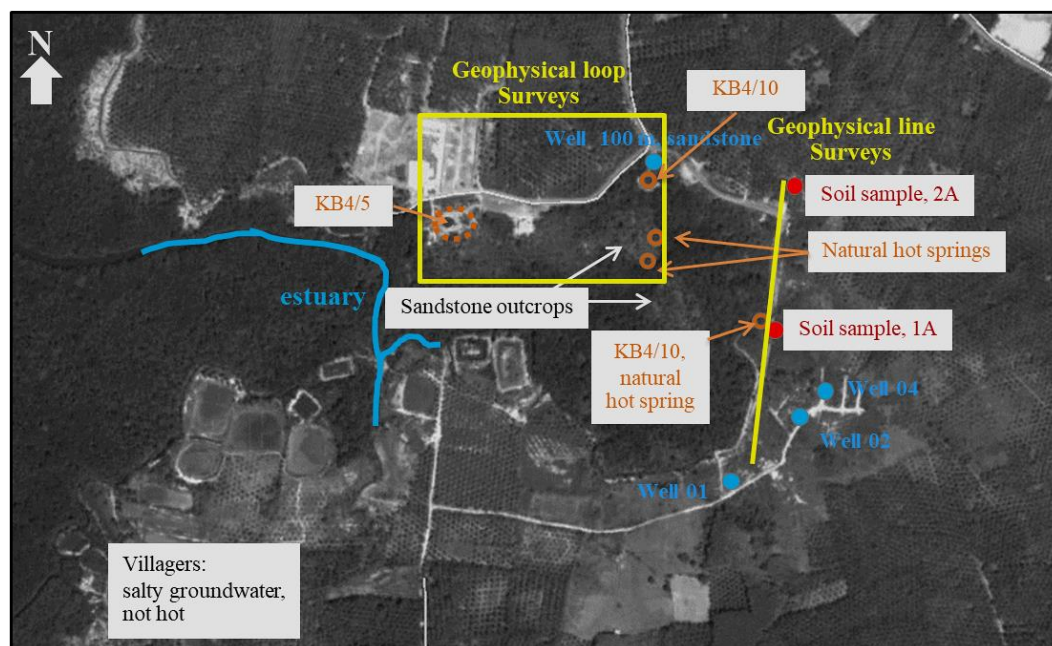
Figure 2.3 Overview map of study area (Google Earth, 2018).

2.4   Self-potential survey

The self-potential method is the main geophysical method survey of this work. This method was carried out in Klongtom saline hot spring which composed of line surveys and loop surveys for understanding the patterns of fluids flow in the shallow subsurface and delineate the anomaly zones.

2.4.1   Field Equipment

In this work, self-potential measurements were performed by using basic equipment consisting of $Pb/PbCl_2$ non-polarizing electrodes connected by cables to the Terrameter SAS 300B (Figure. 2.4). Potential differences between reference and moving electrodes were measured by Terrameter SAS 300B which has high sensitivity able of reading 0.1 mV. For getting normal voltage from the measurements, the reference electrode was connected with negative input of the Terrameter and the moving electrode connected to the positive input.
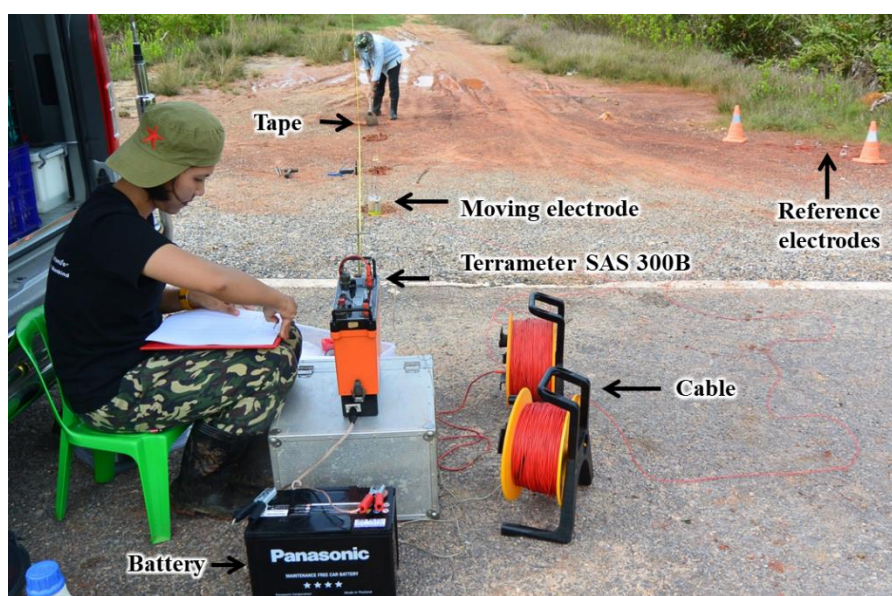
Figure 2.4 Basic equipment for self-potential measurements. Terrameter SAS 300B, which has high sensitivity connected by cables to $Pb/PbCl_2$ non-polarizing electrodes.

A $Pb/PbCl_2$ non-polarizing electrode manufactured by WOLF Chemical Ltd, it is shown in Figure 2.5. This electrode is usable in the very wet environment and under water until a pressure of 10 at. While using, under the moving electrode a watered sponge was placed (Figure 2.6) for a good contact between the electrode and the ground surface. In case of wet soil it was not necessary to use the sponge. Additionally, this work developed a carrier container (Figure 2.6) for carrying the moving electrode while measuring the field survey. The references electrodes were buried into a hole and electrodes were surrounded by mud from the soil which was dug from that hole. After each survey electrodes were cleaned and placed back in their container which has the sponge saturated with salty water at the bottom. The sponge in container have to be always checked during the surveys because it must not be dried up, thus sometimes it should be soaked with distilled water 30 to 50 ml. Electrodes should be stored and transported in their container and protected from sunshine.
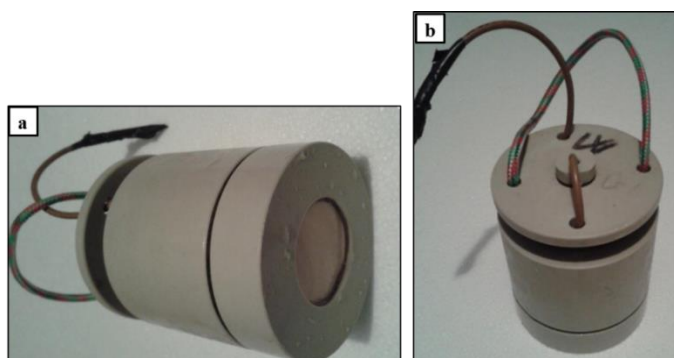
Figure 2.5 Pb/PbCl2 nonpolarizing electrodes: the body is filled up with lead chloride saturated hard gel and a lead spiral is cemented in it, the body-block of electrode has been manufactured from a monolithic PP rod trough turning, and the holder of the ceramic slab connect the block of the electrode by screw-thread and sealed by O-ring, thus it is usable in the very wet environment and under water until pressure 10 at; the electrode mass about 0.6 kg, height 100 mm and diameter 60 mm, (a) bottom of electrode which has surface of the ceramic slab of 7 cm^2, (b) top of electrode.
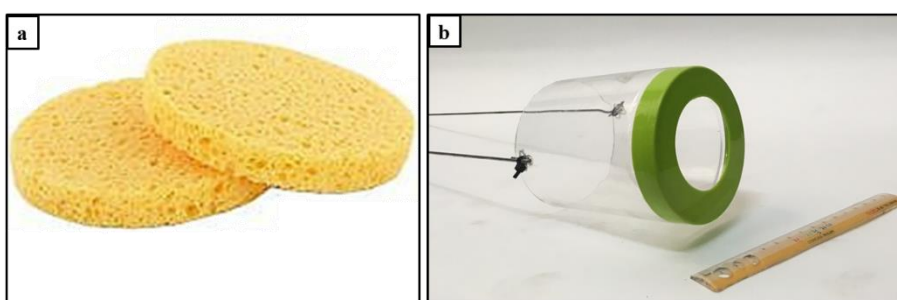
Figure 2.6 Additional equipment: (a) sponges used for a good contact between the electrode and ground surface, diameter of them is 60 mm, while using sponges must not be dry up, (b) container for carrying the moving electrode; the bottom of it was cut out for providing ground contact with a diameter of 52 mm, less than the diameter of the electrode.

2.4.2   Design of self-potential survey and measuring procedure

Self-potential measurements have been done in two parts; all 312 measurement points of this work consisted of two lines parallel to electrical resistivity tomography (ERT) survey line from previous work (Ngansom and Dürrast, 2016) in the eastern area and several loops around in the northern area of the Klongtom saline hot spring area (Figure 2.7a).

Profile line measurements

Two self-potential surveys lines have been done along an ERT survey line with a total of 300 m length (Line 1: 180 m, Line 2: 120 m). The first profile line is parallel to 251-431 m on the resistivity profiles, and the second profile, measured one day after Line 1, is parallel to 130-250 m. Data acquisition was done with fixed base configuration; potential differences were measured between reference and moving electrode. Three non-polarizing electrodes connected in a hole were used as the reference electrode (base); one electrode was moved with 2 m spacing along the self-potential profile which formed the line by using measuring tape.
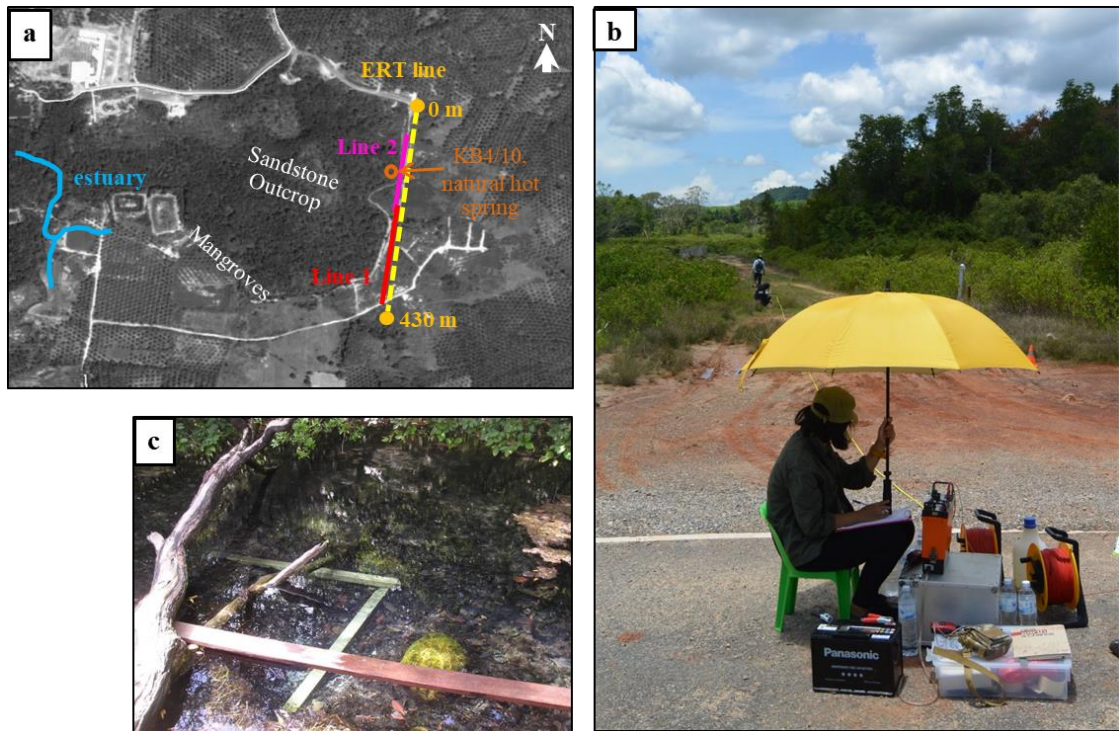
Figure 2.7 (a) Location of survey lines in the eastern area (yellow line, 430 meters), two self-potential measurements and ground temperature measurements were performed parallel along this line (Line 1: 180 m, Line 2: 120 m), the first profile line is parallel to 251-431 meters on yellow line, and the second profile, measured one day after Line 1, is parallel to 130-250 meters (GoogleEarth, 2017). (b) Self-potential measurements in study area, view to South; in the west are mangroves (c) KB4/10 natural hot spring located close to survey lines.

Profile loop measurements

Loop measurements have been done over an area of approximately 0.1km^2 covering the northern part of the study area shown in Figure 2.8. It composed of three loops connected together. All 162 measurement points reconstructed along the loop with the location of each point recorded by GPS meter (Figure 2.9); all loops were closed. Data acquisition was done with the both field technique configuration, fixed base configuration was used in single loop, and leapfrog configuration was used when having to connect the loop with each other.

Figure 2.8 Location of loop survey area in Khlongthom saline hot spring. (Google Earth, 2017).
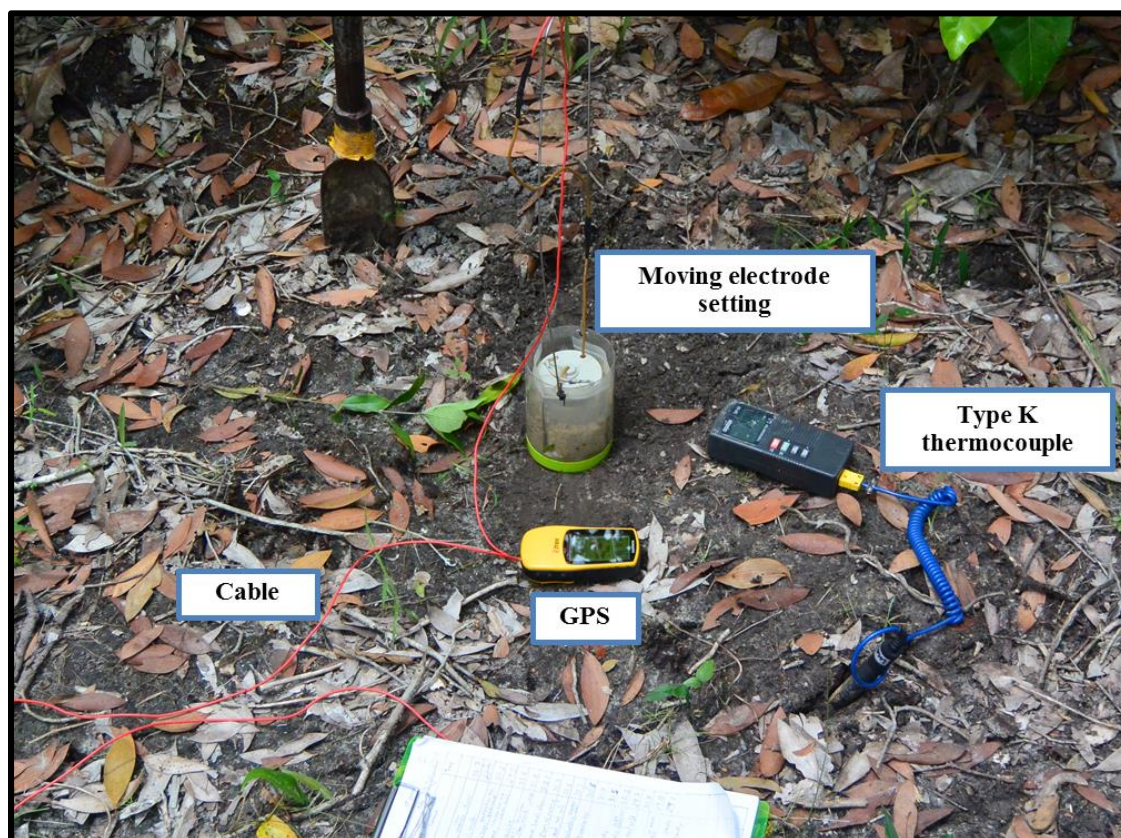
Figure 2.9 Basic equipment was used at measurement points during self-potential loop survey.

2.4.3 Base station

The location where the electrodes were fixed when fixed-base configuration was chosen is the base station, which all measurements refer to. It must be located at a suitable location. The base station is chosen to lie outside any slope, be away from activity of humans, and not be in area of large negative potential or soil condition dried up very fast, for example sand.

After the location for base station was chosen the electrodes was put into dug holes, and surrounded by mud made from the soil that was taken out from that hole before. Normally, one electrode was buried at base station, but to evaluate the self-potential error related with a particular base station, thus three electrodes were buried 30 cm from each other and connected together (Figure 2.10).

Figure 2.10 Three non-polarizing electrodes in holes and connected as base station; they were buried 30 cm from each other to evaluate the self-potential error related with this particular base station.

During the survey, the drift will be observed as it increases usually over a period of time; therefore the moving electrode requires returning to the reference point measurement at the base station every 1-2 hours, and when the last point on the profile was completed it must return there again. It is important that the electrodes at the base station must not be dried up, thus it always checked.

In a large scale survey area like this work extending the measurements of the array for covering the area always requires changing the base station. Then the base station is moved and reference electrode is then at the point of the last measurement station. In case of loop network any measurement point on the profile measured can be chosen for establishing the new base station for the new loop in order to connect both loops.

2.4.4 Self-potential data processing

After the field survey data were processed, which generally requires two corrections steps for the self-potential data. The first step is reference correction, that must be applied to self-potential profiles when the reference electrode position has changed, and the second step is closure correction (or drift correction) which must be corrected. For this work the measurements were performed forming of profiles and loops in order to correct the drift, the details of processing are as following:

1) Processing a self-potential profile

This work uses Microsoft Excel for correct the data and present the self-potential data in graphs as function of distance. During profile measurements this work use only one reference station, thus it does not require the reference correction of the raw self-potential data. The self-potential values of first measurement and the last one at the base station should theoretically be the same; however during the survey a drift were observed because at the same measurement point not obtained the same self-potential values. That drift increase along the time of the survey (Wanfang et al., 1999); this drift must be corrected by using closure correction, based on the equation below.

$$SP_{ci} = SP_i + SP_{drift} \quad\text{..} (2.1)$$

where SP_{ci} is the corrected self-potential value of the drift correction and SPi is the self-potential measurement value for point i and $SPdrift$ is the drift correction value. The drift value has been calculated as following (Wanfang et al., 1999):

$$SP_{drift} = t_i + C_{incrementdrift} \quad\text{..............................} (2.2)$$

and

$$C_{incrementdrift} = \frac{-(SP_{last} - SP_{first})}{\Delta t} \quad\text{...........................} (2.3)$$

where SP_{first} and SP_{last} are the self-potential values at the base station of the first and last measurement, Δt is the absolute time difference of first and last measurement at the base station, $C_{incrementdrift}$ is the value of the gradient of the self-potential value per unit time and t_i is the absolute time difference of the base station and measurement point i. Equation 2.1 was used in case of corrected data by using time recorded data. This work was performed on line surveys because for this one it does not require the UTM records via GPS at every measurement point. UTM locations of the first and last point of the survey lines were recorded in order to check the measurement points on the tape. An example of closure correction calculations for the line surveys is show in Table 2.1.

Table 2.1 Example of drift correction calculation of self-potential data.

Moving electrode on tape (m)	Time (hh:mm)	Average SP (mV)	Δt (min)	SP$_{drift}$	SPc (mV)
base	9:33	0.336	0	0	0.336
4	9:35	0.895	2	-1.96656	-1.07156
6	9:36	0.14	3	-2.94984	-2.80984
8	9:42	0.284	9	-8.84952	-8.56552
10	9:47	-0.317	14	-13.7659	-14.08292
12	9:48	-1.373	15	-14.7492	-16.1222
14	9:50	-2.79	17	-16.7158	-19.50576
16	9:52	-2.15	19	-18.6823	-20.83232
18	9:53	-0.766	20	-19.6656	-20.4316
20	9:54	-2.08	21	-20.6489	-22.72888
22	9:55	6.73	22	-21.6322	-14.90216
24	9:57	-0.455	24	-23.5987	-24.05372
26	9:58	-1.483	25	-24.582	-26.065
28	9:59	-1.734	26	-25.5653	-27.29928
30	10:01	-0.797	28	-27.5318	-28.32884
32	10:02	1.449	29	-28.5151	-27.06612
34	10:03	4.2	30	-29.4984	-25.2984
36	10:05	3.96	32	-31.465	-27.50496
38	10:06	2.4	33	-32.4482	-30.04824
40	10:07	2.28	34	-33.4315	-31.15152
42	10:09	6.45	36	-35.3981	-28.94808
44	10:11	9.83	38	-37.3646	-27.53464
46	10:12	10.54	39	-38.3479	-27.80792
48	10:14	7.51	41	-40.3145	-32.80448
50	10:15	6.15	42	-41.2978	-35.14776
52	10:19	44.5	46	-45.2309	-0.73088
base	10:23	49.5	50	-49.164	0.336

In case of profile loop measurements that cover a large area of Khlongthom saline hot spring including mangrove area and palm forest, the straight line survey was impossible, thus the UTM of every measurement points was measured for closure correction calculation by using Equation 2.4, and an example is show in Table 2.2:

$$SP_{ci} = SP_{ri} - \left(\frac{D}{N}\right) * n \quad\text{.....................................} (2.4)$$

where SP_{ri} is the self-potential value corrected from the reference correction, if the reference electrode positions were not changed SP_i was used for calculation, D is the drift, N is the total number of data point in the profile, n is the place of the data point in the profile.

Table 2.2 Example of closure correction calculation of self-potential data.

Point	UTM		Time	V1	V2	V	SP$_{corrected}$
	E	N	(hh:mm)	(mV)	(mV)	(mV)	(mV)
0	511978	873812	9:44	3.2	3.21	3.205	3.205
1	511979	873824	9:46	12.76	12.65	12.705	12.72844828
2	511976	873831	9:51	1.986	1.961	1.9735	2.020396552
3	511979	873845	9:56	16.46	16.34	16.4	16.47034483
4	511981	873856	10:00	14.68	14.23	14.455	14.5487931
5	511977	873884	10:05	21.4	21.4	21.4	21.51724138
6	511979	873905	10:08	28.2	28	28.1	28.24068966
7	511964	873906	10:13	29.8	30.1	29.95	30.11413793
8	511956	873890	10:19	26.8	26.9	26.85	27.03758621
9	511967	873888	10:22	13.87	13.71	13.79	14.00103448
10	511967	873877	10:26	11.26	11.05	11.155	11.38948276
11	511950	873876	10:30	11.49	11.34	11.415	11.67293103
12	511951	873862	10:34	8.68	8.9	8.79	9.07137931
13	511947	873848	10:44	4.27	4.29	4.28	4.584827586
14	511964	873844	10:46	10.01	10.76	10.385	10.71327586
15	511961	873827	10:53	3.7	4.61	4.155	4.506724138
16	511926	873734	12:03	-0.962	-0.9	-0.931	-0.368241379
17	511906	873735	12:12	-1.229	-1.494	-1.3615	-0.775293103
18	511927	873713	12:23	0.919	0.663	0.791	1.400655172
19	511910	873708	12:33	3.82	3.64	3.73	4.363103448
20	511934	873728	12:41	1.691	1.669	1.68	2.336551724
21	511978	873812	12:53	2.92	2.13	2.525	3.205

2) Processing a dataset of several profile

As mention previously, self-potential measurements were performed forming loops in the study area covered to build a self-potential map. This work composed of three loop profiles; all loops must be connected together in order to build maps of results by using Surfer Software. For correction steps, each profile must be corrected independently for reference correction if reference electrode points were changed. After that all profiles were joined together, with the first loop was choose as reference for the closure correction steps (Cabusson and Finizola, 2012). An example is show in Table 2.3. The steps of closure correction are:

- ➤ Correction of the first reference loop and closed profile.
- ➤ Connecting the next loop to the reference loop
  - 1) Choosing the next loop to be corrected.
  - 2) Shifting the self-potential data of connected points from the reference loop to the new loop and apply closure correction.
- ➤ Connecting the next loop to the data already corrected and performed the same steps than before.

Table 2.3 Example of closure correction calculation for several loops of self-potential data.

point	UTM		SPc loop 1 (mV)	Point	UTM		Average SP loop 3 (mV)	SP shift	SPcorrected loop 3 (mV)
	E	N			E	N			
0	511978	873812	3.205	0	512008	873731	10.38	8.20245	8.20245
1	511982	873782	-0.654931	1	512032	873727	-5.295	-7.4726	-6.5811
2	511964	873779	-0.8813621	2	512025	873709	-9.075	-11.253	-9.4696
3	511945	873776	0.4192069	3	512043	873723	-3.93	-6.1076	-3.4331
4	511988	873767	-1.5322241	4	512051	873731	-11.22	-13.398	-9.8317
5	511973	873759	-1.3926552	5	512040	873710	0.391	-1.7866	2.6708
6	511988	873750	-2.2000862	6	512035	873702	4.18	2.00245	7.35127
7	511996	873728	0.1394828	7	512022	873689	-7.23	-9.4076	-3.1673
8	511980	873729	-7.6234483	8	512038	873686	3.88	1.70245	8.83421
9	511949	873723	-1.8433793	9	512014	873691	-3.335	-5.5126	2.51068
10	511924	873729	-7.3793103	10	512007	873699	2.89	0.71245	9.62715
11	511911	873673	0.1372586	11	512087	873711	0.298	-1.8796	7.92662
12	511930	873690	5.7798276	12	512072	873696	-5.015	-7.1926	3.5051
13	511928	873683	11.916897	13	512062	873691	-8.865	-11.043	0.54657
14	511946	873693	-2.6575345	14	512073	873678	-0.251	-2.4286	10.052
15	511940	873709	-2.2494655	15	512092	873686	-2.56	-4.7376	8.63451
16	511977	873704	-1.5648966	16	512098	873696	-2.51	-4.6876	9.57598
17	511976	873684	7.9801724	17	512008	873731	-4.775	-6.9526	8.20245
18	511994	873686	11.542241						
19	512004	873710	2.1613793						
20	512008	873731	-2.1775517						
21	511992	873831	40.627931						
22	511978	873812	3.205						

Loop 3

Reference loop

Topographic effect

As discussed in the review of the literature several observations obtained that topography can affect the electrical self-potential. In general investigations showed that the self-potential is increasing in downhill direction. Therefore, in this work the effect of terrain was also checked to ensure that the self-potential anomalies caused only from the flow of water in subsurface. Topographic correction was applied after reference and closure corrections were finished.

2.4.5 Field Tests

Self-potential field tests were carried out at the Science courtyard of Prince of Songkla University, Hat-Yai District, Songkhla Province, Southern Thailand (Figure 2.10a). The aims of testing including the understanding of the conditions of environmental effect on self-potential measurements, developing tools for support the electrode, and designing the measurements for the good practices during field surveys. Details of the surveys under different conditions are as following.
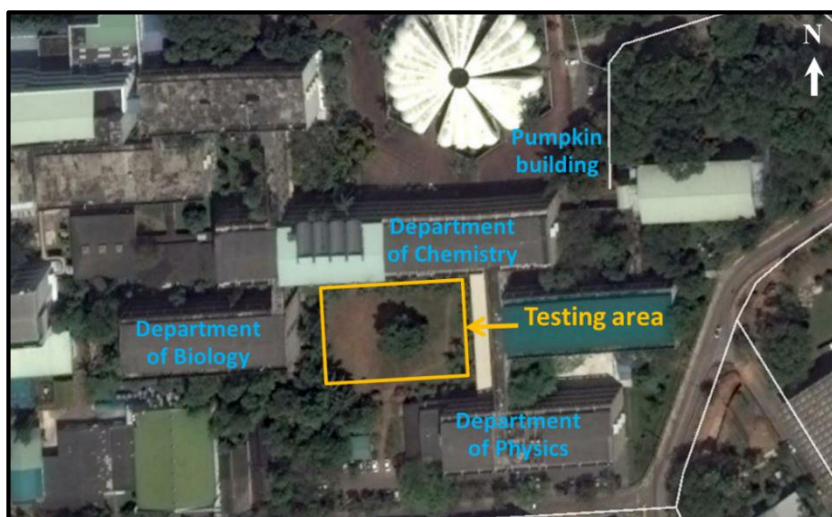
Figure 2.11 Location of the testing area, Science courtyard of Prince of Songkla University, Hat-Yai District, Songkhla Province, Southern Thailand. (Google Earth, 2017).

(1)   Testing efficiency of Pb/PbCl₂ non-polarizing electrodes

The Pb/PbCl2 non-polarizing electrodes were used in this work. Thus, before making the field survey in the study area, the efficiency of every electrode has to be tested, and the acquisition data of them have to be compared with each other for checking the accuracy. The reference electrode was put on the ground and placed onto a watered sponge (Figure 2.13 b); the moving electrode was moved along a survey line and measured at position 0.2, 0.4, 0.6, 0.8 and 1.0 m on a tape, with the last point on line profile measured before the moving electrode was changed to a new one.

Figure 2.12 (a) Testing area at Science courtyard of Prince of Songkla University, (b) efficiency tests of Pb/PbCl2 non-polarizing electrodes.

(2)   Testing of measuring time of moving electrode

The purpose of this test is to obtain the optimal time for measuring after putting the moving electrode on the ground surface at the measurement point. During the survey, moving electrode were removed and dropped at measurement point, as the moving electrode should have time for good contact with the ground; thus this work tried to study about that time. Here, the reference electrode was buried into the ground, the moving electrode was moved along line profile survey and varied the time for reading at each measurement point with 0, 30, 60 and 120 second after placement. The self-potential value was measured and compared with each other.

(3)   Testing of rainfall effect to self-potential measured:

The first field survey carried out at Klongtom saline hot spring had rainfall over the study area, which is not a controlled environment. Because of that, testing was performed to understand the effect of rainfall and what to do in the case of rainfall next time. This testing was set up in the morning of the day after heavy rainfall over night (Figure 2.14a), and immediately after rainfall stopped. Moreover, this testing also checked the base station during rain and compared data with a new base station prepared after rain stopped (Figure 2.14b).
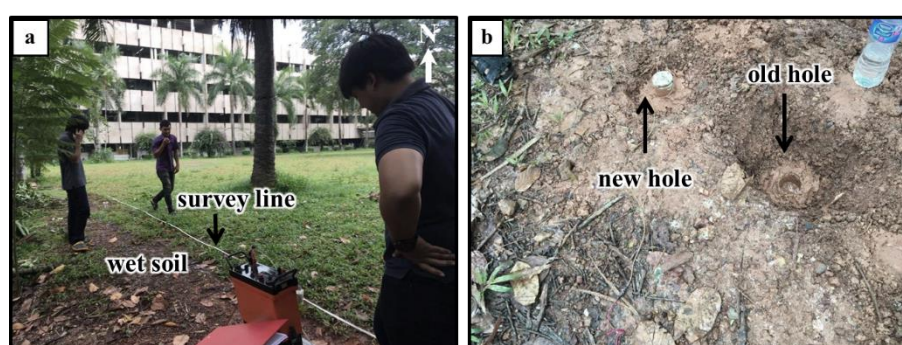
Figure 2.13 (a) Tests of measuring self-potential after rainfall over night, (b) Tests of measured self-potential immediately after stopping of rainfall; a new hole for buried reference electrode was prepare near the old one.

 (4) Testing of water add to sponge for sensor of moving electrode

For having a good contact between the ground and moving electrode a watered sponge was placed under the moving electrode. During surveys the sponge must be soaked all the time, so sometime it was necessary to add water to the sponge. Thus, with this test it was studied to optimize the water addition to the sponge. Normally, the sponge were prepared by soaking in water at least 30 min before measuring; in addition testing varied the water volume as 0.5, 1.0, 1.5, 2.0 and 2.5 cm^3. The obtained data were compared with the standard that also used soaked sponges, but did not add any water.

2.5 Ground temperature survey

A main physical property of the geothermal system is heat, thus a thermal method that directly measures the temperature of the ground was used in the study area. Soil or near surface temperature also was measured at the same point with self-potential measurement; both survey lines and loop surveys. The aim of this method was to understand the hot springs by using the temperature measurement in order to correlate

the data with self-potential method. In this work type k thermocouple which has an accuracy of 0.1°C and capable range of -50.0 °C to +1,300.0 °C was used. The thermocouple was applies as shown in Figure 2.13a. The steps for measuring the ground temperature at each point are as following:

- Using a steel electrode to make a hole at a depth of 30±5 cm.
- Putting type K thermocouple probe into the hole.
- Closing the hole and waiting of about 2-3 minutes; then recording the temperature reading.
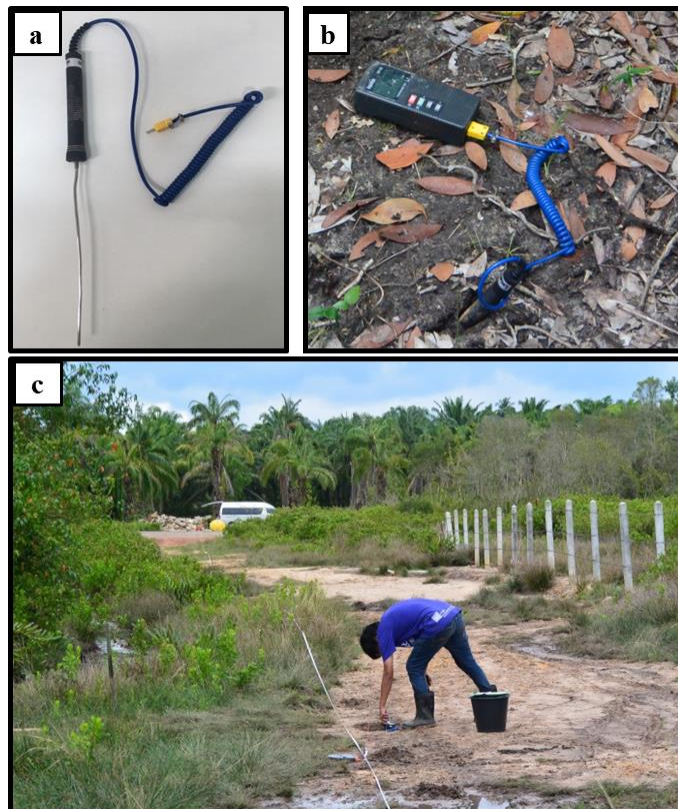
Figure 2.14 (a) Type K thermocouple, (b) Ground temperature measurement set-up and (c) Ground temperature measurement along line survey.

2.6 Vertical electrical sounding survey

Self-potential method is the main method of this work, which can be applied for indicated the location of fluid flow and possible faults in the subsurface of the study area, but it cannot determine geological layers and structures at depth. For improving the interpretation of the subsurface it was necessary to determine the geological layers and structures. The vertical resistivity sounding (VES) can indicate that, thus VES was chosen for this work. Schlumberger array (Figure 2.16) was used in this work.

$$k = [\frac{\left(\frac{AB}{2}\right)^2 - \left(\frac{MN}{2}\right)^2}{2\left(\frac{MN}{2}\right)}]\pi$$
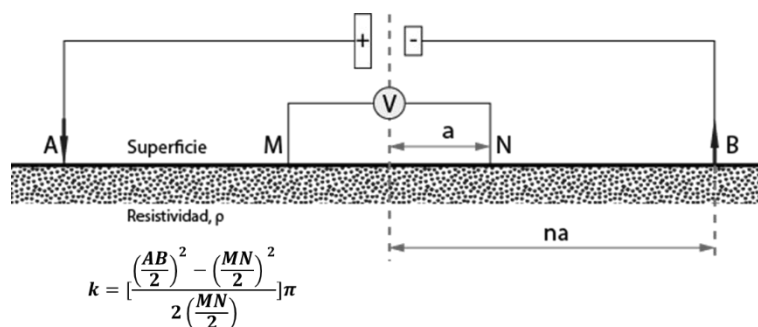
Figure 2.15 Schlumberger array and geometric factor (*K*), with A and B is the current electrode pair, and M and N is potential electrode pair (www.ocsa-geofisica.com/tomografia-electrica.html).

2.6.1 Field Equipment

VES survey requires four steel electrodes put into the ground; two of them for inducing current from a battery source to the ground and two for measuring voltage difference of the respond signal. All electrodes were connected with resistivity meter (Terrameter SAS 1000) by cables; two long cables for current electrodes and two short cables for potential electrodes. The distance from center point was fixed by tape, and also recorded was the UTM of every center line location and the direction of line.

Figure 2.16 Basic equipment for VES measurement, Terrameter SAS 1000 connected by cables to steel electrodes.

2.6.2 Design of VES survey and measuring procedure

The aim of VES survey of this work is determining the geological structures of shallow subsurface. Therefore, VES surveys were designed to cover the same or a larger area of the saline hot spring than the self-potential survey. The VES survey lines were planed

after obtaining data of self-potential anomaly. Positive and negative self-potential anomalies were used for placing the center point of VES lines. Due to the objective of understanding shallow subsurface the AB/2 length was focused at around 100 m; the total length of lines was about 100-240 m. Some lines were slightly shorter due to roads, construction, outcrops of sandstone, and muddy areas.

For measured the resistance value, every measuring points were measured at least two times for obtaining a satisfactory value. Measurement points or electrode spacing of each line were based on following table (Table 2.4), but some for lines the position of some measurement points were changed depending on surface conditions of the area.

Table 2.4 Electrode spacing AB/2 and MN/2 for vertical electrical sounding including geometry factor.

Point	AB/2 (m)	MN/2 (m)	K-Factor
1	1.3	0.5	4.5
2	1.6	0.5	7.3
3	2	0.5	11.8
4	2.5	0.5	18.8
5	3.2	0.5	31.4
6	4	0.5	49.5
7	5	0.5	77.8
8	6.5	0.5	131.9
9	8	0.5	200.3
10	10	0.5	313.4
11	10	2	75.4
12	13	2	129.6
13	16	2	197.9
14	20	2	311.0
15	25	2	487.7
16	32	2	801.1
17	32	5	313.8
18	40	5	494.8
19	50	5	777.5
20	65	5	1,319
21	80	5	2,003
22	100	5	3,134
23	100	10	1,555
24	130	10	2,639

2.6.3 VES data processing

Data obtained from VES surveys are resistivity values (R) used for calculating the apparent resistivity (ρ_a) by multiplication of the resistivity value with the geometric factor (K) of the array (Equation 2.7). Figure 2.18 shows the graph of the relationship between apparent resistivity values with AB/2 in a log-log scale. This work used IPI2win (2008) inversion software for data processing,

$$\rho_a = kR \dots\dots\dots\dots\dots\dots\dots\dots\dots\dots (2.7)$$

Where in case of Schlumberger array k is

$$k = [\frac{(AB/2)^2-(MN/2)^2}{2(\frac{MN}{2})}]\pi \dots\dots\dots\dots\dots (2.8)$$
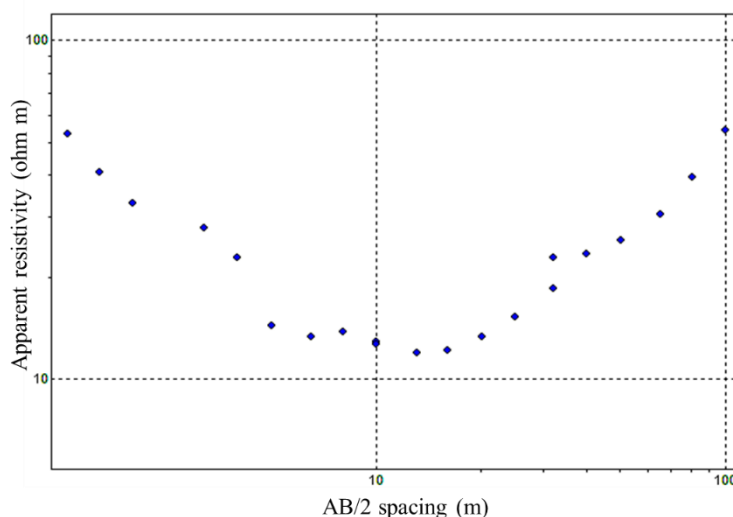
Figure 2.17 Plot between apparent resistivity values (ohm·m) and AB/2 (m) in log-log scale graph (IPI2win, 2008).

After data input the apparent resistivity versus AB/2 into IPI2WIN the program analyzed the number of layers in subsurface, the apparent resistivity and the thickness of subsurface layers by inversion (Figure 2.19, 2.20).
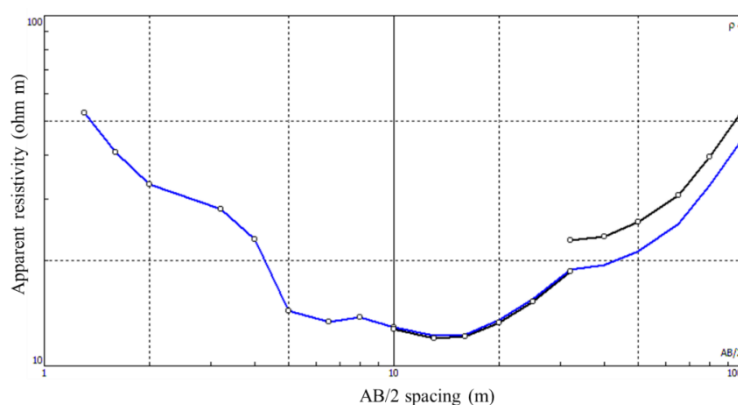
Figure 2.18 Blue curves shows smooth curve that IPI2WIN calculated from input apparent resistivity data (IPIWIN, 2008).
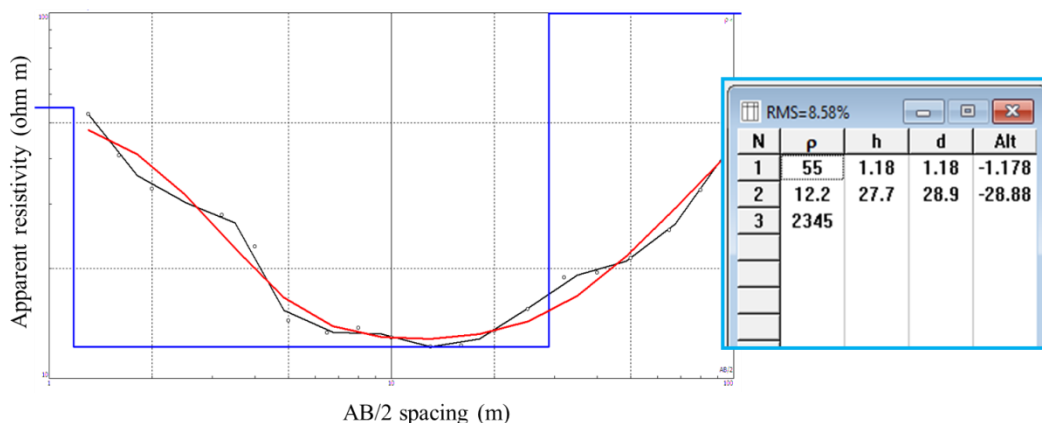
Figure 2.19 Data were analyzed using calculated smooth curve (red curve) to obtained ρ_a, thickness and depth that shows in insert table, black curve present input data and blue line is geoelectrical model of layer (IPIwin, 2008).

2.6.4 Inversion of apparent resistivity data into geoelectrical model

As demonstrates in part of VES data processing data input into the inversion program IPI2win software was used to create a geoelectrical model. This part shows that the inversion can be obtained from the data processing. The case shown in Figure 2.21 there is only one layer with one resistivity value; in this case the inversion of data represent a straight line with the resistivity and the depth of that one layer is infinite.
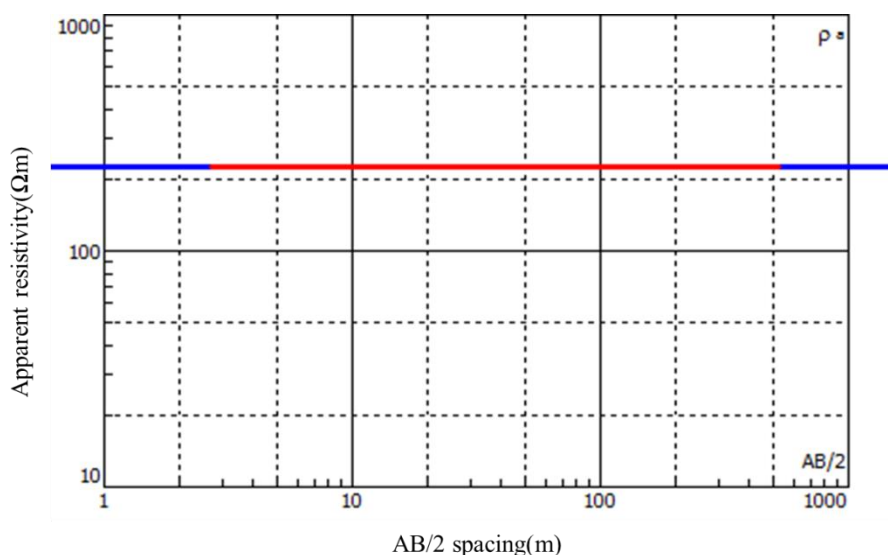
Figure 2.20 Inversion cases of one layer with one resistivity value.

In case of two layers or more with a difference in the apparent resistivity values, the curve calculated from data will not be a straight line as shown in Figure 2.21. In that case the geoelectrical model has two layers.
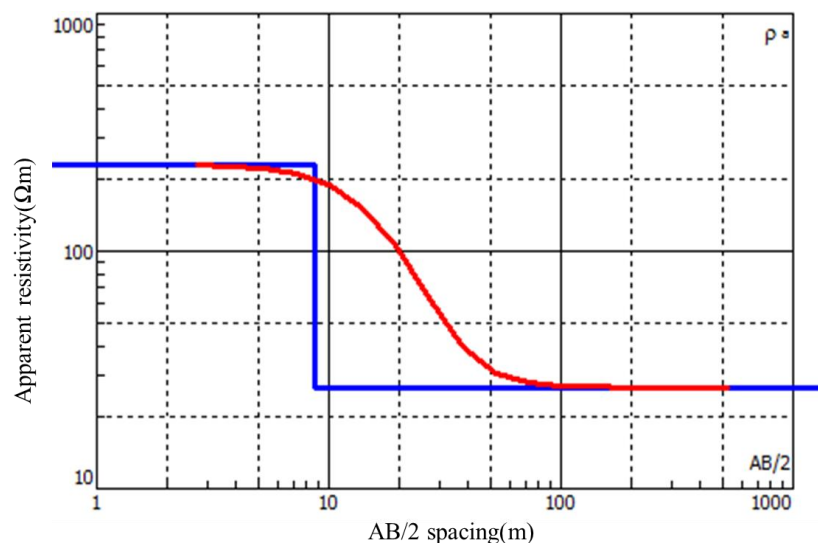
Figure 2.21 Inversion of two layers with apparent resistivity values.

In case of three layers shown in Figure 2.23, the geoelectrical model from the inversion gives three layers. The first one has a higher apparent resistivity then the second layer and the third layer; the second layer has a lower apparent resistivity then other, and the apparent resistivity of this layer will not go down to the true value because of the higher apparent resistivity of the third layer.
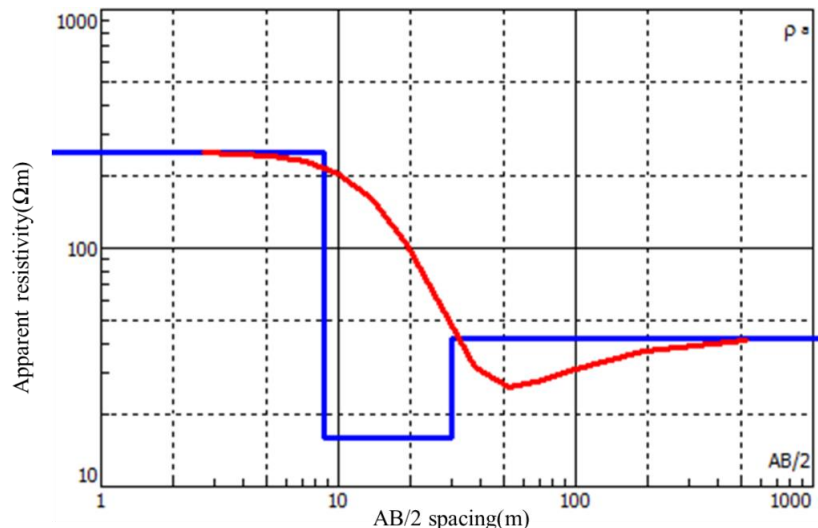
Figure

Figure 2.22 Inversion cases of three layers with apparent resistivity values.

2.7 Electrical resistivity tomography

The electrical resistivity tomography (ERT) is method which used to image the distribution of electrical resistivity. The resistivity data acquisition from field work are filtered on the basis of quality criterions, and after that was inverted by using RES2DINV software (Loke and Barker, 1996).The electrical resistivity results should be compared with other geophysical techniques for estimated to geothermal system. In this work ERT data from previous work was used.

2.8 Work flow

Self-potential is the main methodology for locating and estimating patterns of fluid flow at Khlongthom saline hot spring. For a better understanding of the hot spring system self-potential data can be combined with resistivity and ground temperature measurements, which are used for co-interpretation. Figure 2.23 indicates a work flow of this study. After finishing the step of literature review associated with this research, the planning of the survey design has been done. First, field testing of self-potential measurements in several environmental conditions were conducted as Prince of Songkla University. Then line measurements and loop measurements as Khlongthom saline hot spring were done, respectively.
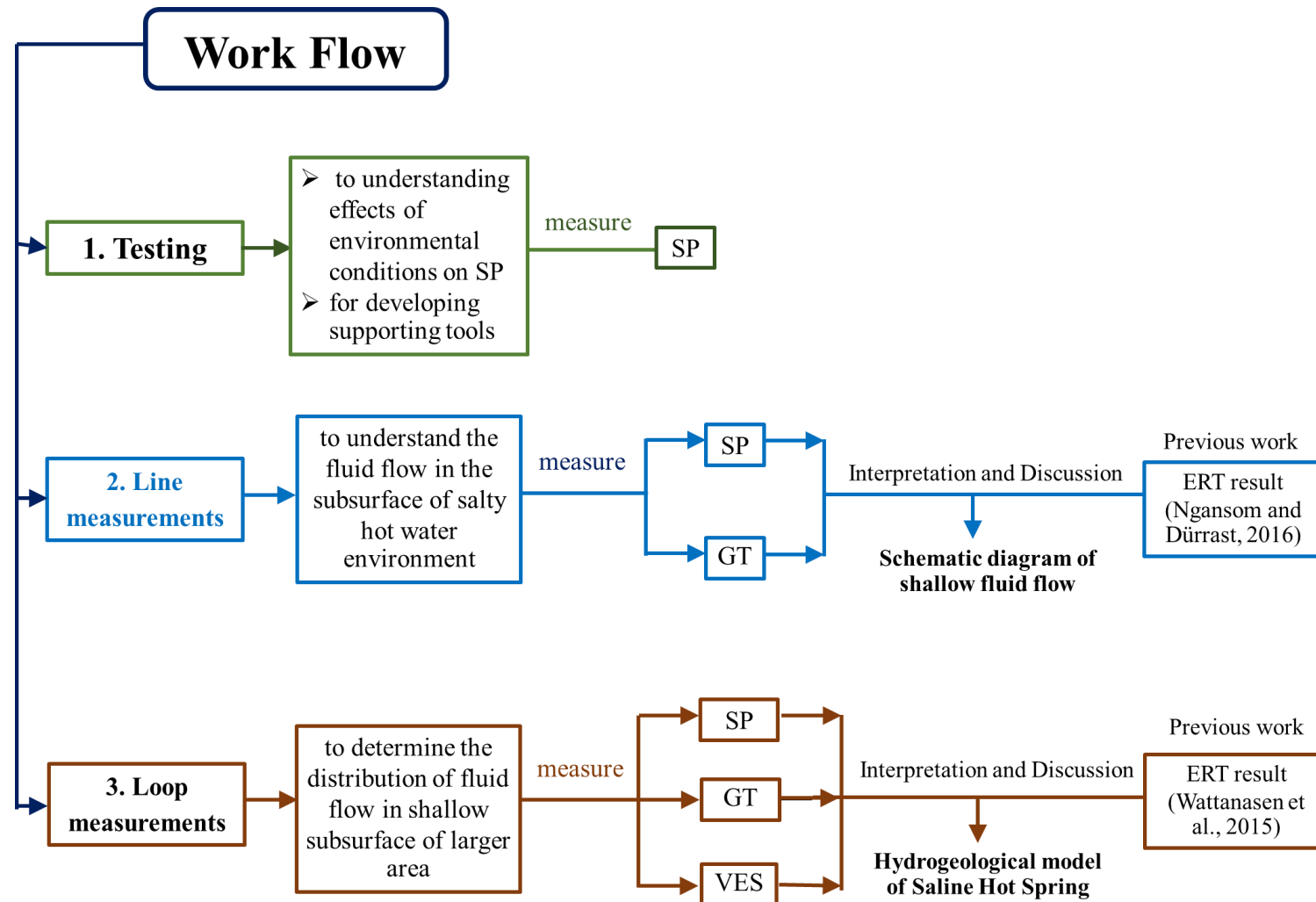
Figure 2.23 Work flow of this study consists of three main parts. First step is field test of self-potential measurements, second is line measurements in the study area, and final step are loop measurements in the study area.

CHAPTER 3

RESULTS

This chapter presents the results and detailed description of geological and geophysical surveys including self-potential measurements, ground surface temperature measurements, and vertical electrical sounding at the Khlongthom saline hot spring in Krabi province. Additionally, results of self-potential testing performed at Science courtyard of Prince of Songkla University are also shown in the first part of this chapter, and then the results of surveys in saline hot spring are following.

3.1 Testing Results

Self-potential field tests were performed at the Faculty of Science courtyard of Prince of Songkla University. The results obtained from each testing are as following.

(1) Result of testing efficiency of Pb/PbCl$_2$ non-polarizing electrodes

The efficiency and accuracy of new Pb/PbCl2 non-polarizing electrodes were tested. All of electrodes were marked by numbers 1 to 6; for this testing electrode number 1 was used as reference electrode and the others were used for moving electrode. There are five short profile lines of self-potential from five moving electrode measured the same location. Acquisition data were plotted with the distance along survey line shown in Figure 3.1. The self-potential measured by different moving electrodes along the same line showed a difference ranging from 0.1 mV to 1.0 mV, and all profiles exhibits the same trend. That shows that the SP value is independent from the electrode. Normally, the mean standard deviation in practical applications is around 2.5 mV, when measured in different time at the same point (Friborg, 1996). Therefore, the values measured from this testing are acceptable when comparing all electrodes with each other.
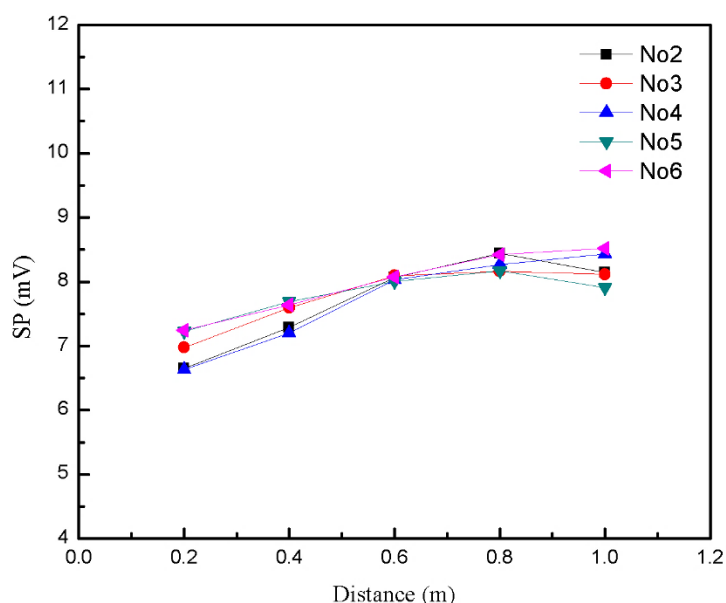
Figure 3.1 Self-potential profile of different moving electrodes along short survey line, Pb/PbCl2 non-polarizing electrodes number 2 to 5 were used for moving electrodes, and electrode number 1 was used for reference electrode.

(2)   Result of testing of measuring time of moving electrode

For checking the suitable time or the optimization time of SP measurements after putting moving electrode on the ground at each measurement point, the self-potential was measured by varying the time reading each measurement points with 0, 30, 60, and 120 seconds.

The self-potential profiles shown in Figure 3.2 presents the values at different time for reading each measurement points; difference are ranging from 0.5 mV to 5 mV, but all profiles exhibit the same trend. The obtained data were compared with published results. Friborg (1996) reported that for normal conditions the first and last reading at each point really seldom differentiate more than 0.5 mV if the electrode was placed in the ground for several minutes, but a second reading could differ by a few millivolts. Friborg (1996) also suggested that reading the data should be always taken as soon as the moving electrodes had been placed to the ground, as it was assumed that a stabilization occurred in a similar character at all points. Waiting for the reading stabilization at all measurement points is consuming more time. Data errors should be reduced by several readings taken at each point, at least two stacking were always recorded if the differences are not more than 5 mV, and four stacking if the difference is more than 10 mV.
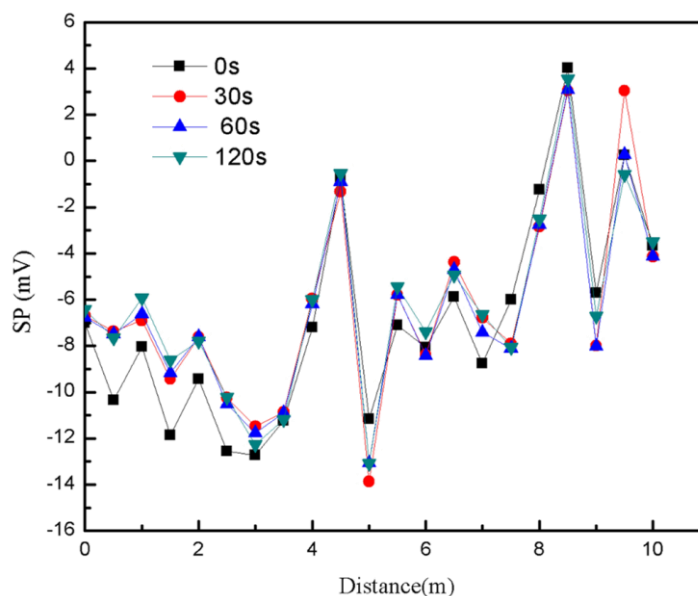
Figure 3.2 Self-potential profiles of differenced time for reading at each measurement point; time varies with 0, 30, 60 and 120 seconds.

(3)   Result of testing rainfall effect on self-potential data

This work also measured the self-potential under uncontrolled conditions of the environment, such as rainfall during the survey. Data measured after heavy rain overnight were compared with results measured under normal conditions. Generally, it is well known that rain is the one of the limitations of self-potential method, but this work aimed to understand the rain effect for good practice in surveying.

Figure 3.3 shows the profiles of self-potentials at two different conditions; firstly normal conditions, and secondly after rain overnight. The two profiles exhibit a different trend line and also present a higher variation when comparing the values between them for each point. Variations range between 0.5 mV and 12 mV. This testing confirms that the self-potential measurement should not be carried out after onset of heavy rain; however, for a short rain shower the survey does not necessary have to stop.
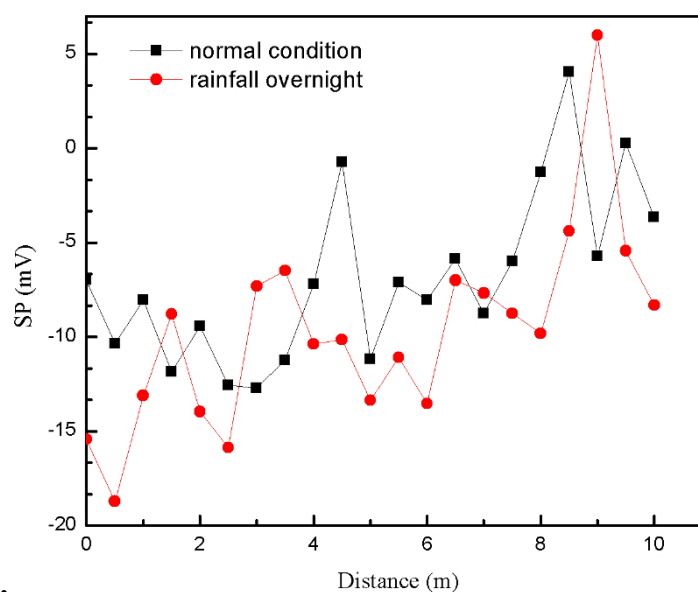
Figure 3.3 Self-potential profiles measured as normal conditions (black line), and measured after rainfall overnight (red line).

Moreover, this work also measured the self-potential after the stop of heavy rain. This was divided into three different conditions. The first one was measured earlier after rain overnight, the second one immediately measured after heavy rain stopped using the reference electrodes that was prepared before the rain started, and the other one was performed when finished measuring the first one but a new reference electrode was prepared close to the old one. The profile of these measured data is presented in Figure 3.4, with all profiles measured on the same day.

From Figure 3.4 it can be observed that all self-potential profiles exhibit the same trend. Considering the profile of self-potential data under rain fall overnight (black line) and the profile after heavy rain by using a new reference station (blue line), the variation of the values for each point is not more than 10 mV. However, the profile of self-potential immediately after heavy rain is showing a very high variation from both other profiles. The explanation of this occurrence is the soil condition; the wet soil when immediately measured after heavy rain can strongly affect SP data. Additionally, the reference electrode holes fill up with rain water due as they were prepared before the rain; this also can affect the self-potential. This testing can conclude that when it is required to measure self-potential after rain then there should be some waiting time before the survey starts and a new hole for the reference electrodes should be prepared.
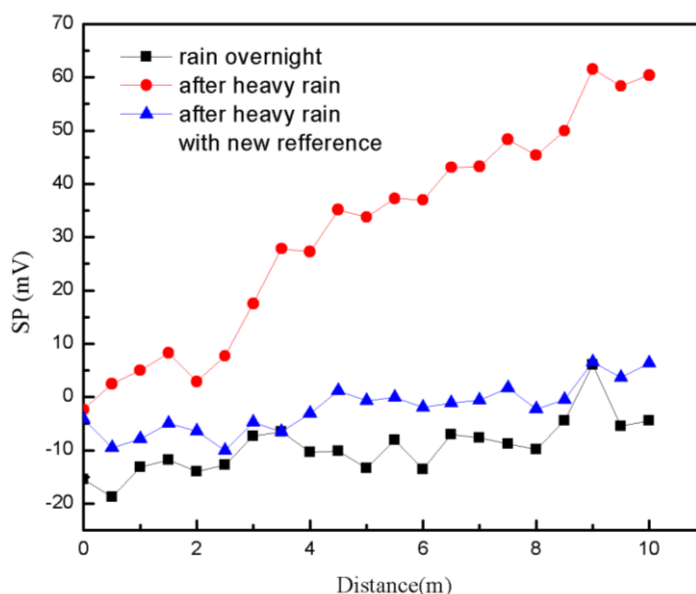
Figure 3.4 Self-potential profiles for three different conditions: black line measured after rainfall overnight, red line measured immediately after stop of heavy rain with a reference electrode used that was prepared before rain, and blue line is measured after the same heavy rain but using a new reference electrode which was prepared close to the old one.

(4)   Result of testing water optimization added to sponge for moving electrode

The aim of this test was to answer the question how much water should be added to sponges without having an impact self-potential data. This testing varied the water added from 0.5, 1.0, 1.5, 2.0, to 2.5 cc. The obtained data were compared with the standard that also used a soaked sponge, but did not add any water. The self-potential profiles are presented in Figure 3.5.
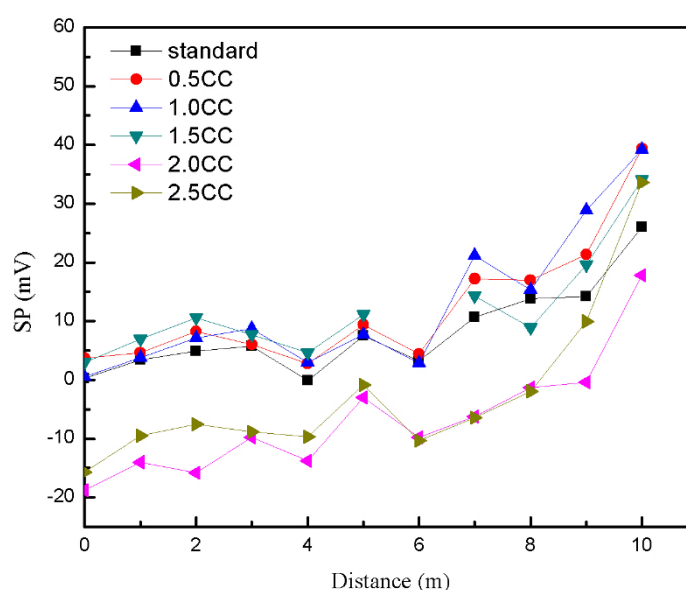
Figure 3.5 Self-potential profiles with varied volume of water added to the sponge, from 0.5, 1.0, 1.5, 2.0, to 2.5 cc, and standard.

All of self-potential profiles in Figure 3.5 show the same trend. Considering the variation of self-potential at each point it can be observed that lower water volumes added to the sponge, 0.5, 1.0 and 1.5 cc, are similar to the standard value. However, for 2.0 and 2.5 cc higher variations of self-potentials were measured when compared to the four previous profiles. From this result it can be assumed that in the surveys not more water should be added than 1.5 cc, thus avoiding variations of the self-potential values.

3.2   Regional Geology Khlongthom saline hot spring

From the geology surveys it was found that most of the hot springs are located on sandstone of the Triassic Sai Bon Formation (Figure 3.6a). The shallow subsurface of alluvial deposits consist of distribution of sand, medium to coarse grained, black marine clay, clay, and plant roots. Two sandstone outcrops (Figure 3.6b) with a height of about 15 meters were found in the area. In addition, calcium carbonate crusts occur around several natural hot springs with a thickness of the crusts of about 30-150 centimeters (Figure 3.6c). They are the results of precipitation from the hot spring water. In the eastern part of the saline hot spring is a salt marsh area, which is seasonally flooded with marine water.
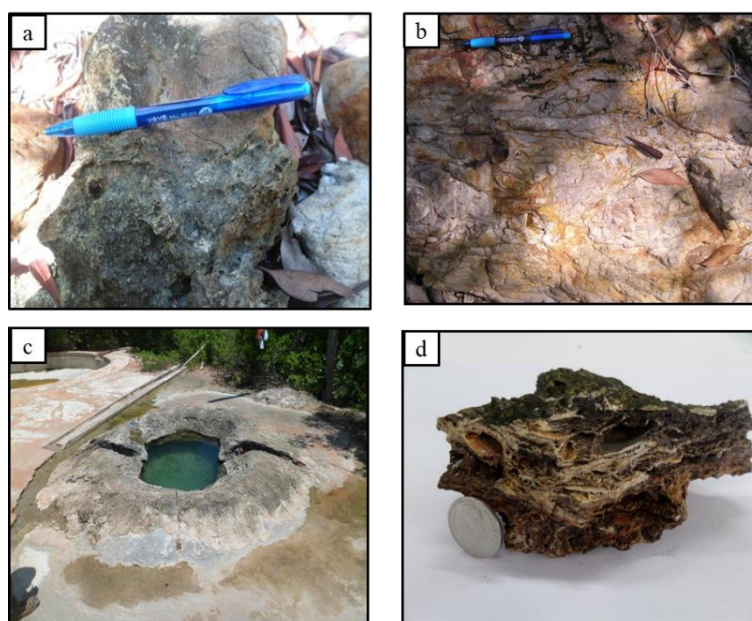
Figure 3.6 Geology in Khlongthom saline hot spring: (a) sandstone (Triassic Sai Bon Formation), (b) sandstone outcrops in a community forest, (c) Calcium carbonate crusts occur around natural hot springs, (d) Layer of carbonate crust with organic material.

3.3   SP Profile Lines

In order to understand the fluid flow in the subsurface of salty hot water environment, self-potential survey lines and ground temperature measurement were performed in the location of the eastern salt marsh area. Two survey lines parallel to 2D resistivity profiles from previous work (Ngansom and Dürrast, 2016) were measured, which are close to the natural hot spring KB4/10 located east of the sandstone outcrops (Figure 3.7)
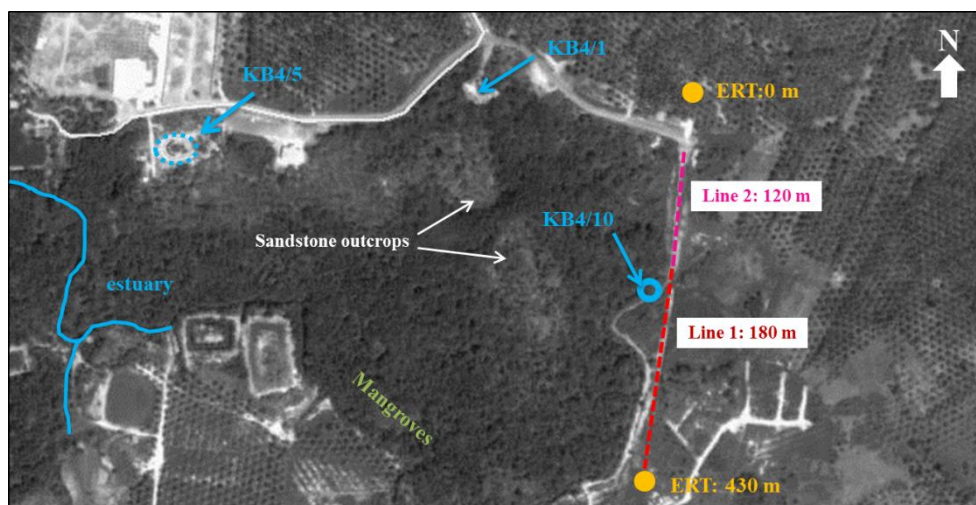
Figure 3.7 Location of self-potential measurement lines and ground temperature measurement lines at salt marsh area; also location of ERT line distance and local hot springs are shown.
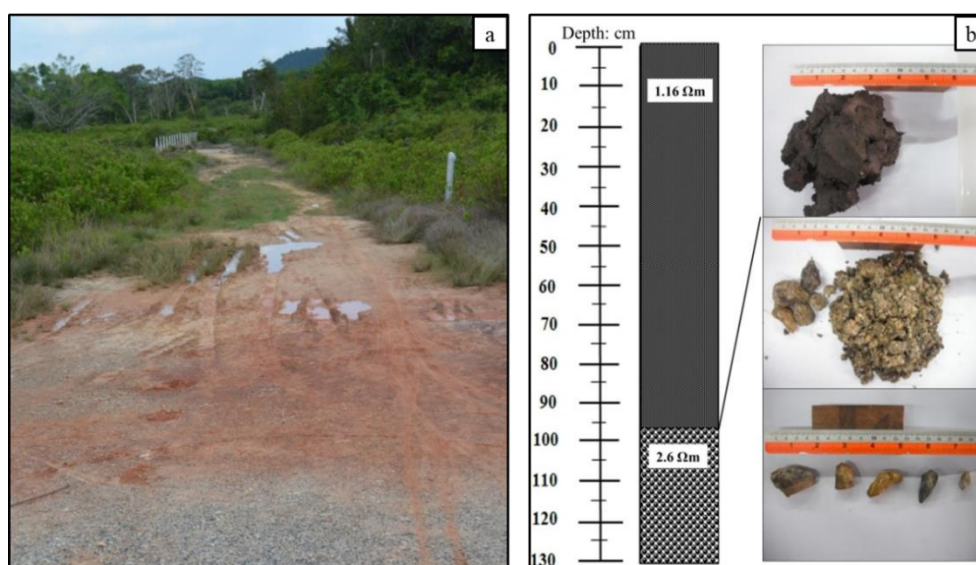
Figure 3.8 (a) Study area: view to the South: to the east salt marsh, in the west mangroves. (b) Soil profile and soil resistivity in the area; upper part: black clay, below: clayey sand with sandstone fragments.

3.3.1 Survey time and weather conditions

Survey lines of self-potential and ground temperature measurements in salt marsh area were carried out in early April; normally that month is summer in Thailand. But during the field survey there was slightly rainfall over the study area. Data from the Thai Meteorological Department (TMD) of Krabi in Figure 3.9a show that the amount of rainfall on the day of survey. The measurements were stopped because of the rain and continued after rainfall on the wet area (Figure 3.9b).
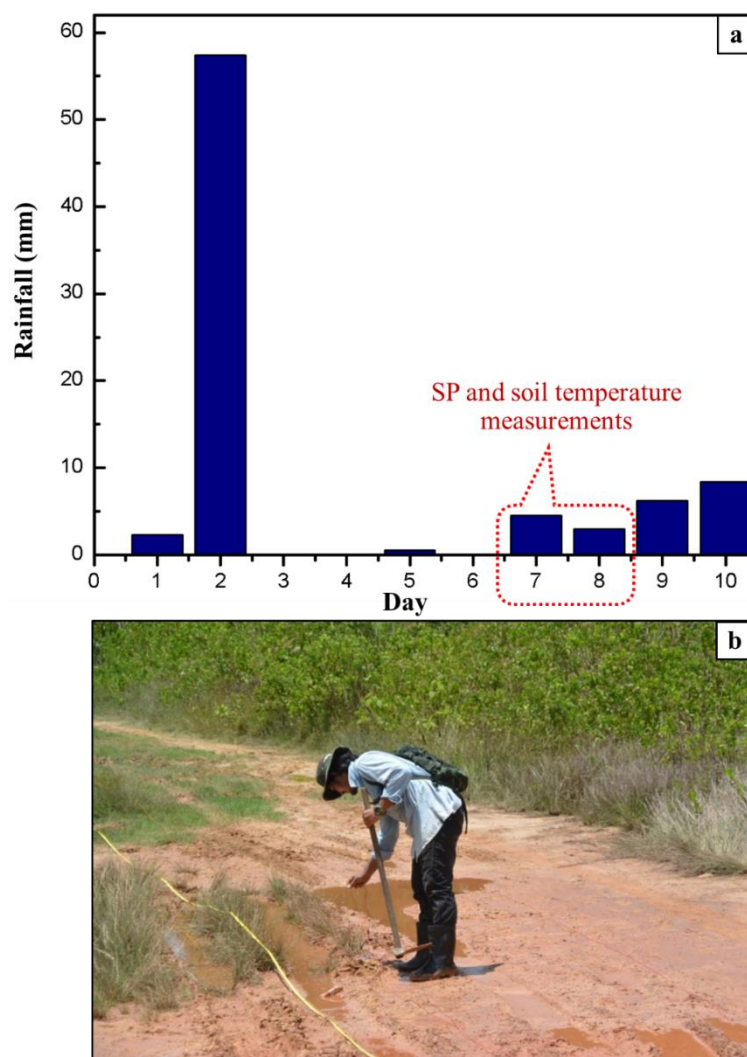
Figure 3.9 Rainfall over study area in April; (a) data of rainfall in early April from TMD Krabi, (b) survey after rainfall.

3.3.2   Result of self-potential surveys

Two self-potential profile line measurements were conducted in salt mash area along ERT profile line studied before. The total length of both self-potential profile lines is 300 m (line 1:180 m, line 2: 120 m). The measurements of line 1 started from UTM 0512459 E, 0873597 N and finished at UTM 0512445 E, 0873511 N, and the reference electrode located at UTM 0512472 E, 0873754 N. For line 2 the measurement started at UTM 0512482 E, 0873762 N and finished at UTM 0512449 E, 0873597 N, and the reference electrode located at UTM 0512475 E, 0873747 N (all WGS-84). Corrections were done as outlined in Chapter 2.
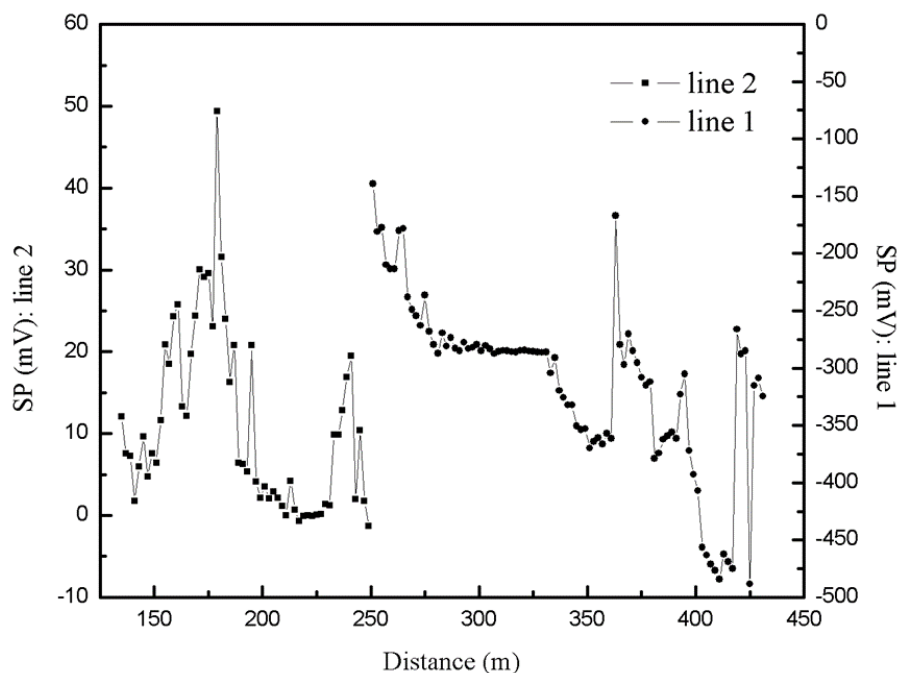
Figure 3.10 self-potential data from two survey lines along a rural way in the Khlongthom Saline Hot Spring area. Both lines were measured along the ERT line from previous work.

Figure 3.10 represents two self-potential profiles obtained from measurements at salt mash area; the self-potential profile line 1 (right) shows values ranging from -488 to -166 mV, and the profile line 2 shows self-potential values ranging from -1 to 49 mV. Both profile lines exhibit clear positive anomalies.

3.3.3   Result of ground temperature measurements
As describe in previous chapters geothermal systems such as hot springs are directly related with heat. Therefore ground temperature was measured along the same line of self-potential measurement points and obtained data were plotted as function of distance along survey line.

Figure 3.11 shows the profile of ground temperature measured at a depth of 30 cm along survey line. The profile shows that temperature data (black line) ranged from 28.5 °C to 32.8 °C, and the temperature average line (red line) exhibits a positive anomaly with a peak at around 220 m of distance on the survey line.
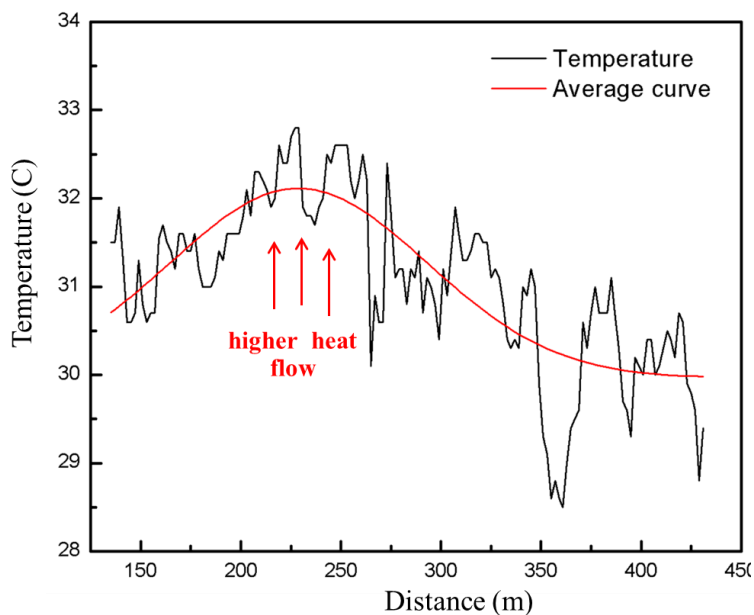
Figure 3.11 Temperature data (black line) along the main survey line of self-potential survey. Average curve of data (red line) exhibits a positive anomaly with a peak at around 220 m.

3.4 SP profile map

In order to determine the fluid flow in the subsurface of the larger saline hot spring area self-potential and ground temperature were measured at 162 measurement points as shown in Figure3.12.
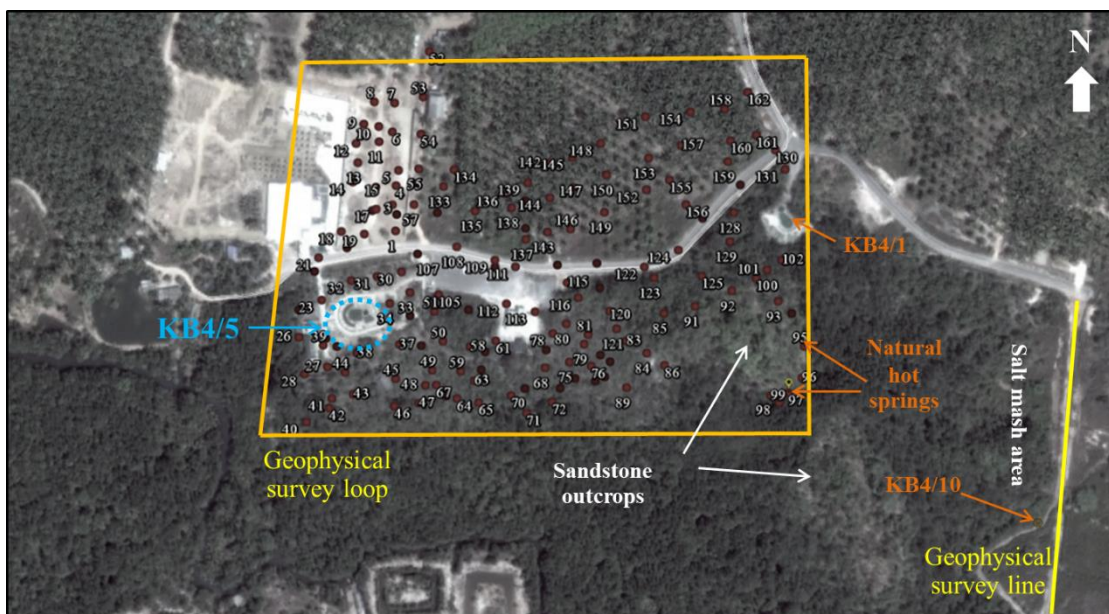
Figure 3.12 Location of profile loop survey (yellow rectangle square) and 162 measurement points (red point) in saline hot spring Khlongthom; KB4/1 and KB/5 are natural hot springs, which were developed as pools for tourism (Google Earth, 2017).

Figure 3.13 Six loops of self-potential measured in Khlongthom saline hot spring area and their measurement points (Google Earth, 2018).

3.4.1 Survey time and weather conditions

The survey was carried out in July, three months after there the SP lines. Loop profile measurement also required to observe the rain. Rain data from TMD Krabi are shown in Figure 3.14a, clearly indicating that there was no rain before and during the days of survey.
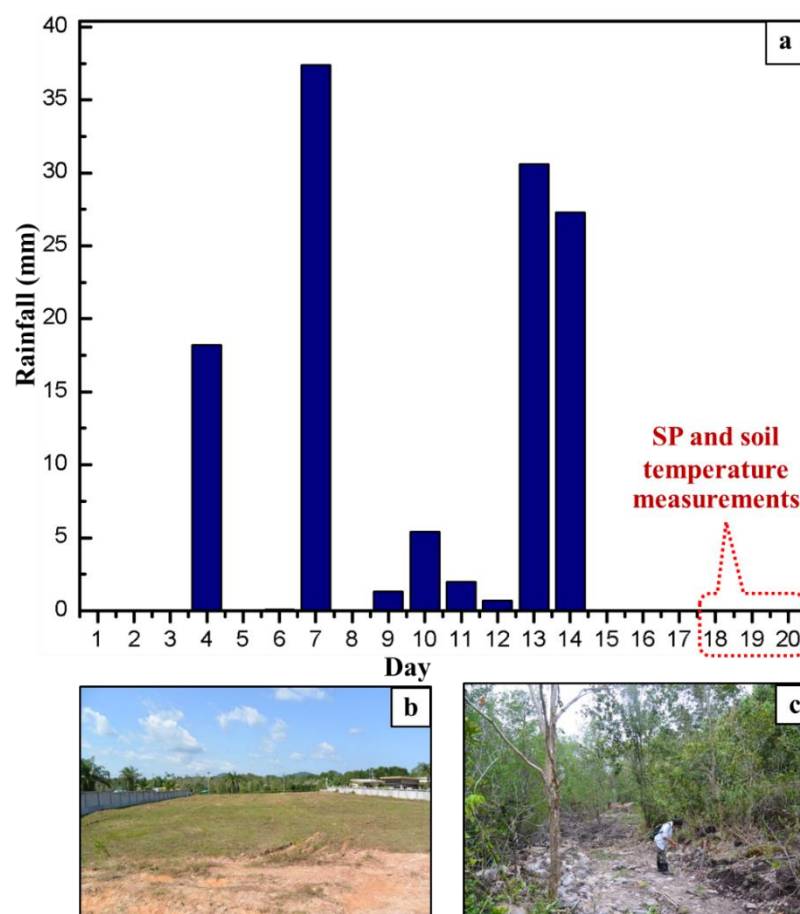
Figure 3.14 (a) Data of rainfall in early July from TMD Krabi, (b) and (c) showing some parts of the study area at that time.

3.4.2 Result of self-potential surveys

Six self-potential profile loops were measured for cover the area of the saline hot spring, thus star network strategy was chosen in order to approach the large mapping area. The first base station was used as a reference for all loops, established at UTM 0511980 E, 0873811 N. The second one is located at UTM 0512009 E, 0873731 N, and the third is located at the same location of first base station. A total of 162 self-potential data was obtained from measurements, corrected and then plotted for building a self-potential distribution map.
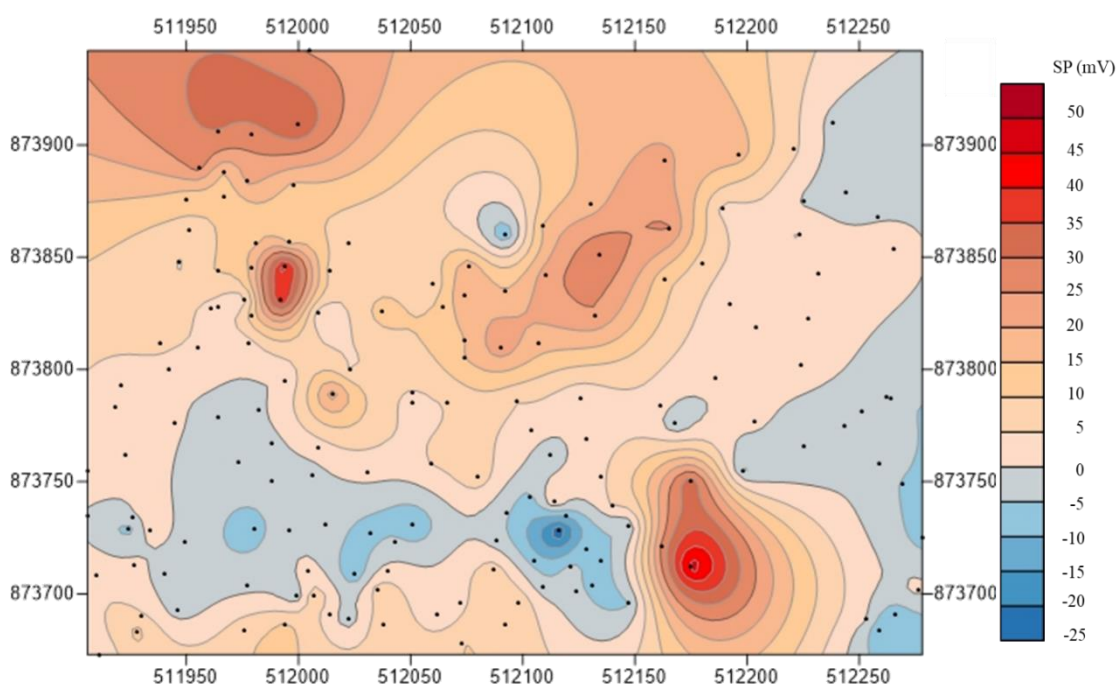
Figure 3.15 Results of self-potential surveys of the area, UTM (Zone 47, WGS-84).

Figure 3.15 shows the drift corrected self-potential data of the study area plotted and contoured. The map shows both positive and negative anomalies; the magnitude of self-potential values range from -25 to 50 mV. Negative anomalies indicated by blue were observed in the north-east, north-west, south-east, and two zones in the middle of the study area; one is at the southern part and another small one is in the northern part of study area. Almost all major negative anomalies were observed as manifestation of hot springs. For positive anomalies indicated by red in the map were observed in the north-west, middle part of northern area, south-east, and south-west.

For this work, the topographic effect on the self-potential data was checked. The data of self-potential values with elevation were plotted as shown in Figure 3.16, but the self-potential data do not significantly correlate with topography of the saline hot spring area (correlation coefficient, $R^2 = 0.159$). The poor correlation may be due to self-potential in study area is dominated by other source especially the salinity, thus resulting to lack of topographic effect. Thus topographic correction is not required for self-potential values of this area.
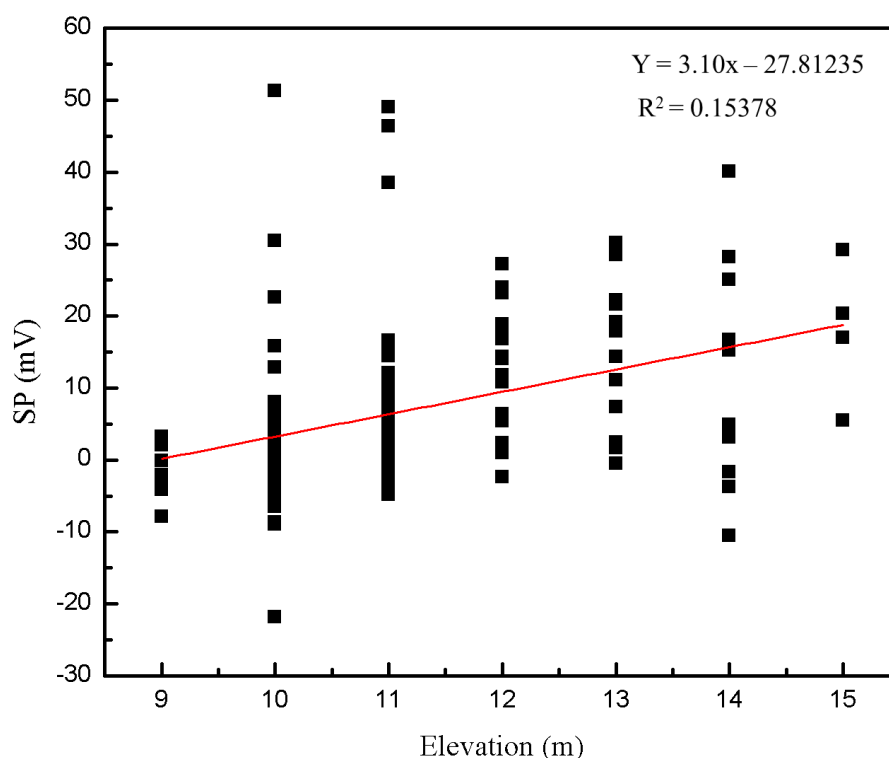
Figure 3.16 Correlation of self-potential values and elevations. The plot shows poor correlation, the elevations parameter probably has no influence on self-potential values.

3.4.3 Result of ground temperature measurements

The purpose of this ground temperature surveys was to understand the saline hot spring system by using shallow temperature measurements, measured at 30 cm depth. In order to provide a map of the ground temperature data values were measured at the same locations of the self-potential measurement points. Ground temperature values were plotted and contoured and shown in Figure 3.17.

Figure 3.17 shows the shallow ground temperature data plotted over the survey area. The temperature distribution map presents several thermal anomalies; the major anomalies are observed in the western part and eastern part of the saline hot spring. Additionally, the map shows that temperature values range from 28 °C to 35 °C, the highest ground temperature in the surveyed area is 35 °C, observed at UTM 0511964 E, 0873779 N.
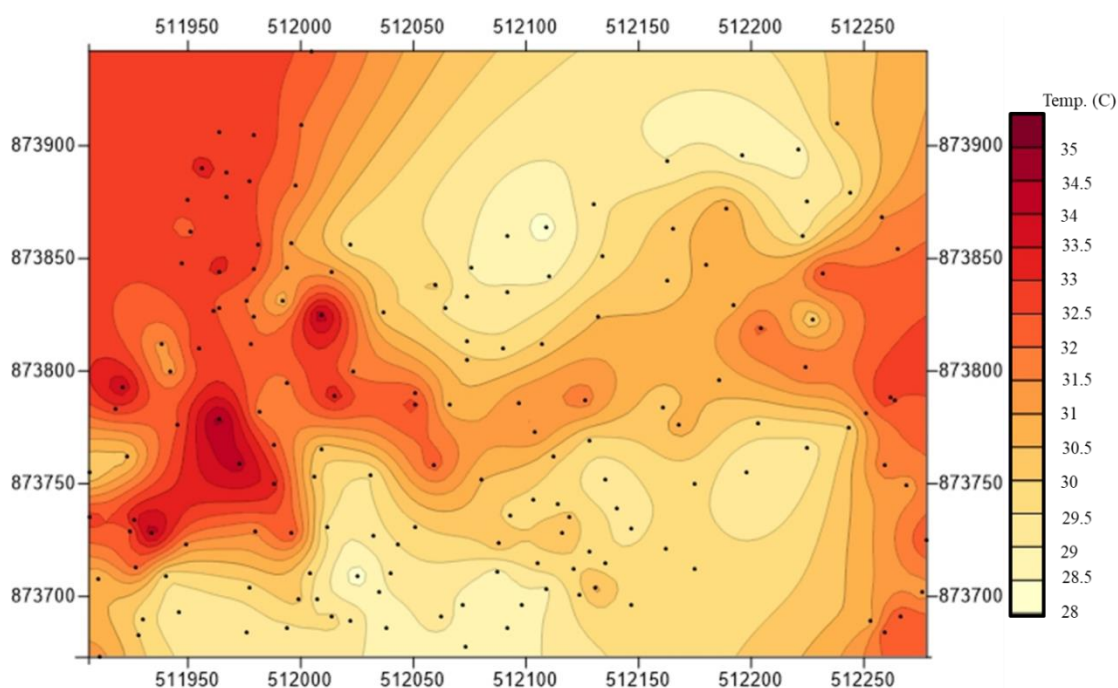
Figure 3.17 Ground temperature data at 30 cm depth plotted and contoured, UTM (Zone 47, WGS-84).

3.5 Result of vertical electrical sounding surveys
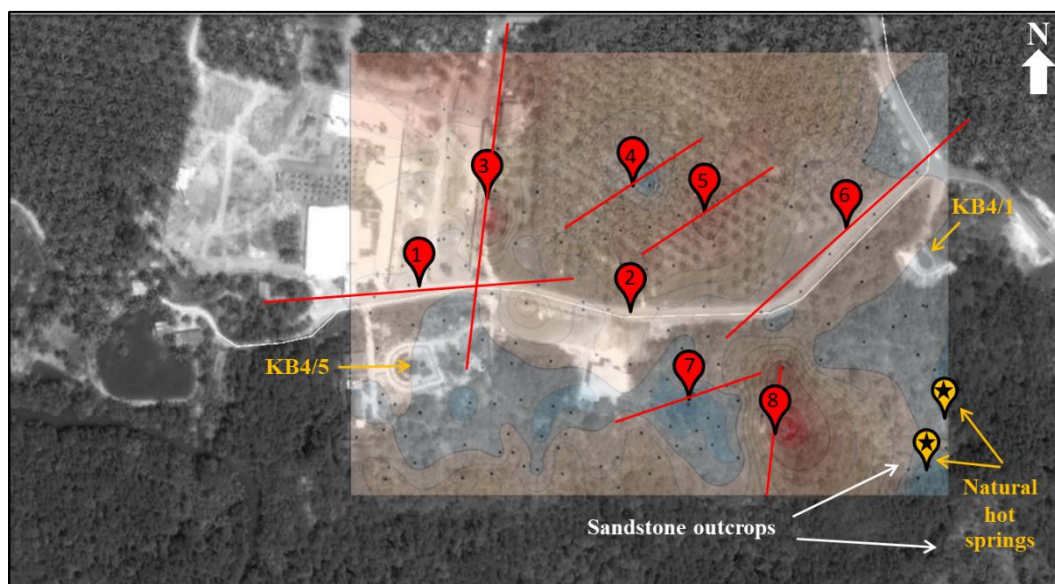
Figure 3.18 Locations of survey points VES 1 to VES 8; red line is 1-D resistivity survey line, KB4/1 and KB4/5 are the natural hot springs which were developed as pools for tourism, numbers in red point is number and center of each VES survey line (Google Earth, 20018).

Table 3.1 Center locations (UTM, Zone 47, WGS-84) and line direction of the VES measurements.

1-D VES (number)	Direction (N over E)	UTM East (m)	UTM North (m)
VES 1	N080E	0511951	0873798
VES 2	N275E	0512082	0873785
VES 3	N195E	0511994	0873852
VES 4	N240E	0512085	0873863
VES 5	N225E	0512129	0873846
VES 6	N215E	0512216	0873834
VES 7	N255E	0512119	0873732
VES 8	N185E	0512172	0873712

3.5.1 Vertical Electrical Sounding 1 (VES 1)

The survey point VES 1 is located at UTM 0511951 E, 0873798 N; the direction of line in azimuth is 240, and maximum AB/2 is 100 m. The resistivity values obtained from field surveys were calculated to apparent resistivity values in order to analyze the resistivity model by IPI2win inversion program.
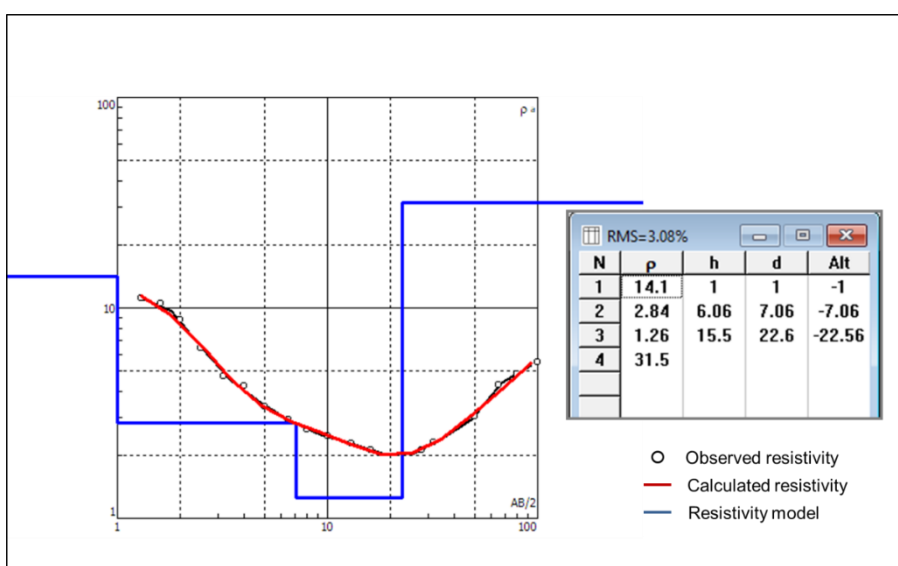
Figure 3.19 VES model of survey line VES1. Result of the analysis of IPI2WIN program. Apparent resistivity values versus AB/2 (left). Inversion results (right table) with N=layer, ρ= resistivity of layer (ohm-m), h=thickness of layer (m), d=depth below surface (m), RMS error is 3.08%.

Figure 3.19 shows that the VES model of survey line VES 1 is interpreted as a four-layer model. The first layer has a resistivity value of 14.1 ohm-m and 1 m of thickness. The second layer has a resistivity value of 2.84 ohm-m and 6.06 m of thickness. The third layer has a resistivity value of 1.26 ohm-m and 15.5 m of thickness. Finally, the forth layer has a resistivity value of 31.5 ohm-m and more than 22.6 m depth.

3.5.2 Vertical Electrical Sounding 2 (VES2)

The survey point VES 2 is located at UTM 0512082 E, 0873785 N; the direction of line in azimuth is 275, and maximum AB/2 is 50 m.
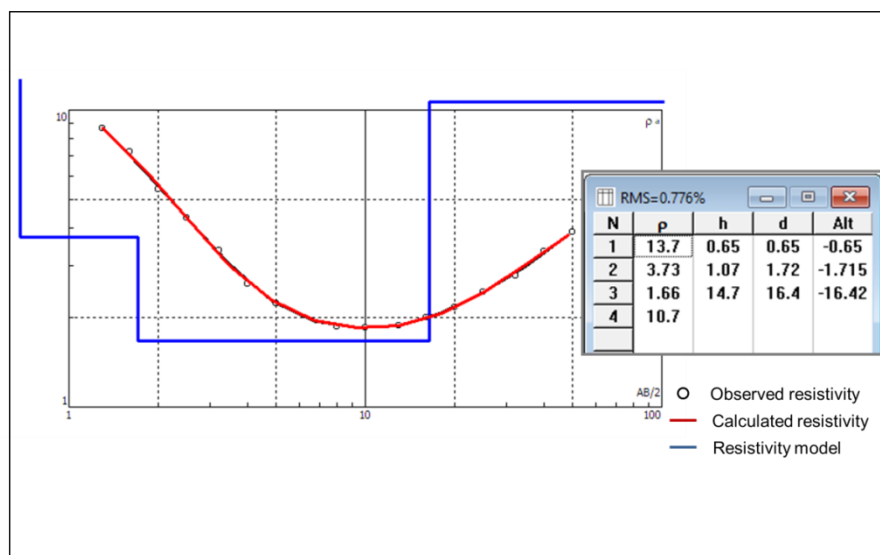
Figure 3.20 VES model of survey line VES2. Result of the analysis of IPI2WIN program. Apparent resistivity values versus AB/2 (left). Inversion results (right table) with N=layer, ρ= resistivity of layer (ohm-m), h=thickness of layer (m), d=depth below surface (m), RMS error is 0.776%.

Figure 3.20 shows that the VES model of survey line VES 2 is interpreted as a four-layer model. The first layer has a resistivity value of 13.7 ohm-m and 0.65 m of thickness. The second layer has a resistivity value of 3.73 ohm-m and 1.07 m of thickness. The third layer has a resistivity value of 1.66 ohm-m and 14.7 m of thickness. Finally, the forth layer has a resistivity value of 10.7 ohm-m and more than 16.4 m depth.

3.5.3 Vertical Electrical Sounding 3 (VES 3)

The survey point VES 3 is located at UTM 0511994 E, 0873852 N; the direction of line in azimuth is 195, and maximum AB/2 is 105 m.

Figure 3.21 shows that the VES model of survey line VES 3 is interpreted as a four-layer model. The first layer has a resistivity value of 108 ohm-m and 1.21 m of thickness. The second layer has a resistivity value of 16.8 ohm-m and 7.33 m of thickness. The third layer has a resistivity value of 1.27 ohm-m and 3.09 m of thickness. Finally, the forth layer has a resistivity value of 12.2 ohm-m and more than 11.6 m depth.
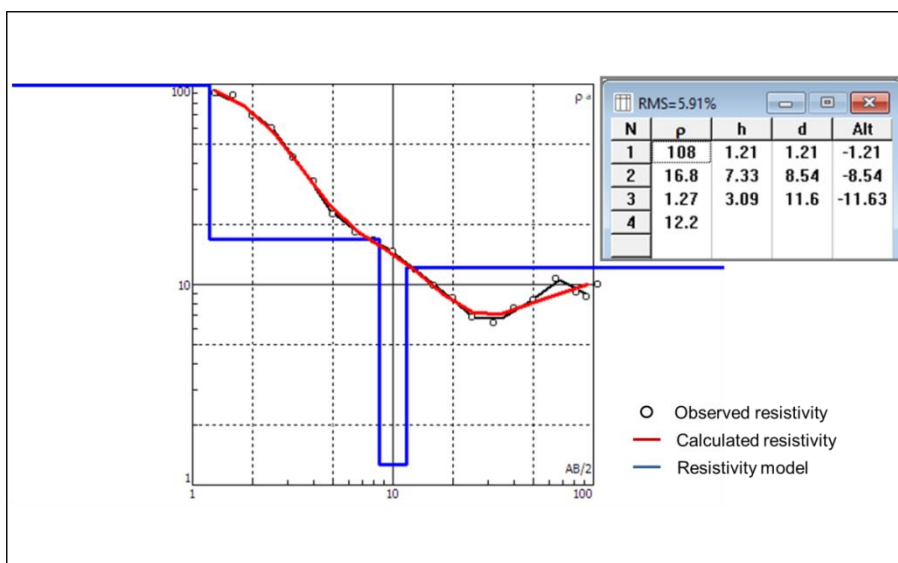
Figure 3.21 VES model of survey line VES3. Result of the analysis of IPI2WIN program. Apparent resistivity values versus AB/2 (left). Inversion results (right table) with N=layer, ρ= resistivity of layer (ohm-m), h=thickness of layer (m), d=depth below surface (m), RMS error is 5.91%.

3.5.4   Vertical Electrical Sounding 4 (VES 4)

The survey point VES 4 is located at UTM 0512085 E, 0873863 N; the direction of line in azimuth is 240, and maximum AB/2 is 50 m.
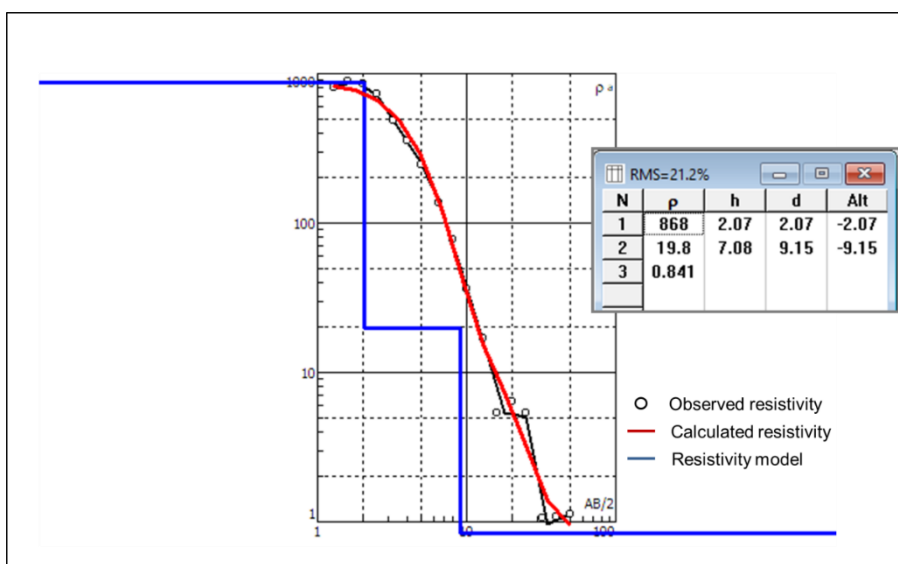
Figure 3.22 VES model of survey line VES4. Result of the analysis of IPI2WIN program. Apparent resistivity values versus AB/2 (left); Inversion results (right table) with N=layer, ρ= resistivity of layer (ohm-m), h=thickness of layer (m), d=depth below surface (m), RMS error is 21.2%.

Figure 3.22 shows the VES model of survey line VES 4 is interpreted as a three-layer model. The first layer has a resistivity value of 868 ohm-m and 2.07 m of thickness. The

second layer has a resistivity value of 19.8 ohm-m and 7.08 m of thickness. Finally, the third layer has a resistivity value of 0.841 ohm-m and more than 9.15 m depth.

3.5.5 Vertical Electrical Sounding 5 (VES 5)

The survey point VES 5 is located at UTM 0512129 E, 08737846 N; the direction of line in azimuth is 225, and maximum AB/2 is 50 m.
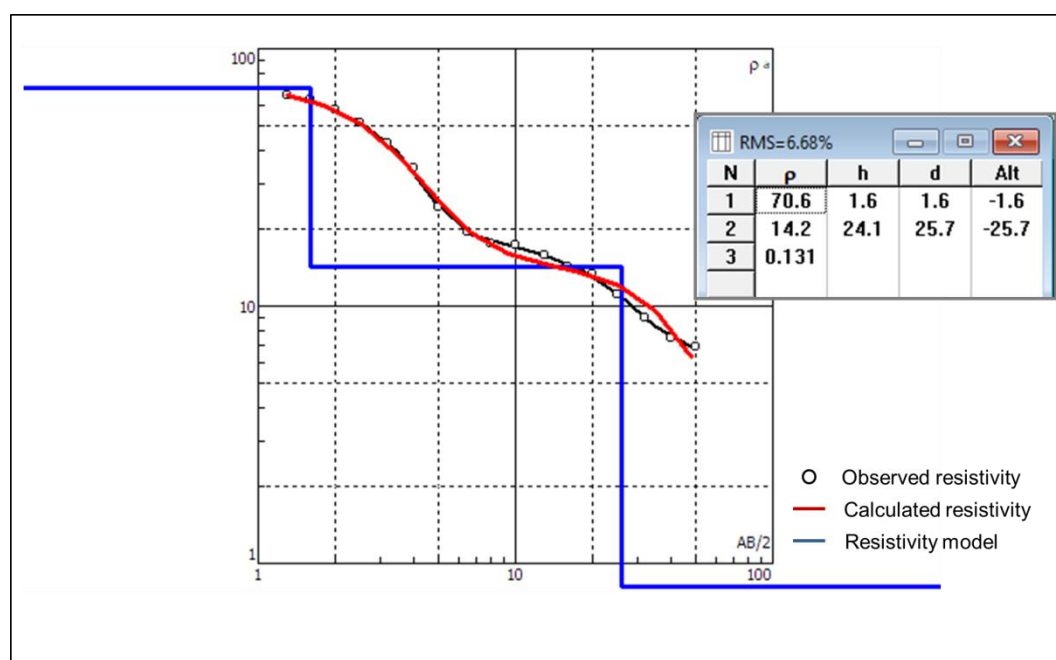
Figure 3.23 VES model of survey line VES5. Result of the analysis of IPI2WIN program. Apparent resistivity values versus AB/2 (left). Inversion results (right table) with N=layer, ρ= resistivity of layer (ohm-m), h=thickness of layer (m), d=depth below surface (m), RMS error is 6.68%.

Figure 3.23 shows the VES model of survey line VES 5 is interpreted as a three-layer model. The first layer has a resistivity value of 70.6 ohm-m and 1.6 m of thickness. The second layer has a resistivity value of 14.2 ohm-m and 24.1 m of thickness. Finally, the third layer has a resistivity value of 0.131 ohm-m and more than 25.7 m depth.

3.5.6 Vertical Electrical Sounding 6 (VES 6)

The survey point VES 6 is located at UTM 0512216 E, 0873834 N; the direction of line in azimuth is 215, and maximum AB/2 is 100 m.

Figure 3.24 shows the VES model of survey line VES 6 is interpreted as four layers model. The first layer has a resistivity value of 70.6 ohm-m and 0.699 m of thickness. The second layer has a resistivity value of 2.02 ohm-m and 4.39 m of thickness. The third layer has a resistivity value of 1.29 ohm-m and 9.45 m of thickness. Finally, the forth layer has a resistivity value of 20 ohm-m and more than 14.5 m depth.
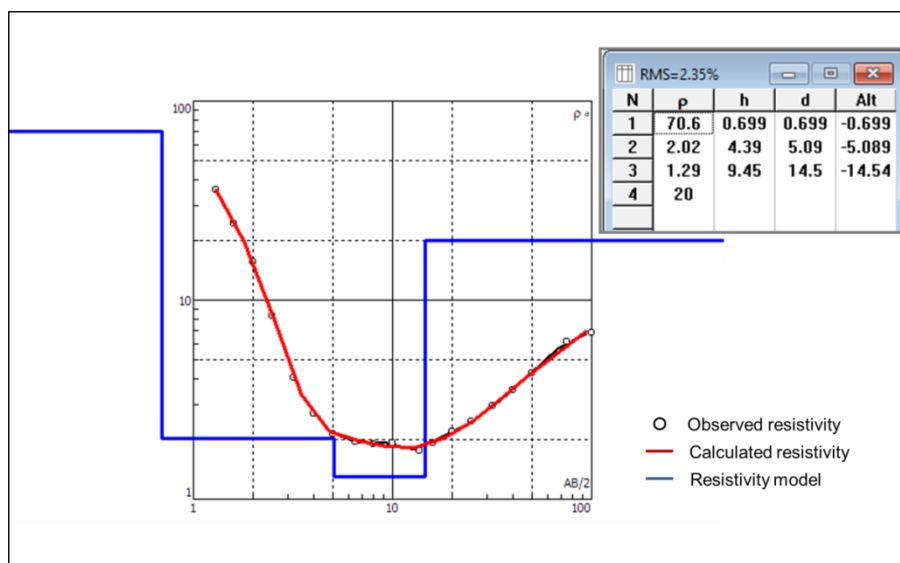
Figure 3.24 VES model of survey line VES6. Result of the analysis of IPI2WIN program. Apparent resistivity values versus AB/2 (left). Inversion results (right table) with N=layer, ρ= resistivity of layer (ohm-m), h=thickness of layer (m), d=depth below surface (m), RMS error is 2.35%.

3.5.7 Vertical Electrical Sounding 7 (VES 7)

The survey point VES 7 is located at UTM 0512119 E, 0873733 N, the direction of line in azimuth is 255, and maximum AB/2 is 50 m.
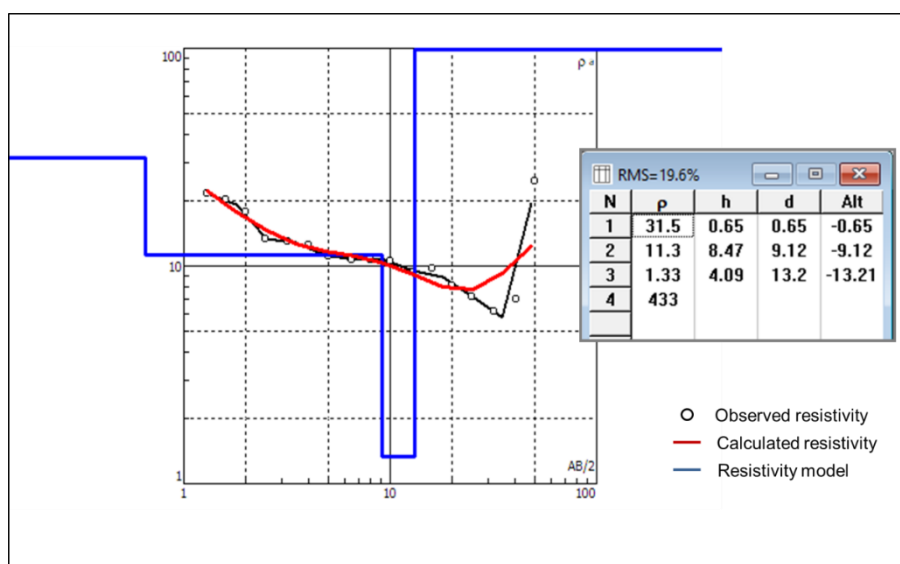
Figure 3.25 VES model of survey line VES7. Result of the analysis of IPI2WIN program. Apparent resistivity values versus AB/2 (left). Inversion results (right table) with N=layer, ρ= resistivity of layer (ohm-m), h=thickness of layer (m), d=depth below surface (m), RMS error is 19.6%.

Figure 3.25 shows the VES model of survey line VES 7 is interpreted as a four-layer model. The first layer has a resistivity value of 31.5 ohm-m and 0.65 m of thickness. The second layer has a resistivity value of 11.3 ohm-m and 8.47 m of thickness. The third layer has a resistivity value of 1.33 ohm-m and 4.09 m of thickness. Finally, the forth layer has a resistivity value of 433 ohm-m and more than 13.2 m depth.

3.5.8   Vertical Electrical Sounding 8 (VES 8)

The survey point VES 8 is located at UTM 0512172 E, 0873712 N; the direction of line in azimuth is 185, and maximum AB/2 is 40 m.
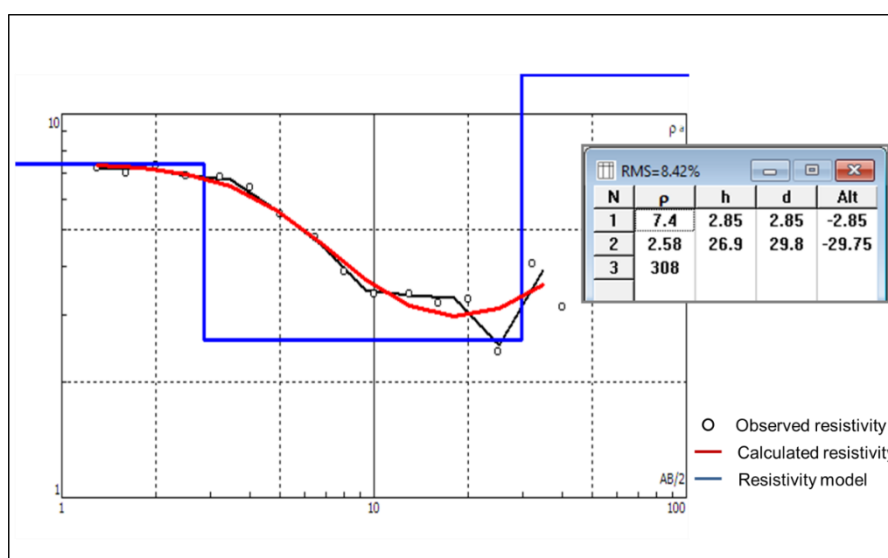
Figure 3.26 VES model of survey line VES8. Result of the analysis of IPI2WIN program. Apparent resistivity values versus AB/2 (left). Inversion results (right table) with N=layer, ρ= resistivity of layer (ohm-m), h=thickness of layer (m), d=depth below surface (m), RMS error is 8.42%.

Figure 3.26 shows the VES model of survey line VES 8 is interpreted as a three-layer model. The first layer has a resistivity value of 7.4 ohm-m and 2.85 m of thickness. The second layer has a resistivity value of 2.58 ohm-m and 26.9 m of thickness. Finally, the third layer has a resistivity value of 308 ohm-m and more than 29.8 m depth.

CHAPTER 4

DISCUSSION AND CONCLUSION

This chapter combines the results of all measurements carried out in this work with the results taken from previous works in the study area in order to make conclusion regarding the objective. In addition illustration and detailed discussion of the measurements are provided for a better understanding.

4.1 Profile lines analysis and interpretation

The self-potential surveys along the rural way in the east of the study area located close to a natural hot spring KB4/10 has been carried out in order to understand the fluid flow in the subsurface of this salty hot water environment. The soil temperature also measured as the same location to support the interpretation of the self-potential data. Another reason for choosing this section was because there is an ERT line that was measured earlier. In general, self-potential can indicate fluid flow in the subsurface but cannot determine geological structures of the subsurface. In some situations the interpretation of self-potential data is more complicated due to multiple source. Therefore, it is preferable combining self-potential result with ERT. Moreover drilling data at well 04 for also were used correlation as it confirmed the result of ERT. Integration of those results included self-potential profile, soil temperature profile, ERT distribution along survey lines, and drilling data as presented in Figure 4.1.

The patterns observed in both self-potential profile lines exhibit clear positive anomalies, however there are difference in the absolute self-potential values, with the first self-potential profile line shows values ranging from -488 to -166 mV, and the second profile line shows self-potential values ranging from -1 to 49 mV, this difference were caused by rain between the measurements of the two lines. During the measurement of the first line rain was falling; then the measurements were paused and started again after rain with the second line. So rain and moisture of the soil caused the changing of self-potential magnitudes.

Soil temperature measurements along the survey line ranged from 28.5 °C to 32.8 °C, and the trend line shows both positive and negative anomalies. From Figure 4.1 can be observed that the trend line exhibits a positive anomaly due to higher heat flow from the geothermal system at depth.

The ERT section that was measured before and parallel with the self-potential and temperature profiles is displayed in Figure 4.1. The bottom part of the ERT section shows high to very high resistivity values corresponding to dense sandstone with almost no water content confirmed by drilling which show here as well 04. Further above parts of the ERT section show very low resistivity values (blue color) corresponding to saline groundwater in clayey sand layers. Some shallow higher resistivity (red color) layers (e.g., 350-400 m) represent dryer sand. The very shallow part with black marine clay on top (see drilling data well 04 and soil profile in Figure 3.10) is not resolved by ERT.
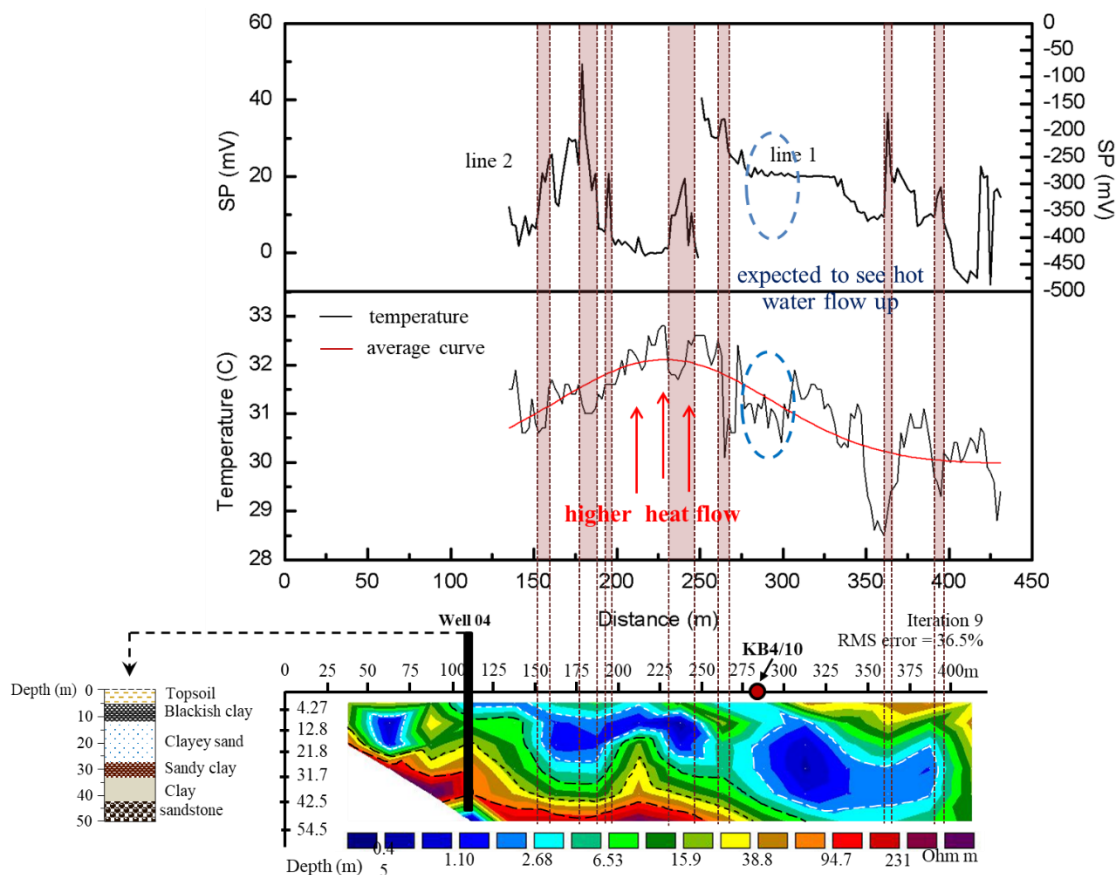
Figure 4.1 Self-potential data from two survey lines (top), temperature data (middle) and electrical resistivity tomography section (bottom) along the main survey line, a rural way in the Khlongthom Saline Hot Spring area.

Ordinary interpreting of self-potential data in this study area is quite complicated. Since 2010 a simple interpretation of self-potential data was provided by Richards et al (2010), where the patterns of profiles are an indicator to determine the direction of groundwater flow in the subsurface; increasing self-potential profiles pattern indicate groundwater flows up and opposite. This work expected to see that positive self-potential anomalies are associated with hot water depths flowing up at a distance of around 275-300 m (blue dashed circle) on the profile surveys and that it should correlate with higher soil temperatures. However, results in this work show an opposite pattern. From Figure 4.1 it can be seen that both self-potential profile lines exhibit clear positive anomalies, which correlate with lower temperatures compared to the overall trend line (pink highlighted bars). However, not all soil temperatures below the trend line can be correlated with positive self-potential anomalies. In order to interpret this complex study area, geochemical data of water were also used for consideration (Table 4.1).

Table 4.1 Geochemical data of saline groundwater analysis from hot spring KB4/5 at Khlongthom saline hot spring.

Parameters	Results (mg/L)	Parameters	Results (mg/L)
Fe	0.008	Cu	Not detected
Mn	0.01	Zn	0.001
Ca	1,097	SO_4	1,330
Mg	544.9	Cl^-	10,413
Na	4,923	F^-	1.3
K	274.4	CO_3	Not detected
HCO_3	122.7	TDS*	16,350
Total hardness	3,471	Noncarbonate hardness	1,227
pH	6.77		
Resistivity	38.31 Ω.cm		

*Total Dissolved Solid. All parameter determined at the Laboratory of the Faculty of Science, Prince of Songkla University, HatYai.

Geochemical data presented in Table 4.1 show that the natural hot spring pool KB4/5 has relatively high concentrations of Na and Cl, causing the saline character of the water. Based on the mechanism of self-potential signal, the salinity can contribute through the diffusion potential to the total self-potential signal in the study area. With a pH of 6.77 the water has a neutral character, which is a common case for the contribution of the streaming potential; therefore is no change in the polarity (positive and negative) of the self-potential signal in term of streaming potential. Moreover, the geochemical data also show Ca, K, and Mg are higher, while Fe is quite low. This can be classified that the water as having bicarbonate and chloride character. As the total hardness of water is higher, it is possible that this can influence on the ionic strength, that decrease the zeta potential even if the surface potential is not effected (Friborg, 1996). However, this can be neglect when considering the magnitude of the streaming potential and the influence of this factor is still not clear.
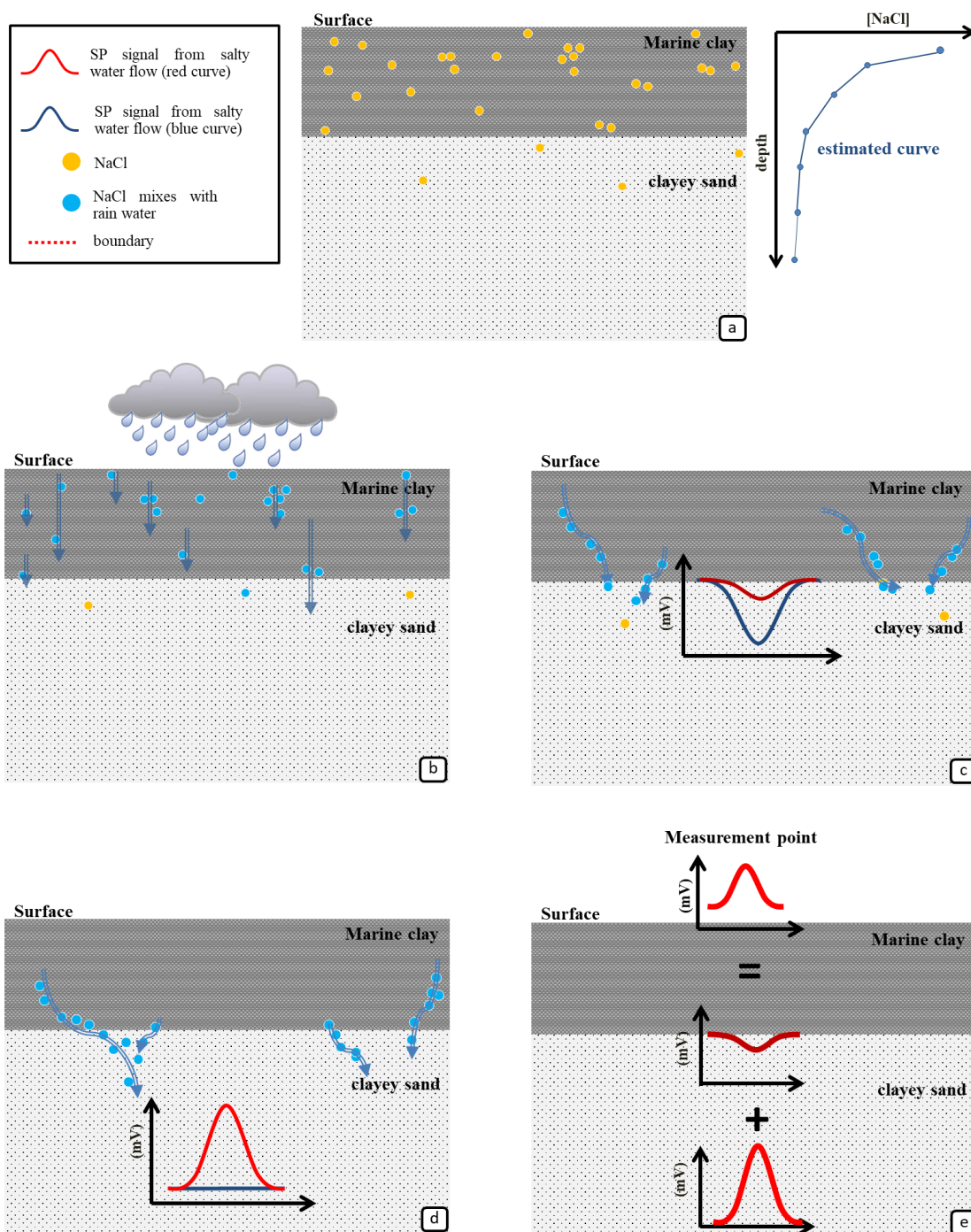
Figure 4.2 Scenario of shallow fluid flow generated self-potential signal in saltmarsh area of Khlongthom saline hot spring. (a) The normal condition of geological structure in subsurface of study area, (b) rain water mixes with NaCl, (c) salty water is flowing down, this generated self-potential signal based on mechanisms of streaming potential, (d) self-potential signal generated from diffusion potential related to NaCl concentration differences, (e) measurement points that performed measuring on the surface taken the total self-potential signal from sum of both sources, streaming potential and diffusion potential.

Figure 4.2 shows the steps of a scenario that can explain all observations. Rain water falling onto the ground picks up NaCl from the highly saline marine clay (salt marsh) at the surface and in the very shallow subsurface, thus becoming saline groundwater. This colder rain water is gravitationally flowing down as groundwater, thus decreasing the near surface soil temperature with respect to the higher temperature trend line due to geothermal heat flow (Figure 4.1 and 4.2). Groundwater flowing down usually creates a negative self-potential base on streaming potential. However, in this case the groundwater flowing down through the porous clayey sand is highly salty, thus reducing the magnitude of the (negative) streaming potential coefficient, which results in a decrease of the self-potential field associated directly with the flow of the groundwater (Ikared et al., 2012).

Further, due to higher salinity in the near surface layer and lower ones in the layers beneath a salinity gradient occurred, which created a diffusion potential of the self-potential field generating a larger positive anomaly (Ikared et al., 2012). The total SP anomaly, a sum of the streaming and diffusion potential, therefore is positive in this environment as measured (Figure 4.1 and 4.2). At locations with negative temperature but not positive self-potential anomalies rain or groundwater is only flowing down into the upper black marine clay layer, but not deeper into the porous clayey sand (see Figure 4.1 and 4.2), as the permeability of the clay layer is relatively low. Flow further down might be along fissures or cracks. Finally, self-potential measurements in combination with soil temperature data have revealed shallow gravitational water flow paths in an overall saline environment resulting in strong positive self-potential anomalies, which override any possible signal from geothermal water flow at depth.

Additionally, a summary schematic diagram has been created as shown in Figure 4.3. All steps of explanation are here illustrated in one figure.
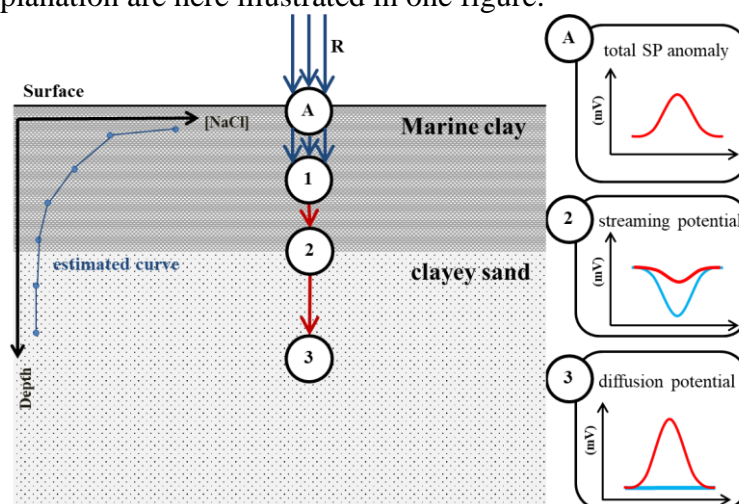
Figure 4.3 Schematic diagram of the shallow fluid flow, which generates the self-potential signal; R: rain water; A: self-potential measurement point (total self-potential anomaly); (1): rain water mixes with NaCl; (2): self-potential signal generated from streaming potential; (3): self-potential signal generated from diffusion potential related to NaCl concentration differences; CL: clay layer; S+CL: clayey sand layer; for (2) and (3): red curve indicates self-potential signal from salty water flow, blue curve self-potential signal from normal groundwater flow.

4.2 Profile map measurements

In order to determine the distribution of fluid flow in shallow subsurface which covers an area requires self-potential mapping. For better interpretation also soil temperature mapping is needed, as well as additional VES data. Self-potential and soil temperature measurements were conducted at the Khlongthom saline hot spring in approximately 0.1 km^2 over few days. VES were conducted after that where the points of VES were chosen based on self-potential anomalies. Reason for choosing them was mentioned before as self-potential can give information about subsurface fluid flow but cannot determine the geological structure of the subsurface. Therefore, for further interpretation VES were measured over self-potential anomaly zone.

Self-potential and temperature exhibit both positive and negative anomalies range from -25 to 50 mV for SP and from 28 °C to 35 °C for soil temperature. Those distribution data will be correlated with each other and with additional geological information, and the locations of hot springs, both natural and man-made, in the study area.
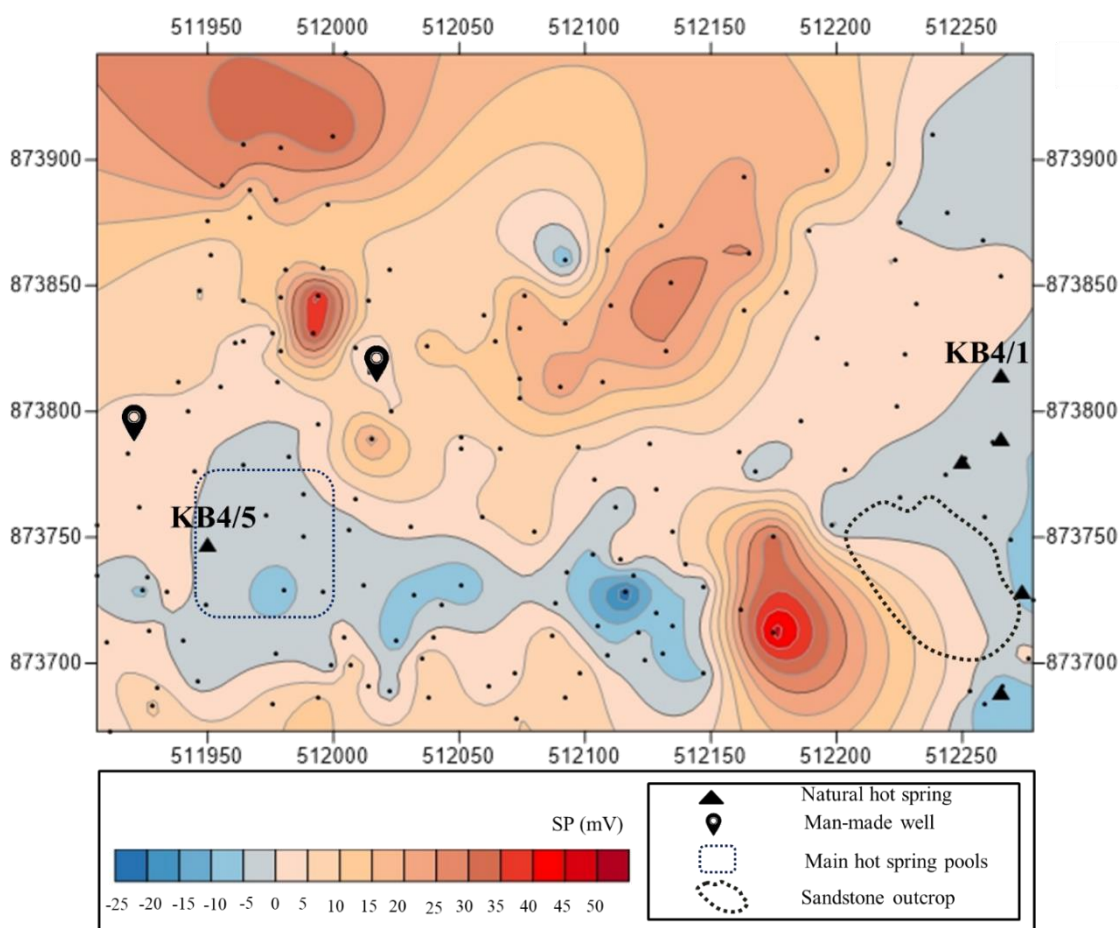
Figure 4.4 Correlation of self-potential mapping with locations of hot spring and wells in study area. KB4/1 and KB/5 are natural hot springs, which were developed as pools for tourism, and the blue dashed line indicates a zone of main pool for tourism. Another four natural hot springs were found in the study area indicated by black triangles.

Figure 4.4 shows self-potential distribution map correlated with locations of natural hot spring and man-made well, in order to make the interpretation and confirmed that observation in profile lines analysis and interpretation discusses earlier. Upward flow of saline hot spring water at Khlongthom created total negative self-potential anomalies. Considering all natural hot springs (black triangles), including KB4/1 and KB4/5, all exhibit negative self-potential anomalies associated with the existence of hot spring. It can be concluded that in case of this study area the upward flow of water in an overall saline environment resulting in negative self-potential anomalies. That confirms the interpretation from earlier measured SP line data, where shallow gravitational water flow in an overall saline environment resulted in strong positive self-potential anomalies. Two man-made wells are located at UTM 511921 E, 873793 N and 512015 E 873816 N (see Figure 4.4); both of them indicate a magnitude of self-potential at almost zero. It is expect to see self-potential signal in same pattern with the location of natural hot spring, but this is not true for the wells. Key difference causing is that there is a pipe inside the man-made well, which is the pathway of the hot saline water up, not porous sand. In general, self-potential signal caused from couple phenomena, which in this case is electrokinetic potential referring to the flux of electrical current induced by a driving force of the flow. In case of the pipes there is no flux of electrical current. Furthermore, a small positive self-potential can be suggested possible of saline water movement in lateral direction (Karakilcik, 2015).

The distribution of the soil temperature also can be compared with the locations of all hot springs in the study area similar to self-potential distribution, as shown in Figure 4.5. Observed zones of higher soil temperatures show a good correlation with all hot springs and included man-made well, as the temperature is measured near the well outflow. In the zone of the natural hot springs dominates higher soil temperature, because of geothermal fluids lose their heat by conduction to the ground which is surrounding them. Figure 4.6 shows the mapping of soil temperature distribution overlain by positive self-potential anomalies (black line) and negative self-potential anomalies (blue line) as observed, both type of survey methods conducted in the same time and similar location.
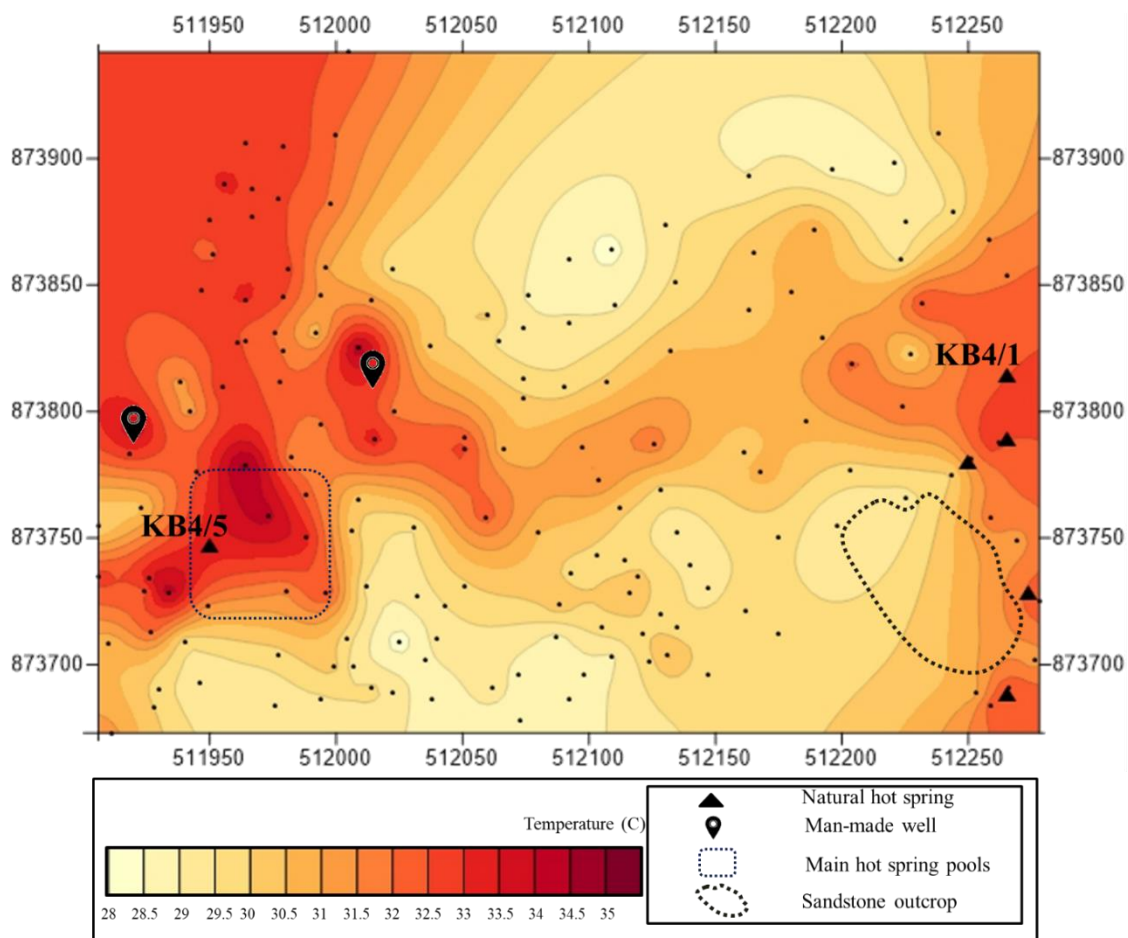
Figure 4.5 Correlation of temperature mapping with location of hot springs and wells in study area. KB4/1 and KB/5 are the natural hot springs which were developed as pools for tourism, and the blue dashed line indicates a zone of main pools for tourism. Another four natural hot springs were found indicated by black triangles.
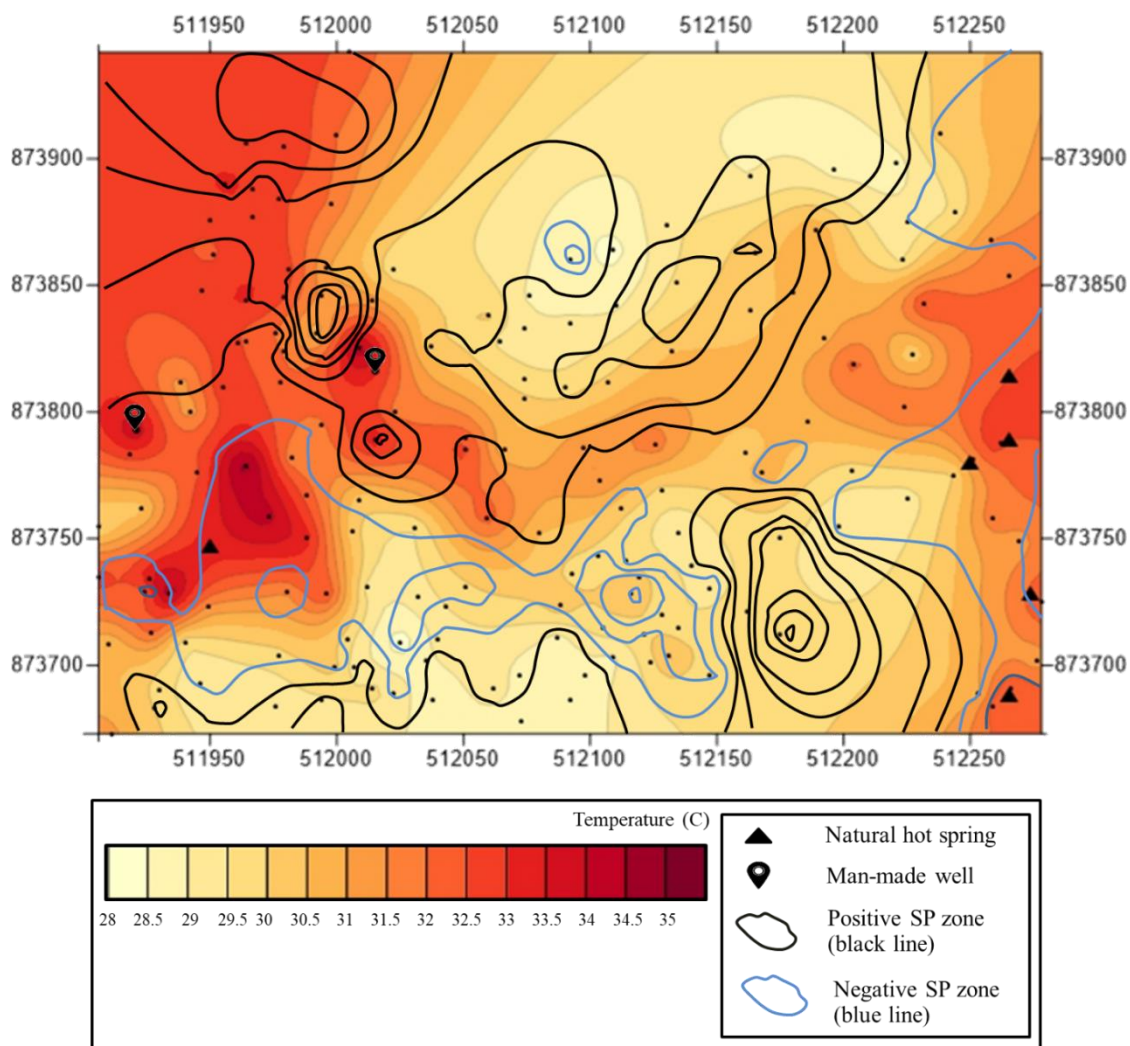
Figure 4.6 Correlation of self-potential anomalies with temperature mapping in study area, positive self-potential (black line) and negative self-potential (blue line) were overlapped with soil temperature map.

Considering the comparison map between self-potential and soil temperature shown in Figure 4.6, the observed correlation can be divided into three cases. The first case is distribution of negative self-potentials related to higher soil temperature, and all of these cases represent locations of hot spring manifestation. It can be concluded that the upward flow of saline hot spring water as the expression hot spring on the ground resulted in generating a negative self-potential anomaly and higher soil temperature. In opposite way, whenever obtains the data of negative self-potential overlap with higher soil temperature this can be referred to the hot saline water upward flow towards the surface.

The second case is distribution of negative self-potential associated with low soil temperature. In this case no observations show hot spring at the surface; an example is the negative self-potential anomaly at UTM 512092 E, 873860 N. This can be referred to saline water moving upward to the very shallow subsurface, but not presents itself on the surface. The explanation behind is the limitation of soil temperature was taken at 30 cm depth, while self-potential method can see deeper. That means that sometimes self-

potential can investigated the subsurface flow but soil temperature cannot. The relationship between self-potential and temperature of such case indicates a hidden saline hot spring.

The third case is the correlation of positive self-potentials with low soil temperature, and also no hot spring was observed on the surface similar to the second case. This result suggested a downward flow of saline water into the subsurface. Whenever the saline hot water moved upwards but cannot expresses itself at the surface it has to find another pathway. The temperature of the hot saline water should decrease by the time and distance from the reservoir, so the saline hot water is getting cooler and also decrease its pressure, so it is possible that it slowly flows lateral and mixes with meteoric water or saline ground water. Finally this saline water should find a way to flow down to a deeper part.

Positive self-potential anomalies related with low temperature may indicate downward flow of meteoric water in a saline environment. However, there are zones of positive self-potential correlated with higher soil temperatures that were observed in the north-western part of the study area, which is different from the third case. Here a final interpretation is not conclusive.

In order to determine the characteristics of the study area results from ERT section and VES data were used to correlate with self-potential, soil temperature and geological data. Wattanasen et al. (2015) investigated the saline hot spring Khlongthom by conducting ERT along a survey line located in the study area defined by a blue line in Figure 4.7; obtained data was used for a correlation in this work as shown in Figure 4.8.
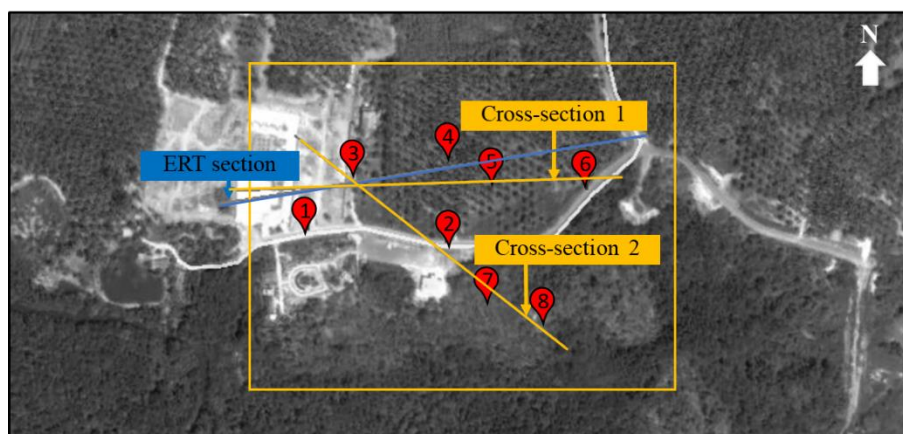
Figure 4.7 Location of self-potential area measurements (yellow rectangle square), ERT section (blue line). Cross-section 1 includes VES 3, VES 4, VES 5, and VES 6 and cross-section 2 comprises VES 3, VES 2, VES 7, and VES 8.
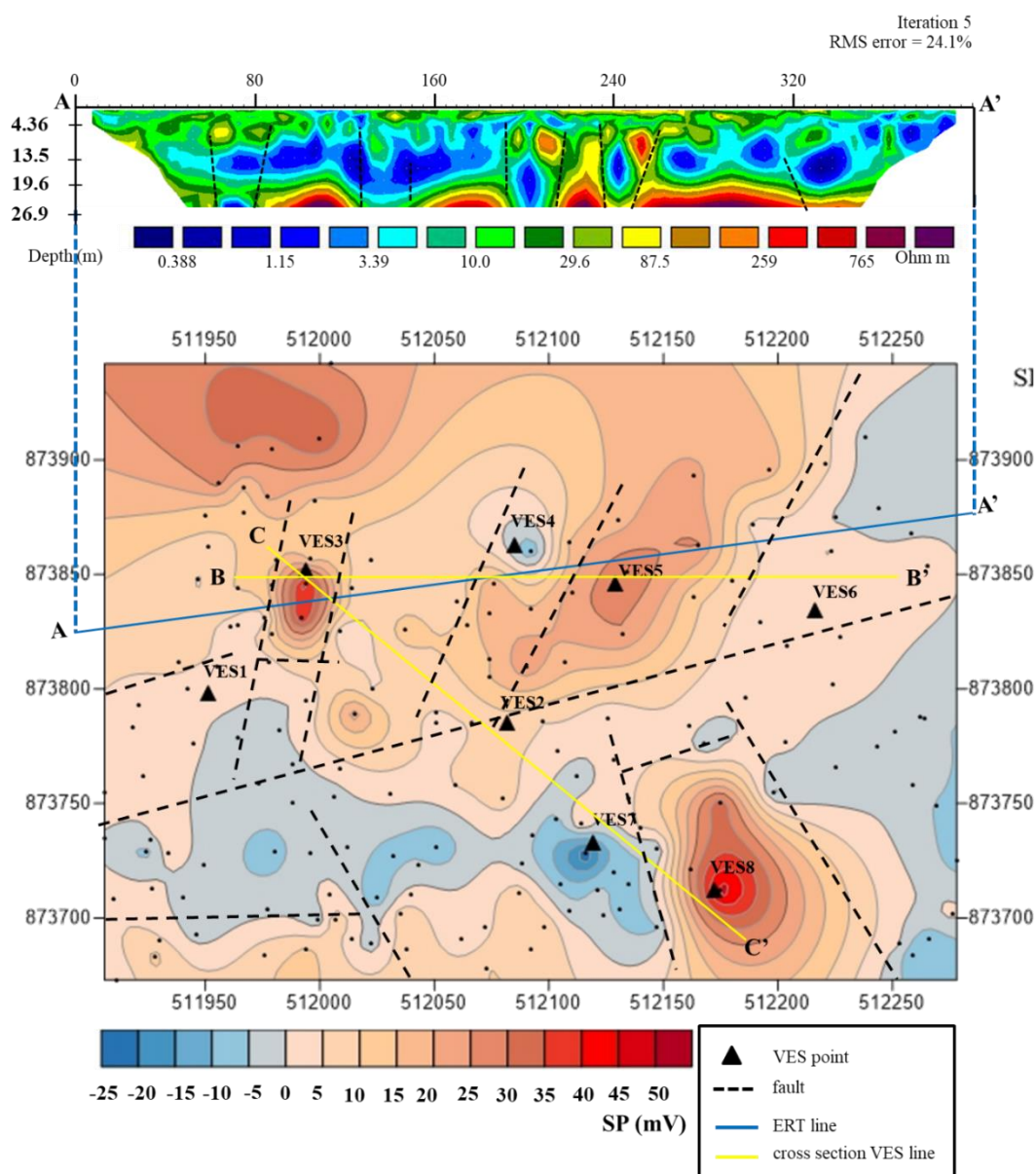
Figure 4.8 Electrical resistivity tomography section with interpretation of possible faults (top), applied from Wattanasen et al. (2015). Self-potential mapping included interpretation of possible faults, location VES points, and cross-section lines for VES (bottom).

Figure 4.8 shows the ERT section (top) with the location of measurement (AA', blue line) on the distribution of the self-potential map. The ERT section suggests that there are three layers of subsurface associated with resistivity values. The first layer exhibit low resistivity value as 5-100 ohm-m (green color), and 0.1-8 m of thickness, this layer can be sand gravel, clayey sand or topsoil. The second layer shows very low resistivity as 0-15 ohm-m (blue color), and associated with 8-22 m depth. In this layer were observed should be saline water as 80-160 m and 320-440 m of ERT section. Finally, the third layer has a resistivity value more than 100 ohm-m, as more than 22 m depth.

This layer can be sandstone. Further, ERT suggests possible faults and fractures at 60, 80, 125, 140, 180, 200, 220, 260 and 330 m on the section.

Considering the distribution of the self-potential anomalies (see Figure 4.8) it can be used for determining possible faults or fractures. Normally, the positive and negative transitions indicates a faulting zone (Karakilcik, 2015), as fault zones allowing or not allowing fluid flow depending on the fault characteristics. In this work, the distribution of self-potential suggested that there are several possible faults or fractures at locations and with orientations indicated by black dashed lines in Figure 4.8. However, exact orientations and locations of these faults cannot be determined using only self-potential. Accordingly, for a subsurface interpretation in the study area a combination with electrical resistivity VES has been done

Eight VES points were conducted in the study area over positive and negative SP anomalies and for further analysis two cross-sections have been constructed connecting several measurement locations. In this work made two straight lines were done as cross-sections (yellow lines in Figure 4.7 and Figure 4.8), first from VES 3 to VES 6, and second, a cross-section from VES 3 to VES 8.

Figure 4.9 presents the cross-section 1 located at BB' (yellow line, Figure 4.8), including VES 3, VES 4, VES 5, and VES 6 with a direction from West to East. In this area there are mainly oil palm plantations. Considering the resistivity values of the top layer which are relatively higher than each other since Figure 4.9 shows the shallowest saline water level is about 6 meter depth (VES 5) and on the other hand, the deepest is about 24 meter with very low resistivity values (VES 6). Therefore, in this cross-section there has to be a vertical fault or fracture between VES 5 and VES 6, and likewise between VES 4 and VES 5; although both points are close the layers are extremely different. Between VES 3 and VES 4 there is a little difference between the layers suggesting no fault, but the self-potential values are quite different, suggesting saline hot water flowing up at VES 4, whereas saline groundwater flowing down at VES 3.

Therefore in cross-section 1 this work suggested at least three faults between the different measuring points, especially between VES 4 and VES 5 in the same way between VES 5 and VES6, but also between VES 3 and VES 4. However, the exact location of each fault cannot be determined.
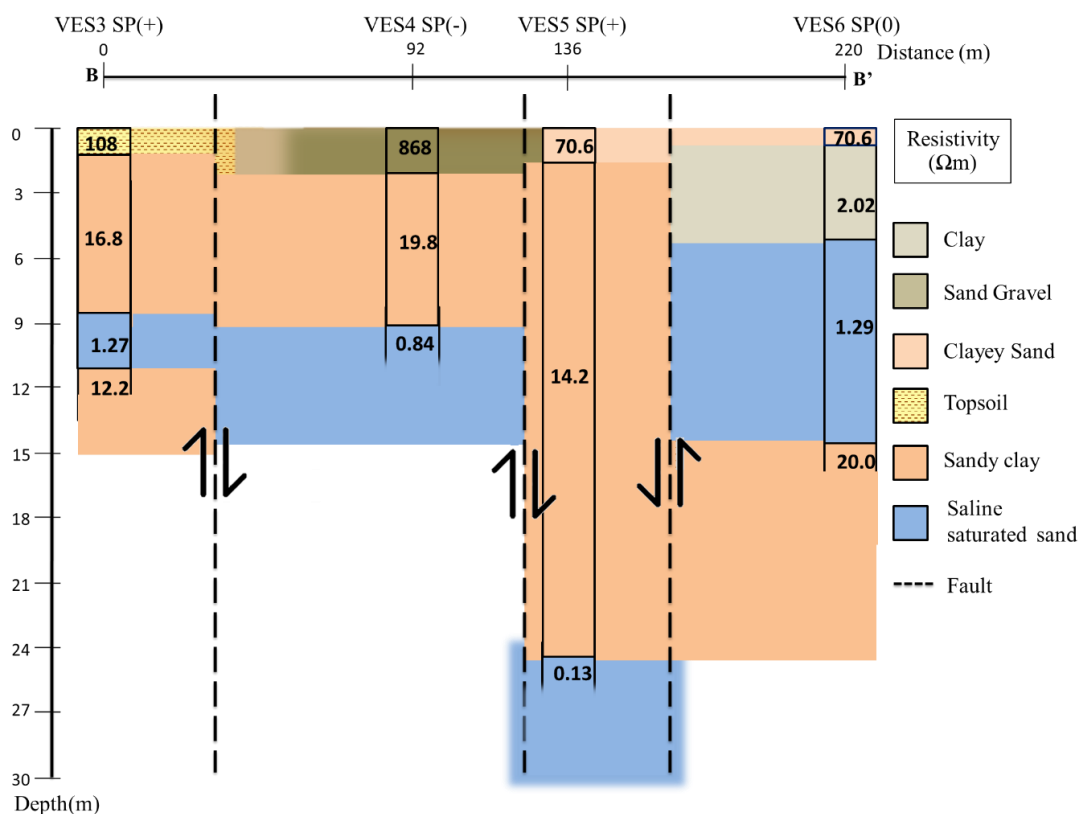
Figure 4.9 Cross-section 1 from West to East with the VES locations shown in bars, with depths, distance, the resistivity of the layers (see also Figure 4.7), as well as interpreted fault locations.

Figure 4.10 present the cross-section 2 located as CC' (yellow line, Figure 4.8), including VES 3, VES 2, VES 7, and VES 8 with line direction from Northwest to Southeast. This second cross-section connects four VES points via a straight line between these points.

In the second cross-section sandstone was found, which is the bedrock in this area. Furthermore, there is a sandstone outcrop nearby VES 8.The resistivity value which was measured is lower than the real resistivity value of sandstone as though it was weathered sandstone and there is saline water inside the pores. Considering VES 7 and VES 8 it was found that the depth of the weathered sandstone layer is very different. For this reason, there should be a fault between both locations. In the same way at VES 2 it was found that the sandstone maybe deeper, but this work has not deeper data. However, the saline water level between VES 2 and VES 7 is very different, also between VES 3 and VES 2. Hence this cross-section should have at least three faults similarly to cross-section 1.
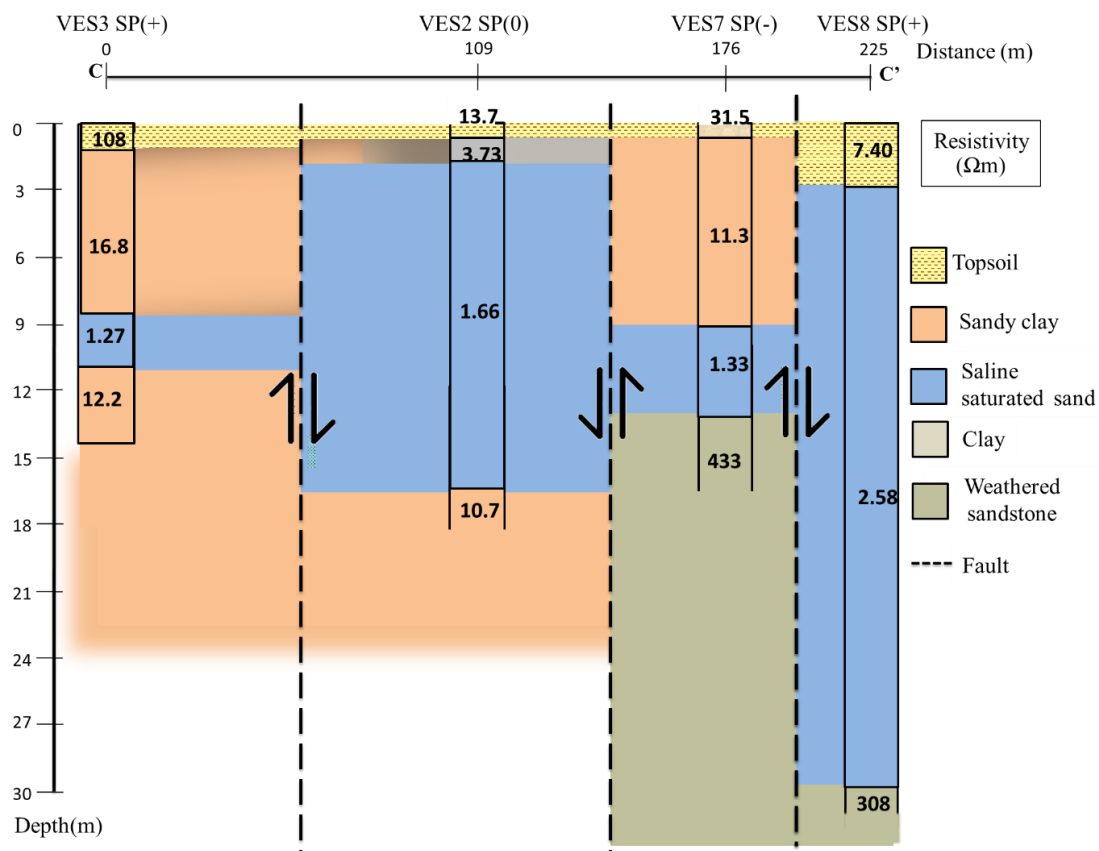
Figure 4.10 Cross-section 2 from Northwest to Southeast with the VES locations shown in bars, with depths, distances, and the resistivity of the layers (see also Figure 4.7).

As a result of VES, at both, the first and second cross-section, three faults were found. Some faults maybe the same fault in particular the fault between VES 3 and VES 2 and VES 2 and VES 4. Nevertheless, there are not enough data for identifying the faults, not only the exact location and direction but also the orientation of these faults as well.

The combination between self-potential data and shallow VES measurements proved to be a good tool for this area, as is believed that the self-potential anomalies have been created by the same geological sources, such as a zone of fluid flow, heat, and ions as self-potential sources (Karakilcik, 2015). Furthermore correlations between self-potential data and VES measurements in this work suggested that self-potential can be investigated the source down to a depth of about 10 m. The negative self-potential anomaly at VES 4 suggests that saline hot water is flowing up as shallow as 9 m but not present itself at the surface because there is high resistivity on the top, likely drier sand. This work has not seen a negative self-potential anomaly coming from saline hot water flowing up deeper than that depth.

The results of this study shows that the saline groundwater and the saline hot spring water in the area of the Khlongthom hot spring are very shallow, often only a few meters deep below surface. Further, the shallow subsurface is seemingly heavily fractured by assumingly vertical fracture (see in Figure 4.11); exact orientation and location of these faults cannot be determined using only VES and self-potential. These fractures can obstruct the pathways of saline hot water and saline groundwater flow.

In case of the manifestation of hot springs hot water can flow up along faults or fractures up to the surface. Section AA' (see Figure 4.8) a hidden hot spring. The flowing up of saline hot water along pathway, vertical faults or fractures, were observed at two parts on the section obtained from negative self-potential values. The first one at 180-200 m, which fluid can flow up until 9 m depth but cannot move to the surface because there are a layer of very high resistivity overlay on the top (868 ohm-m) which data obtained from VES 4, this can be the zone of strongly soil packing and low permeability. When the saline hot water mixes up with meteoric water or saline ground water from seawater intrusion it getting cooling down and find the other way down, thus resulting in saline water possible lateral movement and finally flowing down at some location. The second part of saline hot water flowing up was observed at the western part at 380-400 m of the section, obtained from negative self-potential values. In this zone the hot saline water also cannot presents itself to the surface, as there is a clay layer on top which shows resistivity of 2.02 ohm-m (obtained from ERT, VES 6). A larger zone of positive self-potential were observed at 125–140 m and 220-260 m on AA' section. This corresponds to the flowing down of meteoric water or saline ground water. Furthermore, at the end of eastern part in model section at 0–80 m a zone of water capture is indicated resulting from lateral fluid flow, obtained from small positive self-potential.

Figure 4.11 Location of cross section1 and 2, and the assumed location of possible faults or fracture base on the combination of self-potential with VES.

4.3 Conclusion

In conclusion, self-potential technique as a central survey method in this work is a powerful tool for indicating patterns of fluid flow in the subsurface. Furthermore, self-potential method is an effective tool for mapping fluid flow in shallow subsurface, as shown here with the saline hot spring Khlongthom. However, this method should not be used stand alone in order to determining the overall subsurface structure, which is a complex system such this study area. There are several techniques that can support and confirm the results of self-potential. All obtained results from all surveys show a good correlation.

From the earlier part of this study, it can be concluded that self-potential measurements in combination with soil temperature data have revealed shallow gravitational water flow paths in an overall saline environment resulting in strong positive self-potential

anomalies, which override any possible signal from geothermal water flow at depth. Therefore, the interpretation of self-potential pattern in this area is different from cases associated with normal groundwater flow. The generating of the self-potential signal is always complex and depends also on the concentration of the salinity.

The integration of self-potential methods, soil temperature measurement, electrical resistivity methods with ERT and VES, and geological studies of the area was illustrated in a conceptual model that explains the system of the study area (see Figure 4.12). The conceptual model reflects that the saline groundwater and the saline hot spring water in the area of the Khlongthom saline hot spring are very shallow, often only a few meters deep below surface. This schematic cross section represents the generalized flow pattern of hidden saline hot springs in Khlongthom saline hot spring, where saline hot water is flowing up to the shallow subsurface through vertical fractures. Whenever saline hot water cannot present itself at the surface possible lateral movement and saline hot water mixing with meteoric water can occur. Additionally, self-potential anomalies suggest that in the study area also there are places of fluid circulation down to the depth.

4.4 Recommendations

This work has revealed some of the subsurface characteristics of the saline hot spring. Future work is recommended for identifying and verifying the faults with more data or different methods, especially in oil palm plantation where it is relatively easy to do measurements. Additionally, as the self-potential is directly associated which sources in study area both fluid flow and salinity, repeated measurements over a period of time should be carried out in order to observe changes.

From the conclusion of this work further development in this area should consider these findings when designing buildings or other infrastructure projects. Therefore new buildings should avoid some locations where the saline water level is relatively shallow including areas around VES2 and VES8, as at these locations the saline water level is shallower than three meters. Nevertheless, more surveys should be done in areas where new buildings might be built in order to avoid a negative effect on the hot spring system.
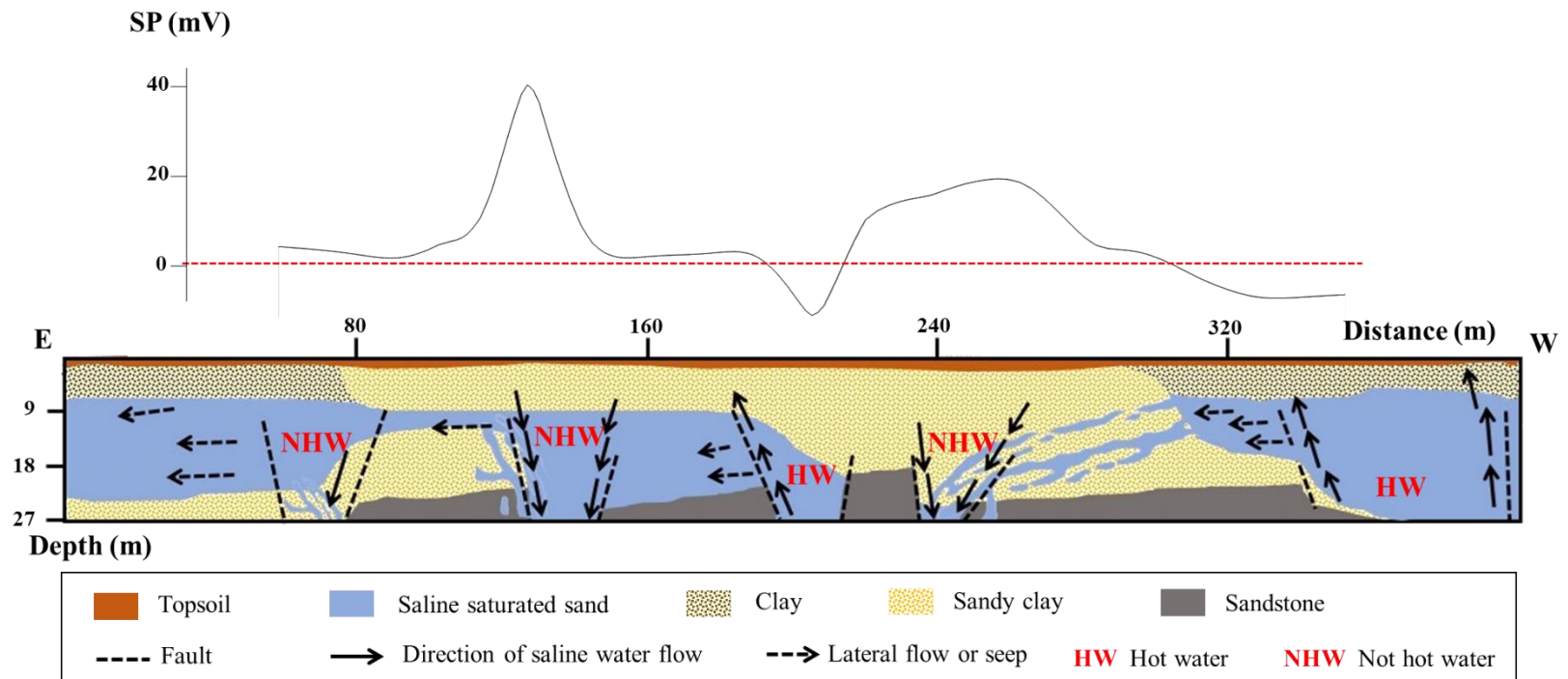
Figure 4.12 Conceptual model of fluid flow pattern in the shallow subsurface at the saline hot spring Khlongthom.

REFFERENCES

Aizawa, H., Yoshida, H. and Sakai, S.-I. (2008). Current results and future perspectives for Japanese recycling of home electrical appliances. Resources, Conservation and Recycling, 52, 1399-1410.

Aubert, M. and Atangana, Q. Y. (1996). Self-Potential Method in Hydrogeological Exploration of Volcanic Areas. Groundwater, 34, 1010-1016.

Axelsson, G. (2013). Conceptual models of geothermal systems introduction. Presented at "Short Course V on Conceptual Modelling of Geothermal Systems", in Santa Tecla, El Salvador, February 24 - March 2, 2013.

Axelsson, G., and Gunnlaugsson, E. (convenors), (2000). Long-term monitoring of high- and lowenthalpy fields under exploitation. World Geothermal Congress 2000, Pre-Congress Course, Kokonoe, Japan, 226 pp.

Barde-Cabusson, S. and Finizola, A. (2012). Tutorial for Self Potential data processing I, Data correction. Version: 10 April 2012.

Bérubé, A.P. (2004). Investigating the Streaming Potential Phenomenon Using Electric Measurements and Numerical Modelling with Special Reference to Seepage Monitoring in Embankment Dams. Doctoral Thesis. Luleå University of Technology Department of Civil and Environmental Engineering, Division of Applied Geophysics, Sweden.

Bowen, R. (1989). Geothermal resources. New York: ELSEVIER SCIENCE PUBLISHING CO., INC.

Bödvarsson G., (1964). Physical characteristics of natural heat sources in Iceland. Proc. UN Conf. on New Sources of Energy, Volume 2: Geothermal Energy, Rome, August 1961. United Nations, New York, 82-89.

Busby, J. Schematic diagram of a geothermal system. Retrieved April 13, 2018, from Natural Environment Research Council: http://www.bgs.ac.uk/research/energy/geothermal.

Corry, C. E., Demoully, G. T. and Gerety, M. T. (1983). Field procedure manual for self potential surveys. Arizona: ZERO Publ.

Corwin, R.F. and Hoover, D.B. (1979). The self-potential method in geothermal exploration. Geophysics, 44(2), 226–245.

Dentith, M. and Mudge, T.S. (2014). Geophysics for the Mineral Exploration Geoscientist. New York. Cambridge University Press.

Dickson, M.H. and Fanelli, M. (2004). https://www.geothermal-energy.org/uploads/pics/ What_is_geothermal_en_06.jpg Accessed: 25/09/2016.

Erchu, R.A. (1988). Geotechnical applications of the self potential (SP) method. Technical report REMR-GT-6. Department of Civil Engineering Virginia Military Institute Lexington, Virginia 24450.

Esmaeili, S., Rahbar, M., Pahlavanzadeh, H., and Ayatollahi, S. (2016). Investigation of streaming potential coupling coefficients and zeta potential at low and high salinity conditions: Experimental and modeling approaches. Journal of Petroleum Science and Engineering 145, 137–147.

Finizola, A., Lénat, J.-F., Macedo, O., Ramos, D., Thouret, J.-C. and Sortino, F. (2004). Fluid circulation and structural discontinuities inside Misti volcano (Peru) inferred from self-potential measurements. Journal of Volcanology and Geothermal Research, 135, 343-360

Friborg, J. (1996). Experimental and theoretical investigations into the streaming potential phenomenon with special reference to applications in glaciated terrain. PhD thesis, Lulea University of Technology, Sweden.

Gupta, H. and Roy, S. (2007). Geothermal energy: an alternative resource for the 21st century. Netherlands: Elsevier B.V.

Ikard, S.J., Revil, A., Jardani, A., Woodruff, W.F., Parekh, M., and Mooney, M. (2012). Saline pulse test monitoring with the self-potential method to nonintrusively determine the velocity of the pore water in leaking areas of earth dams and embankments. Water Resour. Res., 48.

Jaafar, M.Z., Vinogradov, J., and Jackson, M.D. (2009). Measurement of streaming potential coupling coefficient in sandstones saturated with high salinity NaCl brine. Geophysical Research Letters, VOL. 36.

Jackson, D. and Kauahikaua, J. (1987). Regional self-potential anomalies at Kilauea volcano. US Geological Survey Professional Paper, 1350, 947-959.

Jouniaux, L. and Ishido, T. (2013). Electrokinetics in Earth sciences. International Journal of Geophysics, 2013.

Karakilcik, H. (2015). Determination of geothermal Fields at Kizilahaman (Ankara) Using Vertical Electrical Sounding (VES) and Spontaneous Potntial (SP) methods. Progress in Clean Energy, Volume 2: Novel Systems and Applications, 301-311.

Kearey, P., Brooks, N. and Hill, I. (2002). An introduction to geophysical exploration 3rd ed., Blackwell science Ltd., Oxford, England, pp 183-185.

Keller, G.V. and Frischknecht, F.C. (1966). Electrical methods in geophysical prospecting: Pergamon Press, New York, 517 p.

Knödel K, Krummel H, Lange G (1997). Handbuch zur Erkundung des Untergrundes von Deponien und Altlasten. Band 3: Geophysik.

Lal, A.A. (2016) Geophysical investigation of the hot spring sit in Rabula Fiji. A thesis submitted in partial fulfillment of the requirements for the degree of Master of Science. School of Engineering & Physics Faculty of Science, Technology and Environment The University of the South Pacific.

Lénat, J.-F. 2007. Retrieving self-potential anomalies in a complex volcanic environment: an SP/elevation gradient approach. Near Surface Geophysics, 5, 161-170.

Loke M.H. and Barker R.D. (1996). Rapid least-squares inversion of apparent resistivity pseudosections using a quasi-Newton method. Geophysical Prospecting, 44, 131-152.

Loke, M.H. (2000). Electrical imaging surveys for environmental and engineering studies.

Loke, M.H. (2015). Tutorial: 2-D and 3-D electrical imaging surveys.

Mareschal, J.-C., Jaupart, C., Phaneuf, C. & perry, C. (2012). Geoneutrinos and the energy budget of the Earth. Journal of Geodynamics, 54, 43-54.

Martínez-Pagán, P., Jardani, A., Revil, A. and Haas, A. (2010). Self-potential monitoring of a salt plume. GEOPHYSICS,VOL. 75, NO. 4, P.WA17–WA25.

Masum, M. (2015). Low-Temperature Geothermal Systems in Sedimentary Basin andTheir Prospect in Bangladesh.

Mburu, M. (2012). Geothermal energy utilization. Presented at Short Course VII on Exploration for Geothermal Resources, Kenya, Oct. 27 – Nov. 18, 2012.

Milsom, J. 2003. Field Geophysics. Chapter 6: Resistivity Methods. Wiley, U.K., pp. 97-116.

Ngansom, W. and Dürrast, H. (2016). Saline hot spring in Krabi, Thailand: a unique geothermal system. SEG International Exposition and 86th Annual Meeting.

Overbeek, J. T. G. (1952). Electrochemistry of the double layer. Colloid Science, 1, 115-193.

Ogilvy, A., Ayed, M. and Bogoslovsky, V. (1969). Geophysical Studies of Water Leakages from RESERVOIRS*. Geophysical Prospecting, 17, 36-62.

Palacky, G.V. (1987). Resistivity characteristics of geologic targets. Electromagnetic Methods in Applied Geophysics, SEG 1351.

Parasnis, D.S. (1997) Principles of Applied Geophysics, Chapman &Hall, London.

Pearson, A., Pi, Y., Zhao, W., Li, W., Li, Y., Inskeep, W., Perevalova, A., Romanek, C., Li, S. & Zhang, C. L. 2008. Factors controlling the distribution of archaeal tetraethers in terrestrial hot springs. Applied and Environmental Microbiology, 74, 3523-3532.

Rao, M. R. (1953). Self-potential anomalies due to subsurface water flow at Gerimenapenta, Madras State, India. Transaction of the American Institute of Mineralogy, Metallurgy, Petroleum Engineering and Mining Engineering, 400-403.

Revil, A. and Cathles, L. M. (1999). Permeability of shaly sands. Water Resources Research, 35(3), 651–662.

Revil, A. and Jardani, A. (2013). The self-potential method: theory and applications in environmental geosciences, Cambridge University Press.

Reynolds, J.M. (2011). An introduction to applied and environmental geophysics, John Wiley & Sons.

Richards, K., Revil, A., Jardani, A., Henderson, F., Batzle, M. and HAAS, A. (2010). Pattern of shallow ground water flow at Mount Princeton Hot Springs, Colorado, using geoelectrical methods. Journal of Volcanology and Geothermal Research, 198, 217-232.

Ricketts, B. http://www.geological-digressions.com. Coastal Aquifers; Groundwater at Sea Accessed: 25/03/2018.

Saemundsson, K., Axelsson, G. & Steingrímsson, B. (2009). Geothermal systems in global perspective. short course IV on exploration for geothermal resources, 1-22.

Sato, M. and Mooney, H.M. (1960). The electrochemical mechanism of sulfide self-potentials. Geophysics, 25, 226-249

Sasai, Y., J. Zlotnicki, Y. Nishida, Y. Tanaka, P. Yvetot, P. Morat, and H. Murakami. (1997). Electromagnetic monitoring of Miyake-jima Volcano, Izu-Bonin Arc, Japan: A preliminary report, J. Geomagn. Geoelectr., 49, 1293 – 1316

Schiavone, D. and Quarto, R. (1984). Self-potential prospecting in the study of water movements. Geoexploration, 22, 47-58

Stumm, W. (1992). Chemistry of the solid-water interface: processes at the mineral-water and particle-water interface in natural systems, John Wiley & Son Inc.

Telford, W.M., Geldart, L.P. and Sheriff, A.E. (1990). Applied Geophysics, 2nd edition. Cambridge University Press, 792 pp.

Vinogradov, J., M. Z. Jaafar, and M. D. Jackson (2010), Measurement of streaming potential coupling coefficient in sandstones saturated with natural and artificial brines at high salinity, J. Geophys. Res., 115.

Wanfang, Z., Beck, B.F. and Stephenson, J.B. (1999). Investigation of groundwater flow in karst areas using component separation of natural potential measurements. Environmental Geology, 37(1–2), 19–25.

Wattanasen, K., Dürrast, H., Yodkayan, S., and Wattanasen, S. (2015). Geological Characterization of the Klongtom Geothermal Saline Hot Spring, Krabi Province Using Geophysical Methods and Soil-Water Quality Data The Thailand Research Fund, 14982.

APPENDIX

APPENDIX A

Table A 1: Raw data of measured self-potential and ground surface temperature measurement line 1

	UTM_E	UTM_N
SP reference position (base)	512472	873754
First point of line	512482	873762

Distance on tape (m)	Time(hh:mm)	V₁ (mV)	V₂ (mV)	Temp (C)
0				29.8
base	11:41:00	90.3	86.3	30.7
120	11:45:00	1.999	2.31	32.6
122	11:55:00	-0.355	-0.287	32.6
124	11:56:00	4.01	4.1	32.2
126	12:03:00	-1.855	-1.883	32
128	12:04:00	-1.546	-1.473	32.2
130	12:05:00	2.36	2.4	32.5
132	12:07:00	151.6	153.4	32.2
134	12:09:00	52.7	52.3	30.1
136	12:11:00	0.545	0.533	30.9
138	12:14:00	1.065	0.912	30.6
140	12:15:00	-0.331	-0.307	30.6
142	12:17:00	-1.23	-1.271	32.4
144	12:18:00	29	27.5	31.8
146	12:20:00	-573	-0.629	31.1
148	12:23:00	5.08	5.2	31.2
150	12:25:00	4.95	4.95	31.2
base	12:32:00	179.9	178.8	
152	12:36:00	17.86	16.89	30.8
154	12:38:00	6.27	7.86	31.2
156	12:41:00	13.6	12.71	31.1
158	12:43:00	4.44	5.49	31.4
160	12:45:00	2.33	2.31	30.7
base	14:03:00	0.594	0.576	
162	14:08:00	7.76	7.27	31.1
164	14:10:00	2.28	2.16	31
166	14:12:00	4.43	4.42	30.8
168	14:13:00	3.78	3.88	30.4
170	14:16:00	0.889	0.998	31.2

172	14:02:00	5.59	5.67	30.9
174	14:25:00	2.94	3.07	31.4
176	14:27:00	-0.808	-0.943	31.9
178	14:29:00	1.033	1.275	31.6
180	14:32:00	2.09	1.951	31.3
182	14:35:00	2.04	1.948	31.3
184	14:36:00	1.458	1.487	31.4
186	14:38:00	1.217	1.506	31.6
188	14:40:00	2.77	2.73	31.6
190	14:41:00	2.96	2.01	31.5
192	14:43:00	2.31	2.48	31.5
194	14:45:00	2.26	2.25	31.1
196	14:46:00	1.82	1.885	31.2
198	14:48:00	0.363	0.657	31.1
200	14:52:00	2.13	2.19	30.8
base	15:00:00	4.23	4.42	
202	15:05:00	8.12	8.27	30.4
204	15:06:00	30.3	29.1	30.3
206	15:08:00	8.65	8.35	30.4
208	15:09:00	10.67	10.75	30.3
210	15:10:00	6.45	6.71	31
212	15:11:00	11.74	10.83	30.9
214	15:14:00	9.2	9.1	31.2
216	15:15:00	11.09	11.23	31
218	15:16:00	17.1	16.24	29.9
220	15:18:00	10.68	10.51	29.3
222	15:19:00	21.7	21.7	29.1
224	15:21:00	35.4	35.6	28.6
226	15:23:00	40.5	39.8	28.8
228	15:27:00	69.3	67.9	28.6
230	15:29:00	79.7	79.9	28.5
base	15:34:00	185	189.3	
232	15:44:00	234	235	29
234	15:46:00	129.3	127.5	29.4
236	15:48:00	119.8	118.8	29.5
238	15:49:00	150.4	147	29.6
240	15:52:00	147.5	147.7	30.6
242	15:54:00	145	142.8	30.3
244	15:55:00	136.2	137.8	30.7
246	15:56:00	133.3	133.3	31
248	15:57:00	140.2	146	30.7
250	16:00:00	85.2	84.2	30.7

252	16:01:00	93.8	93.1	30.7
254	16:03:00	113.6	113.6	31.1
256	16:04:00	120.7	121.8	30.7
258	16:05:00	127.9	127.8	30.3
260	16:07:00	130.3	130.4	29.7
262	16:08:00	172.8	173.5	29.6
264	16:09:00	194.3	190.6	29.3
266	16:11:00	135.5	132	30.2
268	16:14:00	126.5	125.4	30.1
270	16:16:00	165	163.6	30
base	16:23:00	193.6	193.3	
base	16:29:00	21.4	21.2	
272	16:04:00	9.43	9.66	30.4
274	16:41:00	7.84	8.61	30.4
276	16:43:00	10.66	10.52	30
278	16:44:00	10.6	10.43	30.1
280	16:46:00	13.46	13.39	30.3
282	16:47:00	40.8	40.8	30.5
284	16:49:00	44.8	45.7	30.4
286	16:50:00	34.2	34.9	30.2
288	16:53:00	269	271	30.7
290	16:57:00	277	278	30.6
292	16:58:00	277	279	29.9
294	17:00:00	84.3	82.4	29.8
296	17:02:00	277	274	29.6
298	17:03:00	280	280	28.8
300	17:06:00	280	282	29.4
base	17:18:00	262	264	

Table A 2: Corrected data of measured self-potential line 1

Distance on ERT line (m)	Distance on tape (m)	SPcorrected
251	4	-139.2889768
253	6	-180.8490832
255	8	-177.3045938
257	10	-209.9131683
259	12	-213.4246789
261	14	-213.3391895
263	16	-180.1402108
265	18	-178.2812321
267	20	-238.0772534
269	22	-249.0187853

271	24	-254.2352959
273	26	-262.7753172
275	28	-236.3658278
277	30	-268.0968491
279	32	-279.388381
281	34	-287.1594023
283	36	-269.310743
285	38	-280.9064133
287	40	-273.5849188
289	42	-282.7505891
291	44	-284.8662594
293	46	-277.4478384
295	48	-283.06447
297	50	-282.0511016
299	52	-279.4494173
301	54	-284.8653647
303	56	-280.4376279
305	58	-283.4292068
307	60	-287.3138384
309	62	-285.60947
311	64	-284.7574173
313	66	-285.0123647
315	68	-285.6626805
317	70	-286.0403121
319	72	-284.6239437
321	74	-284.5022594
323	76	-285.288891
325	78	-285.4755226
327	80	-285.9838384
329	82	-286.39047
331	84	-286.0837331
333	86	-304.2231449
335	88	-290.8950273
337	90	-319.538792
339	92	-325.7106743
341	94	-332.1525567
343	96	-332.114439
345	98	-350.4100861
347	100	-353.7719684
349	102	-353.0138508
351	104	-369.9376155
353	106	-364.1694978

355	108	-360.9732625
357	110	-366.3770273
359	112	-356.980792
361	114	-361.4883214
363	116	-166.929954
365	118	-279.5182806
367	120	-296.9066071
369	122	-270.2507703
371	124	-284.9832601
373	126	-295.3715867
375	128	-308.1157499
377	130	-314.9599132
379	132	-312.0040765
381	134	-378.8365663
383	136	-374.1807295
385	138	-362.2690561
387	140	-359.1132193
389	142	-355.8573826
391	144	-361.3457091
393	146	-322.7898724
395	148	-305.2340357
397	150	-371.9223622
399	152	-392.754852
401	154	-407.0431785
403	156	-456.3540765
405	158	-463.2841581
407	160	-471.1443214
409	162	-476.544403
411	164	-484.3645663
413	166	-462.3646479
415	168	-469.0448112
417	170	-474.9848928
419	172	-266.2051377
421	174	-287.5654642
423	176	-284.9055459
425	178	-488.2857091
427	180	-315.2658724
429	182	-308.605954
431	184	-324.6261989

Table A 3: Raw data of measured self-potential and ground surface temperature measurement line 2

	UTM_E	UTM_N
SP reference position (base)	512472	873754
First point of line	512482	873762

distance on tape (m)	Time(hr:m)	V_1(mV)	V_2(mV)	Temp (C)
base	11:41:00	0.791	1.166	30.7
4	11:42:00	12.09	13	31.5
6	11:43:00	7.52	7.4	31.5
8	11:45:00	7.21	5.88	31.9
10	11:46:00	1.752	2.28	31.3
12	11:48:00	5.95	4.78	30.6
14	11:49:00	9.6	8.13	30.6
16	11:51:00	4.66	3.93	30.7
18	11:52:00	7.46	4.34	31.3
20	11:53:00	6.37	5.77	30.8
22	11:54:00	11.54	11.12	30.6
24	11:55:00	20.8	23.6	30.7
26	11:57:00	18.4	20.5	30.7
28	11:58:00	24.2	24.3	31.54
30	12:00:00	25.6	26	31.7
32	12:02:00	13.13	14.06	31.5
34	12:03:00	12.03	11.28	31.4
38	12:10:00	19.53	20.6	31.6
40	12:11:00	24.2	25.2	31.6
42	12:13:00	29.8	30.7	31.4
44	12:14:00	28.9	29.3	31.4
46	12:15:00	29.3	30	31.6
48	12:16:00	22.8	23.4	31.2
50	12:17:00	49.1	49.1	31
52	12:18:00	31.3	31	31
54	12:20:00	23.7	23.1	31
56	12:21:00	16.02	18.65	31.1
58	12:22:00	20.5	23.3	31.4
60	12:24:00	6.12	6.12	31.3
62	12:25:00	5.92	5.35	31.6
66	12:29:00	5.03	5.03	31.6
68	12:31:00	20.4	20.8	31.6

70	12:33:00	3.73	3.68	31.6
72	12:34:00	1.724	1.723	31.8
74	12:34:00	3.16	3.14	32.1
76	12:36:00	1.645	1.64	31.8
78	12:37:00	2.52	2.49	32.3
80	12:38:00	1.717	1.699	32.3
82	12:39:00	0.744	0.748	32.2
84	12:41:00	-0.435	-0.476	32.1
86	12:42:00	3.786	3.7	31.9
88	12:43:00	0.251	0.253	32
90	12:44:00	-1.14	-1.137	32.6
92	12:45:00	-0.576	-0.566	32.4
94	12:46:00	-0.472	-0.486	32.4
96	12:47:00	-0.561	-0.563	32.7
98	12:47:00	-0.445	-0.449	32.8
100	12:48:00	-0.356	-0.366	32.8
102	12:49:00	0.853	1.081	31.9
104	12:50:00	0.676	0.671	31.8
106	12:51:00	9.32	9.52	31.8
108	12:53:00	9.34	9.41	31.7
110	12:54:00	12.27	12.36	31.9
112	12:55:00	16.37	16.41	32
114	12:56:00	18.96	8.99	32.5
116	12:57:00	1.425	1.425	32.4
118	12:58:00	9.84	9.89	32.6
base	13:28:00	-0.012	-0.017	

Table A 4: Corrected data of measured self-potential line 2

distance on ERT line (m)	distance on tape (m)	SPcorrected
135	4	12.09750467
137	6	7.535009346
139	8	7.240018692
141	10	1.789523364
143	12	6.00253271
145	14	9.660037383
147	16	4.735046729
149	18	7.542551402
151	20	6.460056075

153	22	11.63756075
155	24	20.90506542
157	26	18.52007477
159	28	24.32757944
161	30	25.74258879
163	32	13.28759813
165	34	12.1951028
167	36	19.74763551
169	38	24.42514019
171	40	30.04014953
173	42	29.14765421
175	44	29.55515888
177	46	23.06266355
179	48	49.37016822
181	50	31.5776729
183	52	23.99268224
185	54	16.32018692
187	56	20.80769159
189	58	6.442700935
191	60	6.250205607
193	62	5.390224299
195	64	20.77523364
197	66	4.120242991
199	68	2.121747664
201	70	3.557747664
203	72	2.057757009
205	74	2.940261682
207	76	2.144766355
209	78	1.179271028
211	80	0.014558152
213	82	4.243785047
215	84	0.71628972
217	86	-0.667205607
219	88	-0.095700935
221	90	0.015803738
223	92	-0.065691589
225	94	0.050308411
227	96	0.146813084

229	98	1.363317757
231	100	1.19382243
233	102	9.845327103
235	104	9.880336449
237	106	12.81784112
239	108	16.92534579
241	110	19.52285047
243	112	1.99535514
245	114	10.41785981
247	116	1.770364486
249	118	-1.282121495

Table A 5: Self-potential data and ground surface temperature data loop 1

Number	UTM		Time(hr:m)	V_1(mV)	V_2(mV)	SPCorrected (mV)
	E	N				
0	511978	873812	9:44	3.2	3.21	3.205
1	511979	873824	9:46	12.76	12.65	12.72845
2	511976	873831	9:51	1.986	1.961	2.020397
3	511979	873845	9:56	16.46	16.34	16.47034
4	511981	873856	10:00	14.68	14.23	14.54879
5	511977	873884	10:05	21.4	21.4	21.51724
6	511979	873905	10:08	28.2	28	28.24069
7	511964	873906	10:13	29.8	30.1	30.11414
8	511956	873890	10:19	26.8	26.9	27.03759
9	511967	873888	10:22	13.87	13.71	14.00103
10	511967	873877	10:26	11.26	11.05	11.38948
11	511950	873876	10:30	11.49	11.34	11.67293
12	511951	873862	10:34	8.68	8.9	9.071379
13	511947	873848	10:44	4.27	4.29	4.584828
14	511964	873844	10:46	10.01	10.76	10.71328
15	511961	873827	10:53	3.7	4.61	4.506724
16	511964	873828	10:59	3.1	4.19	4.020172
17	511938	873812	11:07	6.51	7.49	7.398621
18	511955	873810	11:10	3.85	3.97	4.332069
19	511942	873800	11:19	0.87	0.811	1.286017
20	511921	873793	11:26	2.07	2.06	2.533966
21	511918	873783	11:41	2.27	2.35	2.802414
22	511923	873762	11:49	1.398	1.323	1.876362
23	511906	873755	11:57	3.39	4.11	4.28931

24	511926	873734	12:03	-0.962	-0.9	-0.36824
25	511906	873735	12:12	-1.229	-1.494	-0.77529
26	511927	873713	12:23	0.919	0.663	1.400655
27	511910	873708	12:33	3.82	3.64	4.363103
28	511934	873728	12:41	1.691	1.669	2.336552
29	511978	873812	12:53	2.92	2.13	3.205

Table A 6: Self-potential data and ground surface temperature data loop 2

Number	UTM		Time(hr:m)	V_1(mV)	V_2(mV)	SPcorrected (MV)
	E	N				
0	511978	873812	12:53			3.205
1	511982	873782	14:16	-0.57	-0.524	-0.654931034
2	511964	873779	14:23	-0.636	-0.695	-0.881362069
3	511945	873776	14:27	0.753	0.733	0.419206897
4	511988	873767	14:34	-1.106	-1.095	-1.532224138
5	511973	873759	14:42	-0.832	-0.874	-1.392655172
6	511988	873750	14:53	-1.558	-1.547	-2.200086207
7	511996	873728	15:03	0.889	0.901	0.139482759
8	511980	873729	15:12	-6.58	-6.94	-7.623448276
9	511949	873723	15:19	-0.877	-0.867	-1.84337931
10	511924	873729	15:30	-6.7	-5.9	-7.379310345
11	511911	873673	15:43	1.32	1.329	0.137258621
12	511930	873690	16:02	7.15	7	5.779827586
13	511928	873683	16:09	13.37	13.27	11.91689655
14	511946	873693	16:22	-1.179	-1.114	-2.657534483
15	511940	873709	16:30	-0.63	-0.631	-2.249465517
16	511977	873704	16:41	0.186	0.138	-1.564896552
17	511976	873684	16:50	9.78	9.85	7.980172414
18	511994	873686	16:56	13.42	13.55	11.54224138
19	511999	873699	17:01	-1.857	-1.853	-3.905689655
20	512004	873710	17:16	4.07	4.57	2.16137931
21	512008	873731	17:27	0.093	0.085	-2.177551724
22	512006	873753	17:38	0.623	0.883	-1.621482759
23	512005	873942	18:03	26.5	27.4	24.46758621
24	512000	873909	18:08	37.4	38	35.10965517
25	511998	873882	18:13	16.44	16.57	13.80672414
26	511996	873857	18:17	15.4	15.69	12.7387931
27	511994	873846	18:32	46.2	46	43.18586207
28	511992	873831	18:36	43.5	43.8	40.62793103
29	511978	873812	18:48	6.38	6.29	3.205

Table A 7: Self-potential data and ground surface temperature data loop 3

Number	UTM		Time(hr:m)	V_1(mV)	V_2(mV)	SPcorrected
	E	N				
0	512008	873731	9:40	10.57	10.19	8.202448
1	512032	873727	10:23	-5.33	-5.26	-6.58108
2	512025	873709	10:32	-9	-9.15	-9.46961
3	512043	873723	10:41	-4.01	-3.85	-3.43314
4	512051	873731	10:48	-11.19	-11.25	-9.83167
5	512040	873710	10:56	0.331	0.451	2.670801
6	512035	873702	11:03	4.01	4.35	7.351272
7	512022	873689	11:11	-7.19	-7.27	-3.16726
8	512038	873686	11:20	4.14	3.62	8.834213
9	512014	873691	11:29	-3.47	-3.2	2.510684
10	512007	873699	11:37	2.99	2.79	9.627154
11	512087	873711	11:56	0.316	0.28	7.926625
12	512072	873696	12:02	-5.02	-5.01	3.505095
13	512062	873691	12:07	-8.82	-8.91	0.546566
14	512073	873678	12:14	-0.229	-0.273	10.05204
15	512092	873686	12:23	-2.65	-2.47	8.634507
16	512098	873696	12:30	-2.45	-2.57	9.575978
17	512008	873731	12:40	-4.63	-4.92	8.202448

Table A 8: Self-potential data and ground surface temperature data loop 4

Number	UTM		Time(hr:m)	V_1 (mV)	V_2(mV)	SPcorrected (mV)
	E	N				
0	512008	873731	13:59:00	-5.37	-5.35	-7.97659
1	512109	873703	14:10:00	-0.257	-0.311	-3.12061
2	512105	873715	14:18:00	-4.24	-4.33	-7.34163
3	512121	873712	14:22:00	-0.204	-0.319	-3.53814
4	512088	873724	14:31:00	1.215	1.1032	-2.33756
5	512093	873736	14:37:00	-0.824	-0.831	-4.54417
6	512116	873728	14:41:00	-21.3	-21.4	-25.2867
7	512103	873743	14:45:00	-2.64	-2.46	-6.70671
8	512119	873735	14:50:00	-4.7	-4.93	-9.19172
9	512128	873720	14:58:00	-0.849	-0.78	-5.41124
10	512147	873730	15:05:00	-0.265	-0.227	-5.06275
11	512162	873721	15:11:00	31.7	31.1	26.36323
12	512175	873750	15:16:00	39.9	38.2	33.79321
13	512175	873712	15:23:00	52.9	54.1	48.0232
14	512131	873704	15:34:00	-1.488	-1.411	-7.14632

15	512135	873715	15:43:00	-1.016	-1.05	-6.94984
16	512147	873696	15:50:00	0.57	0.571	-5.56635
17	512124	873701	15:56:00	3.5	3.38	-2.91687
18	512198	873755	16:25:00	0.986	0.982	-5.59288
19	512225	873766	16:31:00	2.76	2.91	-3.9619
20	512259	873758	16:37:00	6.4	6.46	-0.58692
21	512269	873749	16:42:00	1.638	1.78	-5.52793
22	512278	873725	16:47:00	0.484	0.427	-7.00145
23	512276	873702	16:54:00	9.59	9.57	1.903036
24	512266	873691	16:57:00	-0.69	-0.698	-8.59098
25	512259	873684	17:05:00	-1.541	-1.811	-9.793
26	512253	873689	17:09:00	9.06	9.03	0.707987
27	512243	873775	17:22:00	5.24	5.55	-3.16203
28	512251	873781	17:29:00	6.62	6.74	-2.09704
29	512262	873788	17:35:00	6.56	6.89	-2.27206
30	512264	873787	17:40:00	4.55	4.74	-4.57208
31	512008	873731	17:57:00	1.457	1.464	-7.97659

Table A 9: Self-potential data and ground surface temperature data loop 5

Number	UTM		Time(hr:m)	V_1(mV)	V_2(mV)	SPcorrected (mV)
	E	N				
0	511978	873812	9:40	2.49	2.34	5.62
1	511994	873795	9:42	-2.55	-2.89	0.470345
2	512009	873765	9:49	-1.034	-0.743	2.28719
3	512031	873754	9:57	-1.151	-1.166	2.002534
4	512015	873789	10:02	19.48	19.56	22.66638
5	512023	873800	10:08	1.355	1.558	4.588224
6	512051	873790	10:25	1.808	1.764	4.903069
7	512051	873785	10:34	-0.745	0.756	3.107914
8	512066	873785	10:44	2.12	2.33	5.312759
9	512059	873758	10:56	2.18	2.16	5.243103
10	512080	873752	11:02	5.03	5.14	8.143448
11	512097	873786	11:09	2.16	2.15	5.198793
12	512104	873773	11:16	0.16	0.107	3.162638
13	512112	873762	11:23	-5.94	-5.97	-2.94052
14	512114	873741	11:28	1.973	1.886	4.929328
15	512126	873787	11:37	-2.37	-2.22	0.690172
16	512128	873769	11:48	-0.64	-0.644	2.328517
17	512135	873752	11:56	1.236	1.236	4.191862
18	512140	873739	12:00	2.53	2.61	5.511207
19	512161	873784	12:14	-3.64	3.78	2.996552

20	512168	873776	12:22	-7.23	-7.2	-4.3031
21	512186	873796	12:33	-1.809	-1.81	1.087741
22	512203	873777	12:41	-0.85	-0.853	2.031086
23	512204	873819	12:50	-1.087	-1.619	1.514931
24	512232	873843	13:00	-0.37	-0.314	2.511276
25	512227	873823	13:07	-0.955	-1.064	1.829121
26	512224	873802	13:13	-0.41	-0.521	2.358466
27	512258	873868	13:22	-3.18	-3.2	-0.38069
28	512265	873854	13:28	-0.511	-0.539	2.269655
29	511978	873812	13:43	3.31	2.37	5.62

Table A 10: Self-potential data and ground surface temperature data loop 6

Number	UTM		Time(hr:m)	V_1(mV)	V_2(mV)	SPcorrected (mV)
	E	N				
0	511978	873812	13:43	3.31	2.37	6.045
1	512009	873825	15:14	-1.904	-1.908	1.278531
2	512014	873844	15:21	4.68	4.68	7.844063
3	512022	873856	15:27	3.77	3.59	6.823594
4	512037	873826	15:37	9.26	9.69	12.59813
5	512060	873838	15:42	2.83	3.42	6.227656
6	512074	873805	15:47	11.86	11.88	14.95219
7	512064	873828	15:51	8.23	8.69	11.52172
8	512076	873846	15:55	15.35	15.89	18.66125
9	512074	873813	16:00	11.52	11.68	14.62078
10	512074	873833	16:04	16.36	16.85	19.60531
11	512092	873860	16:08	-12.99	-12.81	-9.92016
12	512090	873810	16:14	20.7	20.4	23.50938
13	512092	873835	16:17	11.93	12	14.90391
14	512109	873864	16:20	12.76	12.77	15.68344
15	512107	873812	16:25	14.34	13.94	17.03797
16	512110	873842	16:29	19.81	19.77	22.6675
17	512130	873874	16:04	14.33	14.43	17.23703
18	512132	873824	16:40	21.6	21.6	24.43656
19	512134	873851	16:43	25.9	26.1	28.81609
20	512163	873893	16:47	17.98	18.08	20.82563
21	512163	873840	16:53	8.76	8.81	11.56016
22	512165	873863	16:57	22.8	22.9	25.60469
23	512196	873896	17:02	14.73	14.7	17.44922
24	512180	873847	17:06	5.1	5	7.76375
25	512192	873829	17:08	-0.57	-0.581	2.117781
26	512189	873872	17:13	0.943	0.672	3.480313

27	512221	873898	17:18	3.27	3.4	5.987344
28	512223	873860	17:22	2.71	2.74	5.356875
29	512225	873875	17:25	-3.88	-2.73	-0.69359
30	512244	873879	17:28	-5.89	-5.85	-3.27906
31	512238	873910	17:33	-4.47	-4.15	-1.73953
32	511978	873812	17:45	3.6	3.39	6.045

APPENDIX B

Table B 1: Data from VES survey at VES 1.

AB/2	MN/2	K-Factor	R	Rho app
[m]	[m]	[m]	[ohm]	[ohm m]
1.3	0.5	4.5	2.4628	11.14
1.6	0.5	7.3	1.444	10.48
2	0.5	11.8	0.74094	8.73
2.5	0.5	18.8	0.3438	6.48
3.2	0.5	31.4	0.15161	4.76
4	0.5	49.5	0.0857	4.24
5	0.5	77.8	0.043836	3.41
6.5	0.5	131.9	0.022228	2.93
8	0.5	200.3	0.013196	2.64
10	0.5	313.4	0.0078488	2.46
10	2	75.4	0.035066	2.64
13	2	129.6	0.018833	2.44
16	2	197.9	0.011423	2.26
28	2	612.6	0.0036964	2.26
32	2	801.1	0.0030672	2.46
32	5	313.8	0.0081157	2.55
50	5	777.5	0.0043525	3.38
65	5	1,319	0.0036413	4.80
80	5	2,003	0.0026865	5.38
100	5	3,134	0.0019645	6.16

Table B 2: Data from VES survey at VES 2.

AB/2	MN/2	K-Factor	Rho app
[m]	[m]	[m]	[ohm m]
1.3	0.5	1.9249	8.71
1.6	0.5	0.99465	7.22
2	0.5	0.45933	5.41
2.5	0.5	0.22944	4.32
3.2	0.5	0.10708	3.36
4	0.5	0.052566	2.60

5	0.5	0.028778	2.23
8	0.5	0.0092914	1.86
10	0.5	0.0059077	1.85
10	2	0.026671	1.97
13	2	0.015416	2.00
16	2	0.010789	2.13
20	2	0.0074468	2.31
25	2	0.0053085	2.59
32	2	0.0036881	2.95
32	5	0.0092458	2.89
40	5	0.0070671	3.49
50	5	0.005125	4.04

Table B 3: Data from VES survey at VES 3.

AB/2	MN/2	K-Factor	Rho app
[m]	[m]	[m]	[ohm m]
1.3	0.5	4.5	90.22
1.6	0.5	7.3	88.26
2	0.5	11.8	69.81
2.5	0.5	18.8	60.34
3.2	0.5	31.4	43.07
4	0.5	49.5	32.47
5	0.5	77.8	22.47
6.5	0.5	131.9	18.18
8	0.5	200.3	16.52
10	0.5	313.4	14.52
10	2	75.4	13.91
13	2	129.6	11.36
16	2	197.9	9.46
20	2	311.0	8.23
25	2	487.7	6.55
32	2	801.1	6.15
32	5	313.8	5.84
40	5	494.8	6.91
50	5	777.5	7.62
65	5	1,319	9.69
82	5	2,105	8.33
93	5	2,709	7.88
93	10	1,343	6.69
105	10	1,716	7.69

Table B 4: Data from VES survey at VES 4.

AB/2	MN/2	K-Factor	Rho app
[m]	[m]	[m]	[ohm m]
1.3	0.5	4.5	800.64
1.6	0.5	7.3	891.86
2	0.5	11.8	847.55
2.5	0.5	18.8	729.43
3.2	0.5	31.4	483.45
4	0.5	49.5	355.24
5	0.5	77.8	246.41
6.5	0.5	131.9	136.85
8	0.5	200.3	78.01
10	0.5	313.4	35.93
10	2	75.4	34.17
13	2	129.6	16.12
16	2	197.9	5.10
20	2	311.0	6.02
25	2	487.7	5.14
32	2	801.1	1.01
32	5	313.8	9.16
40	5	494.8	9.33
50	5	777.5	9.66

Table B 5: Data from VES survey at VES 5.

AB/2	MN/2	K-Factor	Rho app
[m]	[m]	[m]	[ohm m]
1.3	0.5	4.5	65.56
1.6	0.5	7.3	63.23
2	0.5	11.8	57.87
2.5	0.5	18.8	51.46
3.2	0.5	31.4	42.78
4	0.5	49.5	34.61
5	0.5	77.8	24.34
6.5	0.5	131.9	19.44
8	0.5	200.3	17.41
10	0.5	313.4	17.25
10	2	75.4	16.86
13	2	129.6	15.33
16	2	197.9	13.85
20	2	311.0	13.01
25	2	487.7	10.85
32	2	801.1	8.82

32	5	313.8	9.64
40	5	494.8	8.04
50	5	777.5	7.41

Table B 6: Data from VES survey at VES 6.

AB/2	MN/2	K-Factor	Rho app
[m]	[m]	[m]	[ohm m]
1.3	0.5	4.5	35.98
1.6	0.5	7.3	24.29
2	0.5	11.8	15.63
2.5	0.5	18.8	8.33
3.2	0.5	31.4	4.05
4	0.5	49.5	2.69
5	0.5	77.8	2.14
6.5	0.5	131.9	1.94
8	0.5	200.3	1.88
10	0.5	313.4	1.92
10	2	75.4	1.85
13.6	2	142.1	1.69
16	2	197.9	1.85
20	2	311.0	2.10
25	2	487.7	2.35
32	2	801.1	2.82
32	5	313.8	2.71
40	5	494.8	3.27
50	5	777.5	3.96
75	5	1,759	5.75
100	5	3,134	6.31

Table B 7: Data from VES survey at VES 7.

AB/2	MN/2	K-Factor	Rho app
[m]	[m]	[m]	[ohm m]
1.3	0.5	4.5	21.58
1.6	0.5	7.3	20.27
2	0.5	11.8	17.64
2.5	0.5	18.8	13.28
3.2	0.5	31.4	12.90
4	0.5	49.5	12.47

5	0.5	77.8	11.08
6.5	0.5	131.9	10.66
8	0.5	200.3	10.68
10	0.5	313.4	10.60
10	2	75.4	9.40
13	2	129.6	8.35
16	2	197.9	8.64
20	2	311.0	7.23
25	2	487.7	6.42
32	2	801.1	5.47
41	2	1317.11	6.22
50	2	1960.35	21.86

Table B 8: Data from VES survey at VES 8.

AB/2	MN/2	K-Factor	Rho app
[m]	[m]	[m]	[ohm m]
1.3	0.5	4.5	7.21
1.6	0.5	7.3	7.01
2	0.5	11.8	7.37
2.5	0.5	18.8	6.88
3.2	0.5	31.4	6.85
4	0.5	49.5	6.41
5	0.5	77.8	5.49
6.5	0.5	131.9	4.75
8	0.5	200.3	3.87
10	0.5	313.4	3.39
10	2	75.4	5.52
13	2	129.6	5.52
16	2	197.9	5.24
20	2	311.0	5.34
25	2	487.7	3.90
32	2	801.1	6.62
32	5	313.8	9.50
40	5	494.8	7.33

APPENDIX B

ENETT12-RE-278
การสำรวจแหล่งความร้อนใต้พิภพโดยวิธีการการทางธรณีฟิสิกส์
Geoscientific Investigations of Geothermal Systems Case Study Khlongthom, Krabi.

เมธิภา ผลาการ, ไกรพัฒน์ เพชรฤทธิ์* วิภาดางานสม และ Helmut Dürrast

Geophysics Research Center, Department of Physics, Faculty of Science, Prince of Songkla University, 90112 HatYai
*E-mail: woody_kraiapt@hotmail.com, โทรศัพท์ 074-288736 โทรสาร 074-558849

บทคัดย่อ

พลังงานความร้อนใต้พิภพถือเป็นพลังงานหมุนเวียนรูปแบบหนึ่งซึ่งเป็นพลังงานที่สะอาด และไม่ส่งผลกระทบต่อสิ่งแวดล้อมในปัจจุบันจึงมีการสำรวจแหล่งความร้อนใต้พิภพเพื่อนำมาใช้ประโยชน์หนึ่งในวิธีการสำรวจแหล่งความร้อนใต้พิภพที่นำมาใช้คือการสำรวจทางธรณีฟิสิกส์ซึ่งเป็นการศึกษาลักษณะโครงสร้างหรือองค์ประกอบต่างๆภายใต้ผิวโลกโดยอาศัยหลักการความแตกต่างของคุณสมบัติทางกายภาพของวัตถุต่างชนิดกันอย่างเช่นค่าสภาพต้านทานไฟฟ้าเป็นต้นในการสำรวจวัดสภาพต้านทานไฟฟ้านั้นเป็นการวัดค่าความต่างศักย์ไฟฟ้าโดยการปล่อยกระแสไฟฟ้าลงไปในผิวดินด้วยตัวกำเนิดไฟฟ้ากระแสตรงสิ่งที่มีผลต่อค่าการเปลี่ยนแปลงของความต่างศักย์ไฟฟ้าคือคุณสมบัติทางกายภาพของดิน-หินที่ประกอบด้วยแร่องค์ประกอบรูพรุนของเหลวในรูพรุนในรายงานฉบับนี้ได้นำเสนอการสำรวจแหล่งน้ำพุร้อนเค็มคลองท่อมจังหวัดกระบี่โดยวิธีการสำรวจวัดสภาพต้านทานไฟฟ้าแบบหยั่งลึกแนวดิ่ง (VES) และการสร้างภาพตัดขวางค่าสภาพต้านทานไฟฟ้าใต้ผิวดิน (ERT) ผลการสำรวจพบว่าบริเวณที่มีการสะสมตัวของน้ำร้อนเค็มนั้นอยู่ในชั้นของหินทราย (sandstone) ซึ่งมีความสอดคล้องกับข้อมูลทางธรณีวิทยา และข้อมูลหลุมเจาะในพื้นที่

คำสำคัญ: แหล่งความร้อนใต้พิภพ น้ำพุร้อน การสำรวจสภาพต้านทานไฟฟ้า

Abstract

Geothermal energy is a renewable energy source based on the almost unlimited amount of heat generated by the Earth interior. Geothermal areas depend on a reservoir of hot water, which will be recharged after taking it out, thus making it a sustainable energy source. Geoscientific exploration provides a range of methods for the exploration of geothermal sources, with a variety of geological, geophysical and geochemical methods. Geophysical exploration surveys utilize differences in the physical properties of the earth's materials. This paper further presents results from a case study, the saline hot spring in Khlongthom District of Krabi Province. Different methods have been applied and based on that a final geological model has been drawn.

*Keywords*: Geothermal system, hot spring, Geophysics, Resistivity survey

1. บทนำ

ปัจจุบันทั่วโลกกำลังประสบกับปัญหาความขาดแคลนพลังงานอย่างรุนแรง การค้นหาแหล่งพลังงานทดแทนจึงถือเป็นพันธกิจหลักของนักวิจัยพลังงานทุกคน สร้างความร่วมมือและเครือข่ายการแก้ปัญหาอย่างจริงจัง นอกจากปัญหาด้านพลังงานขาดแคลน ปัญญาการปล่อยก๊าซคาร์บอนไดออกไซด์ที่ปล่อยออกสู่ชั้นบรรยากาศที่เกินค่ามาตรฐานและมีแนวโน้มสูงขึ้นทุกปี หนึ่งในสาเหตุหลักก็มาจากกระบวนการผลิตกระแสไฟฟ้าด้วยเชื้อเพลิงถ่านหินและน้ำมัน ดังนั้นหากเรา

สามารถหาแหล่งพลังงานทดแทนสะอาดเพื่อการผลิตกระไฟฟ้าเป็นผลสำเร็จก็เท่ากับว่าเราสามารถลดการปล่อยก๊าซคาร์บอนไดออกไซด์สู่ชั้นบรรยากาศอีกหนึ่ง โดยผลการสำรวจกลุ่มพลังงานทดแทนที่ปล่อยก๊าซคาร์บอนไดออกไซด์น้อยที่สุดได้ระบุให้พลังงานความร้อนใต้พิภพ (Geothermal energy) เป็นพลังงานสะอาดและถูกให้จัดเป็นแหล่งพลังงานหมุนเวียนที่ใช้ไม่มีหมดสิ้น

ความร้อนใต้พิภพ คือ พลังงานความร้อนที่ถูกกักเก็บไว้ใต้ผิวโลกในบริเวณที่มีหินหนืดสะสมตัวอยู่ในระดับตื้น หรือ

บริเวณที่มีการเคลื่อนตัวของเปลือกโลกทำให้มีการถ่ายเทความร้อนจำนวนขึ้นมาบนผิวโลก ตัวอย่างที่มีให้เห็นกันทั่วไปเช่นใน

รูปของน้ำพุร้อน (hot spring) ซึ่งเป็นปรากฏการณ์ธรรมชาติที่มีน้ำร้อนไหลขึ้นมาจากใต้ผิวดิน โดยกระบวนการเกิดน้ำพุร้อน (รูปที่ 1) เมื่อน้ำจากผิวดินไหลซึมผ่านช่องว่างของหินลงไปใต้ผิวโลกจนไปถึงบริเวณของชั้นหินที่ทำหน้าที่เป็นแหล่งกักเก็บ แล้วต่อมาเมื่อน้ำได้รับการถ่ายเทความร้อนจากแหล่งของความร้อนที่อยู่ใต้โลก ส่งผลให้น้ำเย็นที่ถูกกักเก็บอยู่นั้นแปรเปลี่ยนสภาพเป็นน้ำร้อน เกิดมีแรงดันขึ้นมาแล้วไหลขึ้นสู่ข้างบนผิวโลกด้วยแรงลอยตัวตามบริเวณของรอยแตกและรอยเลื่อนของหิน ทำให้เกิดปรากฏการณ์ธรรมชาติที่เรียกกันโดยทั่วไปว่าน้ำพุร้อนขึ้น
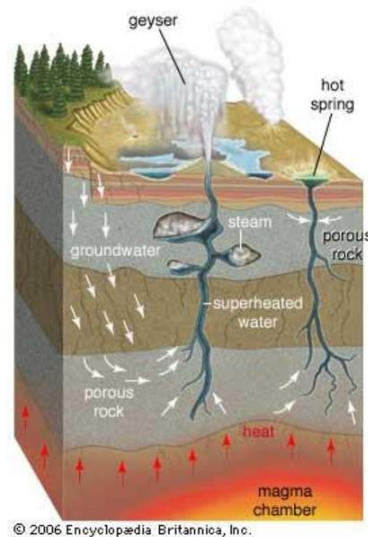
รูปที่ 1 การเกิดน้ำพุร้อน (hot spring) [1]

สำหรับรายวิจัยฉบับนี้ได้นำเสนอวิธีการสำรวจแหล่งน้ำพุร้อนเค็มคลองท่อม จังหวัดกระบี่ โดยวิธีการทางธรณีฟิสิกส์เพื่อศึกษาโครงสร้างทางธรณีวิทยาใต้พื้นดินทั้งในระดับตื้นและลึก และการสร้างแบบจำลองลักษณะโครงสร้างทางธรณีวิทยาเพื่อประเมินศักยภาพของแหล่งน้ำพุร้อน ต่อไป

2. การสำรวจทางธรณีวิทยา

การสำรวจลักษณะหินและธรณีวิทยาโครงสร้างเป็นการศึกษาลำดับชั้นหินการแบ่งขอบเขตและการกำหนดอายุของชุดหินรวมไปถึงศึกษาคุณสมบัติพื้นฐานของหินแต่ละชนิด

วิธีการได้มาซึ่งข้อมูลทางธรณีวิทยานั้นอย่างเช่นการใช้วิธีหยั่งลึกหลุมเจาะ (Well logging)

3. การสำรวจทางธรณีเคมี

การศึกษาองค์ประกอบทางเคมีของแหล่งน้ำพุร้อน เพื่อวิเคราะห์ชนิดและคุณสมบัติของแร่ธาตุที่ละลายอยู่ในแหล่งน้ำ โดยวิธีการวิเคราะห์ไอโซโทปกัมมันตรังสี เป็นต้น

4. การสำรวจทางธรณีฟิสิกส์

การสำรวจทางธรณีฟิสิกส์คือการศึกษาลักษณะโครงสร้าง หรือ องค์ประกอบต่างๆ ภายใต้ผิวโลก โดยอาศัยหลักการความแตกต่างของคุณสมบัติทางกายภาพของวัตถุต่างชนิดกัน (physical property) ด้วยเครื่องมือที่มีการออกแบบมาเพื่อสำรวจความแตกต่างของคุณสมบัติเฉพาะตัวทางกายภาพของวัตถุได้ คุณสมบัติทางกายภาพของวัตถุมีอยู่หลายชนิด ซึ่งสามารถศึกษาได้โดยการสำรวจทางธรณีฟิสิกส์ที่แตกต่างกันออกไป อย่างเช่น การศึกษาคลื่นไหวสะเทือน เพื่อหาความเร็วของคลื่นในชั้นดิน การสำรวจสนามแม่เหล็ก เพื่อศึกษาค่าสภาพยอมรับได้ทางแม่เหล็กของหินและแร่ การสำรวจค่าสนามโน้มถ่วงเพื่อหาค่าสนามโน้มถ่วงผิดปกติและค่าความหนาแน่นของผิวดินการสำรวจค่าสภาพต้านทานไฟฟ้า เพื่อศึกษาค่าสภาพต้านทานไฟฟ้าของชั้นหิน เป็นต้น[2]

ตารางที่ 1 การสำรวจทางธรณีฟิสิกส์

| วิธีการสำรวจ	คุณสมบัติทางกายภาพที่ศึกษา
การสำรวจคลื่นไหวสะเทือน	ความเร็วคลื่นในชั้นดิน-หิน (Seismic velocity, V_p, V_s)
การสำรวจสนามแม่เหล็ก	ค่าสภาพยอมรับได้ทางแม่เหล็ก (Magnetic susceptibility, k)
การสำรวจค่าสนามโน้มถ่วง	ค่าความหนาแน่นของชั้นดิน (Density)
การสำรวจสภาพต้านทานไฟฟ้า	ค่าสภาพต้านทานไฟฟ้าในชั้นดิน (Resistivity, ρ)

รายงานฉบับนี้ มุ่งเน้นไปที่การศึกษาและสำรวจแหล่งพลังงานความร้อนใต้พิภพด้วยวิธีการสำรวจวัดสภาพต้านทานไฟฟ้า (Resistivity survey) การสำรวจวัดสภาพต้านทานไฟฟ้าเป็นการวัดค่าความต่างศักย์ไฟฟ้าโดยการปล่อยกระแสไฟฟ้าลงไปในผิวดินด้วยตัวกำเนิดไฟฟ้ากระแสตรง สิ่งที่มีผลต่อค่าการเปลี่ยนแปลงของความต่างศักย์ไฟฟ้า คือคุณสมบัติทางกายภาพของดิน-หินที่ประกอบด้วย แร่องค์ประกอบ รูพรุนของเหลวในรูพรุน และองค์ประกอบอื่นๆ ที่มีอยู่ในเนื้อดิน-หิน ดังนั้นประโยชน์ที่ได้จากการสำรวจสภาพต้านทานไฟฟ้าจึงได้แก่ ใช้หาชั้นดินที่มีองค์ประกอบของแร่ รูพรุนและค่าการซึม

ผ่านที่แตกต่างกัน ใช้หาชั้นหินอุ้มน้ำหรือชั้นน้ำบาดาล ใช้หา
ขอบเขตของการแทรกตัวของชั้นน้ำเค็ม ใช้หาโพรงใต้ผิวดิน
หรือสำรวจระดับน้ำใต้ผิวดินเป็นต้น [2]

หลักการเบื้องต้นในการสำรวจสภาพต้านทานไฟฟ้า
สภาพต้านทานไฟฟ้าของวัตถุ

ค่าสภาพต้านทานไฟฟ้าของวัตถุ (Resistivity, ρ) เป็น
คุณสมบัติเฉพาะทางกายภาพของวัตถุที่บอกให้ทราบว่า วัตถุ
นั้นมีความต้านทานไฟฟ้า หรือยอมให้กระแสไฟฟ้าไหลผ่านมาก
น้อยเพียงใด จากรูปที่ 2 เมื่อมีวัตถุความยาว L พื้นที่หน้าตัด A
และค่าความต้านทาน R สามารถคำนวณสภาพต้านทานไฟฟ้า
ของวัตถุได้ดังนี้ [3]

$$\rho = \frac{RL}{A} \qquad (1)$$
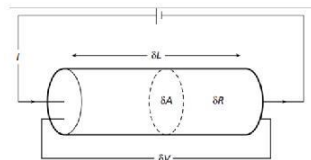
รูปที่ 2 การคำนวณหาสภาพต้านทานไฟฟ้า เมื่อวัตถุมีความ
ยาว L พื้นที่หน้าตัด A ค่าความต้านทานไฟฟ้า R

การวัดสภาพต้านทานไฟฟ้าใต้ผิวดิน

จากรูปที่ 3 เมื่อทำการปักขั้วไฟฟ้าทั้งสี่ขั้วลงบนผิวดิน
โดยให้ขั้วไฟฟ้า A และ B เป็นขั้วที่ใช้ในการปล่อยกระแสไฟฟ้า
และขั้วไฟฟ้า M และ N เป็นขั้วที่ใช้ในการปล่อยกระแสไฟฟ้า
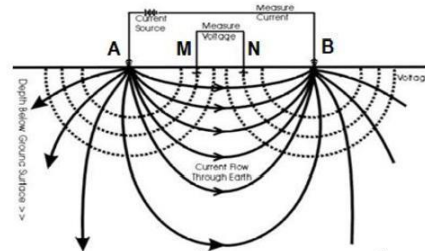จะสามารถคำนวณค่าสภาพต้านทานไฟฟ้าใต้ผิวดินได้โดย
สมการ

$$\rho = \frac{\Delta V_{MN}}{I} \left(\frac{2\pi}{\frac{1}{AM} - \frac{1}{BM} - \frac{1}{AN} + \frac{1}{BN}} \right) \qquad (2)$$

เมื่อ ΔV_{MN} คือความต่างศักย์ไฟฟ้าระหว่างขั้ว M และ
N (V), คือ กระแสไฟฟ้าที่ใช้ในการปล่อยลงสู่ใต้ผิวดิน (A), AM,
BM, AN และ BN คือ ระยะห่างระหว่างขั้วไฟฟ้า (m)

จากสมการที่ (2) ค่าสภาพต้านทานไฟฟ้าสามารถ
คำนวณได้จากสมการ

$$\rho = Rk \qquad (3)$$

เมื่อ R คือค่าความต้านทานไฟฟ้าที่ได้ (Ohm), K คือค่า
Geometric factor ซึ่งขึ้นอยู่กับการจัดเรียงขั้วไฟฟ้า (m)

รูปที่ 3 รูปแบบการจัดเรียงขั้วไฟฟ้า เมื่อ A และ B คือขั้วไฟฟ้า
ที่ใช้ในการปล่อยกระแส และ M และ N คือขั้วไฟฟ้าที่ใช้ในการ
วัดศักย์ไฟฟ้า [3]

ตารางที่ 2 ค่าสภาพต้านทานไฟฟ้า และค่าการนำไฟฟ้า [3]

| Material	Resistivity (Ωm)	Conductivity (Siemen/m)
Igneous and Metamorphic Rocks		
Granite	5×10^{3} - 10^{6}	10^{-6} - 2×10^{-4}
Basalt	10^{3} - 10^{6}	10^{-6} - 10^{-3}
Slate	6×16^{2} - 4×10^{7}	2.5×10^{-8} - 1.7×10^{-3}
Marble	10^{2} - 2.5×10^{8}	4×10^{-9} - 10^{-2}
Quartzite	10^{2} - 2×10^{8}	5×10^{-9} - 10^{-2}
Sedimentary Rocks		
Sandstone	8 - 4×10^{3}	2.5×10^{-4} - 0.125
Shale	20 - 2×10^{3}	5×10^{-4} - 0.05
Limestone	50 - 4×10^{2}	2.5×10^{-3} - 0.02
Soils and waters		
Clay	1 - 100	0.01 - 1
Alluvium	10 - 800	1.25×10^{-3} - 0.1
Groundwater (fresh)	10 - 100	0.01 - 0.1
Sea water	0.2	5
Chemicals		
Iron	9.074×10^{-8}	1.102×10^{7}
0.01 M Potassium chloride	0.708	1.413
0.01 M Sodium chloride	0.843	1.185
0.01 M acetic acid	6.13	0.163
Xylene	6.998×10^{16}	1.429×10^{-17}

เครื่องมือและอุปกรณ์

เครื่องมือหลักที่ใช้ในการสำรวจค่าสภาพต้านทานไฟฟ้า
ประกอบด้วยเครื่องวัดค่าสภาพต้านทานไฟฟ้า ขั้วไฟฟ้าโลหะ
และสายไฟใช้ในการเชื่อมต่ออุปกรณ์ทั้งหมดด้วยกัน นอกจากนี้
ยังมีอุปกรณ์จำเป็นอื่นๆ ในการเก็บข้อมูลภาคสนามเช่น ค้อน
ตลับเมตร เครื่องวัดพิกัดตำแหน่ง (GPS) เป็นต้น

การสำรวจสภาพต้านทานไฟฟ้าแบบหยั่งลึกแนวดิ่ง

การสำรวจสภาพต้านทานไฟฟ้าแบบหยั่งลึกแนวดิ่ง
(Vertical electrical sounding, VES) เป็นการสำรวจสภาพ
ต้านทางไฟฟ้าที่จุดใดจุดหนึ่งลึกลงไปใต้ผิวดิน ผลที่ได้จากการ
สำรวจคือค่าสภาพต้านทานไฟฟ้าของชั้นดินที่เปลี่ยนแปลงตาม
ความลึก ซึ่งสามารถนำผลที่ได้ไปแปลความรวมกับข้อมูลทาง
ธรณีวิทยาเพื่อให้ได้ชนิดและความหนาของชั้นดิน (อ้างอิงได้
จากข้อมูลค่าสภาพต้านทานไฟฟ้าของชั้นแต่ละชนิด)
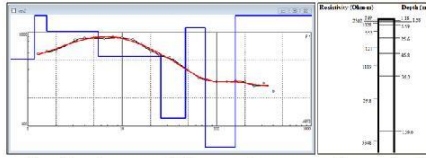
รูปที่ 4 ตัวอย่างของผลที่ได้จากการสำรวจสภาพต้านทานไฟฟ้า
แบบหยั่งลึกแนวดิ่ง ค่าสภาพต้านทานไฟฟ้าของชั้นดินที่
เปลี่ยนแปลงตามความลึก

รูปที่ 6 พื้นที่ศึกษา

การสร้างภาพตัดขวางค่าสภาพต้านทานไฟฟ้า

การสร้างภาพตัดขวางค่าสภาพต้านทานไฟฟ้าใต้ผิวดิน (Electrical resistivity tomography, ERT) เป็นการสำรวจค่าสภาพต้านทานไฟฟ้าของชั้นดินใน 2 มิติ เพื่อศึกษาการกระจายตัวของค่าสภาพต้านทานไฟฟ้าใต้ผิวดินทั้งในแนวดิ่งและแนวราบ ผลที่ได้จากการสำรวจจะทำให้ทราบถึงลักษณะโครงสร้างใต้ผิวดิน
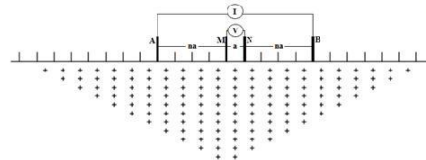
รูปที่ 5 ตัวอย่างการสร้างภาพตัดขวางค่าสภาพต้านทานไฟฟ้า

5. การสำรวจแหล่งน้ำพุร้อนเค็มคลองท่อม จังหวัดกระบี่

การสำรวจในครั้งนี้มีเป้าหมายเพื่อศึกษาและทำความเข้าใจโครงสร้างทางธรณีวิทยาในระดับตื้นของแหล่งน้ำพุร้อนเค็มคลองท่อม จังหวัดกระบี่ด้วยวิธีการสำรวจสภาพต้านทานไฟฟ้าแบบหยั่งลึกแนวดิ่ง และการสร้างภาพตัดขวางค่าสภาพต้านทานไฟฟ้าพื้นที่ที่ทำการศึกษาตั้งอยู่ในตำบลห้วยน้ำขาว อำเภอคลองท่อม แนวที่ทำการสำรวจอยู่บริเวณทางตอนใต้ของบ่อน้ำพุร้อนเค็มหลักและทางตอนใต้ของป่าชายเลน ภายในป่าชายเลนมีแม่น้ำที่เชื่อมต่อกับอ่าวกระบี่เพื่อไหลไปสู่ทะเลอันดามันภูมิศาสตร์โดยทั่วไปของพื้นที่เป็นป่าชายเลนที่มีน้ำพุร้อนเค็ม ในทางตอนเหนือ และมีสวนปาล์มน้ำมันและยางพาราในทางตอนใต้ [4]

บริเวณหลักของน้ำพุร้อนคือ KB4/5 และสระน้ำพุร้อนที่ถูกสร้างขึ้นหลายสระโดยแบ่งตามอุณหภูมิสำหรับใช้ในการอาบ KB4/5 นั้นมีน้ำร้อนอยู่สระเดียว และKB4/10 เป็นบ่อน้ำพุร้อนธรรมชาติ

ข้อมูลการสำรวจธรณีเคมีจาก KB4/5 แสดงให้เห็นว่า Na และCl มีความเข้มข้นสูงในบริเวณที่เป็นน้ำเค็มนอกจากนั้นยังพบว่า Ca, K และ Mg จะมีความเข้มข้นสูงเมื่อ Fe มีค่าค่อนข้างต่ำน้ำสามารถจำแนกได้ตามลักษณะเด่นของไบคาร์บอเนตและคลอไรด์

ลักษณะทางธรณีวิทยาโดยส่วนใหญ่ของน้ำพุร้อนตั้งอยู่บนหินทราย (Triassic Sai Bon Formation) ชั้นหินปูนเกิดขึ้นรอบๆน้ำพุร้อนซึ่งเป็นผลมาจากการตกตะกอนของน้ำร้อนจากน้ำพุร้อน

วิธีการการสำรวจ

การสำรวจแบบ VES ได้มีการกระจายจุดสำรวจออกเป็น 7 จุด ครอบคลุมพื้นที่แหล่งน้ำพุร้อน แนวสำรวจมีความยาวประมาณ 200-300 เมตร ทำให้ความลึกสูงสุดที่ได้จากการสำรวจอยู่ที่ 60 เมตร ผลการสำรวจได้ถูกนำมาตีความต่อโดยการนำข้อมูลมาวิเคราะห์รวมกันเพื่อสร้างภาพตัดขวางหาขอบเขตของแหล่งน้ำพุร้อน จากข้อมูลการสำรวจสามารถสร้างภาพตัดขวางได้ 2 แนว (รูปที่ 7)และการสำรวจERT มีทั้งหมด 2 แนวสำรวจ (Line1 และ Line 2) อยู่ในทิศตะวันออกเฉียงเหนือของกลุ่มแนวสำรวจ VES แนวสำรวจมีความยาวประมาณ 400 เมตรความลึกสูงสุดจากการสำรวจอยู่ที่ประมาณ 55 เมตร [5]

การตีความตีความข้อมูล

การตีความข้อมูลทำได้โดยการ นำผลข้อมูลที่ได้จากการสำรวจทางธรณีฟิสิกส์มาแปลผลรวมกับข้อมูลทางธรณีวิทยาอย่างเช่น ข้อมูลลักษณะของชั้นตะกอนในพื้นที่ข้อมูลจากบ่อเจาะเป็นต้น ซึ่งจะทำให้ทำให้การตีความข้อมูลมีความแม่นยำมากขึ้น
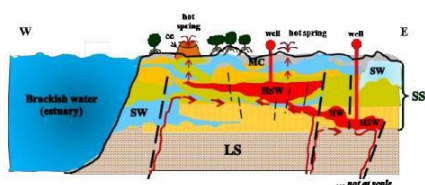
รูปที่ 7 a) การเก็บตัวอย่างน้ำเพื่อวัดผลทางธรณีเคมีที่บ่อน้ำพุร้อน KB4/10 และการเกิดแผ่นหินปูนรอบบ่อน้ำพุร้อน
b) การสำรวจทางธรณีวิทยา มีหินทรายในพื้นที่บ่อน้ำพุร้อน c) การสำรวจสภาพต้านทานไฟฟ้าแบบหยั่งลึกแนวดิ่งในพื้นที่ศึกษา
d) การสำรวจแบบสร้างภาพตัดขวางสภาพต้านทานไฟฟ้า e) ภาพตัดขวางสภาพต้านทานไฟฟ้าที่บริเวณบ่อน้ำพุร้อน KB4/10

6. สรุปผล

การสำรวจทางธรณีฟิสิกส์สามารถใช้ในการศึกษาโครงสร้างต่างๆ ภายใต้ชั้นผิวดินได้เป็นอย่างดี ทั้งนี้ยังสามารถใช้ในการศึกษา อธิบาย และหาขอบเขตของแหล่งพลังงานความร้อนใต้พิภพได้อีกเช่นกัน ในการตีความเพื่อสรุปผลข้อมูลนั้นจำเป็นต้องตีความร่วมกับข้อมูลอื่นๆ อย่างเช่น ข้อมูลทางธรณีวิทยา ข้อมูลจากบ่อเจาะ เป็นต้น เพื่อให้การสรุปผล และอธิบายลักษณะโครงสร้างใต้ผิวดินมีความแม่นยำมากยิ่งขึ้นข้อมูล

รูปที่ 8 แผนภาพแสดงลักษณะโครงสร้างทางธรณีวิทยา LS คือหินปูน SS คือหินทราย cc คือแผ่นหินปูน MC คือดินเหนือดินเค็ม HW คือน้ำร้อน HSW คือน้ำร้อนเค็ม SW คือน้ำเค็ม น้ำร้อนจากแหล่งกักเก็บในระดับลึก และเค็มจากทะเลแทรกเข้ามาในชั้นน้ำบาดาลระดับตื้น ผสมและอยู่รวมกันเกิดเป็นน้ำพุร้อนตามธรรมชาติขึ้นมาสู่ผิวดิน

7. กิตติกรรมประกาศ

ขอขอบคุณภาควิชาฟิสิกส์ และ สถานีวิจัยธรณีฟิสิกส์ มหาวิทยาลัยสงขลานครินทร์สำหรับข้อมูลและเครื่องมือการสำรวจธรณีฟิสิกส์ภาคสนาม

8. เอกสารอ้างอิง

[1] Encyclopedia Britannica (2006)

[2] Sartarak, P., (2007). Exploration geophysics, Faculty of Technology,KhonKaen University

[3] Kearey, P., Brooks, N. and Hill, I. (2002). An introduction to geophysics exploration 3rd ed., Blackwell science Ltd., Oxford, England, pp 183-185

[4] Pothaworn, K. andDürrast, H., (2015). Shallow subsurface structure around the north western part of the saline hot spring in Khlongthom, Krabi, from 1-D VES., Department of physics, Faculty of Science, Prince of Songkla University

[5] Chaiyarak, N., Ngasom, W and Dürrast, H., (2016). Shallow geological structure of Khlongthom hot spring area, Krabi, Thailand, from 2D-resistivity, Department of physics, Faculty of Science, Prince of Songkla University

Near surface flow characteristics from self-potential measurements at the Khlongthom Saline Hot Spring in Krabi, Southern Thailand

Maytipa Phalakarn and Helmut Dürrast
Geophysics Research Center and Department of Physics, Faculty of Science, Prince of Songkla University, HatYai 90112 Thailand
E-mail: kati_aar_@hotmail.com; helmut.j@psu.ac.th

Abstract

Self-potential or streaming potential (SP) anomaly measurements is one geophysical method which is often used to localize fluid flow pathways in porous rock and soil, as the SP response is directly linked to subsurface fluid movement. Here, measurements of SP in the Khlongthom saline hot spring area, located in Southern Thailand, are presented. Self-potential profiles were combined with soil temperature and electrical tomography resistivity data to identify preferential fluid flow pathways in the subsurface. Due to water flow in an overall higher saline environment the SP signal is positive, a sum of streaming and diffusion potential, thus reflecting only relative shallow groundwater flow.

Introduction

Khlongthom saline hot spring (7.904° N, 99.110° E) is located in the southern part of Krabi Province, Thailand, about 85 km east of Phuket; it is close to one of tributaries of the Phela River system, which connects to the Andaman Sea. The hot spring water reaches temperatures of around 40-47 °C; it is salty (around 2 ppt) because of the mixing of hot water, which emerges from the subsurface, and salty groundwater related to river water influx. The area is surrounded by mangrove forests, salt marsh, and palm oil plantations (Fig. 1). The saline hot springs are located on Triassic sandstone; the shallow subsurface consist of alluvial deposits with of medium to coarse grained sand, clay, black marine clay (Fig. 2). Additionally, calcium carbonate crusts found around several natural hot springs as the result of precipitation from the hot spring waters. Self-potential (SP) surveys have been carried out in order to understand the fluid flow in the subsurface of this salty hot water environment.

Figure 1: Study area, view to South; to resistivity;
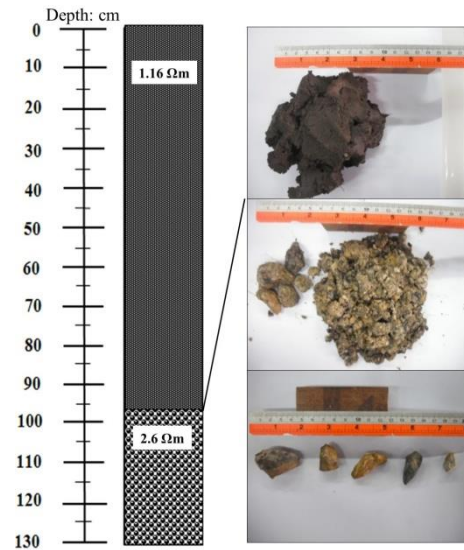the east salt marsh, in the west mangroves. sand

Figure 2: Soil profile and soil

upper part: black clay, below: clayey

with sandstone fragments.

SP measurements are usually used to characterize subsurface fluid flow and to localize fluid pathways in various geophysical surveys, such as in geothermal areas or for saline aquifers (Jaafar et al., 2009). This method is a passive measurement of the naturally potential that is occurring and distributed in the Earth. This natural potential is results of fluid flow passing through a porous media or capillaries thus generating an electrical field; this process is also called streaming potential (Friborg, 1996). Streaming potentials arise from the electrical double layers occurring at solid-fluid interfaces. Main key petrophysical property associated with streaming (∇V) and fluid (∇P) potential gradients is the streaming potential coupling coefficient (C); when the total current density (j) is zero C is expressed (Sill, 1983):

$$C = \left.\frac{\nabla V}{\nabla P}\right|_{j=0} \quad \text{..} (1)$$

In the case of an environment related to salty water flow in the subsurface, the magnitude and sign of streaming potential coupling coefficient depends on the salinity, which is the electrical potential associated with the counter charge in electrical double layer at the mineral-fluid interface (Jaafar et al., 2009). The transport of the conductive salty water through the porous rock changes the localized streaming potential coupling coefficient, which is associated with the advective drag of the excess charge of the pore water and is also responsible for a diffusion current associated with the salinity gradient (Ikard et al., 2012). Several studies found that the magnitude of the streaming potential coupling coefficient decreases when salinity increases (Jaafar et al., 2009; Vinogradov et al., 2010; Ikard et al., 2012). When salty water moves in a porous material, e.g. porous rock or sand, the total source of the current density generated self-potential signal is associated with two contributions. The first one is streaming potential, which occurred

by the flow of pore water itself. The second is the diffusion current density, which related to gradient of the salinity (Ikard et al., 2012).

Materials and Methods

An electrical resistivity tomography (ERT) survey was carried out in 2015 using dipole-dipole configuration, along a 430 m profile line, with electrode spacing of 25 m, n=8, and an effective depth of 50 m. Data processing was done with RES2DINV software to produces a cross section of the electrical resistivity (Ngansom and Dürrast, 2016). Two SP surveys have been done in April 2017 along the ERT survey line with a total of 300 m length (Line 1: 180 m, Line 2: 120 m). The first profile line is parallel to 251-431 m on the ERT line, and the second profile, measured one day after Line 1, is parallel to 130-250 m. SP were performed by using $Pb/PbCl_2$ non-polarizing electrodes connected to Terrameter SAS 300. Data acquisition was done with fixed base configuration; potential differences were measured between reference and moving electrode. Three non-polarizing electrodes connected in a hole were used as the reference electrode (base); one electrode was moved with 2 m spacing along the SP profile. Soil temperature was measured along the SP profiles on the SP data locations shortly after SP measurements. A type K thermocouple was put into the ground at a depth of 30 cm.

Results and Discussion

ERT profile with parallel SP and temperature data are displayed in Fig. 3. The bottom part of the ERT section shows high to very high resistivity values corresponding to dense sandstone with almost no water content; confirmed by drilling (not shown here). Further above parts of the ERT section show very low resistivity values corresponding to saline groundwater in clayey sand layers. Some shallow higher resistivity layers (e.g., 350-400 m) represent dryer sand. The very shallow part with black marine clay on top (see Fig. 2) is not resolved by ERT. The first SP profile line shows values ranging from -488 to -166 mV, and the second profile line show SP values ranging from -1 to 49 mV; difference in the absolute SP values were caused by rain between the measurements of the two lines. Both SP profile lines exhibit clear positive anomalies, which correlate with lower temperatures compared to the overall trend line. The temperature trend line exhibits a positive anomaly with a peak at around 220 m due to higher heat flow from the geothermal system. However, not all soil temperatures below the trend line can be correlated with positive SP anomalies (Fig. 3).
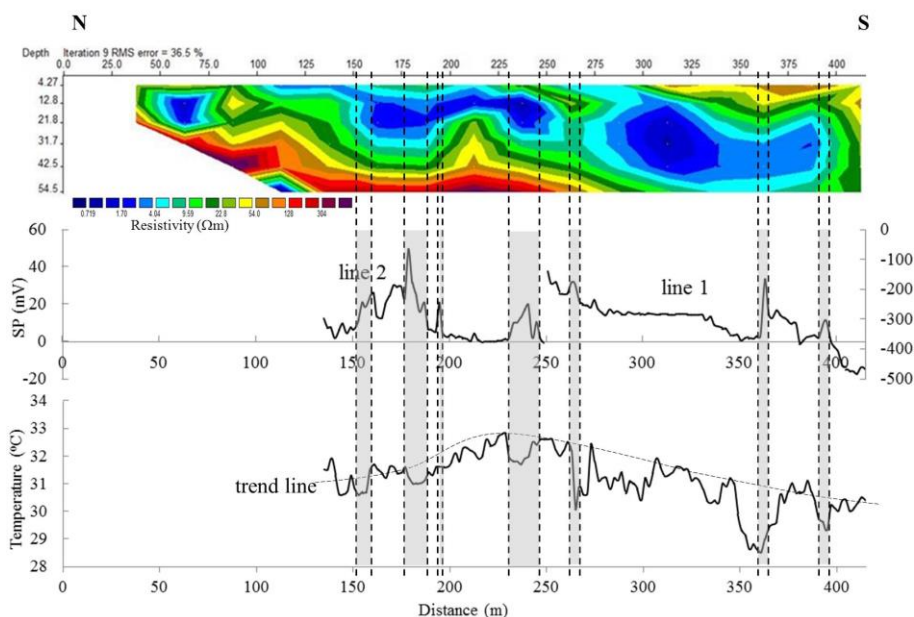
Figure 3: Electrical resistivity tomography section (top), self-potential data from two survey lines (middle), and temperature data (bottom) along the main survey line, a rural way in the Khlongthom Saline Hot Spring area (see Fig. 1).

Following scenario might explain all observations (see Fig. 4): Rain water falling onto the ground picks up NaCl from the highly saline marine clay (salt marsh) at the surface and in the very shallow subsurface, thus becoming saline groundwater. This colder rain water is gravitationally flowing down as groundwater, thus decreasing the near surface soil temperature with respect to the higher temperature trend line due to geothermal heat flow (Fig. 3). Groundwater flowing down usually creates a negative SP streaming potential. However, in this case the groundwater flowing down through the porous clayey sand is highly salty, thus reducing the magnitude of the (negative) streaming potential coefficient, which results in a decrease of the SP field associated directly with the flow of the groundwater (Ikared et al., 2012).

Further, due to higher salinity in the near surface layer and lower one in the layers beneath a salinity gradient occurred, which created a diffusion potential of the SP field generating a larger positive anomaly (Ikared et al., 2012). The total SP anomaly, a sum of the streaming and diffusion potential, therefore is positive in this environment as measured (Fig. 3). At locations with negative temperature but not positive SP anomalies rain/groundwater is only flowing down into the upper black marine clay layer, but not deeper into the porous clayey sand (see Fig. 3), as the permeability of the clay layer is relatively low. Flow further down might be along fissures or cracks.
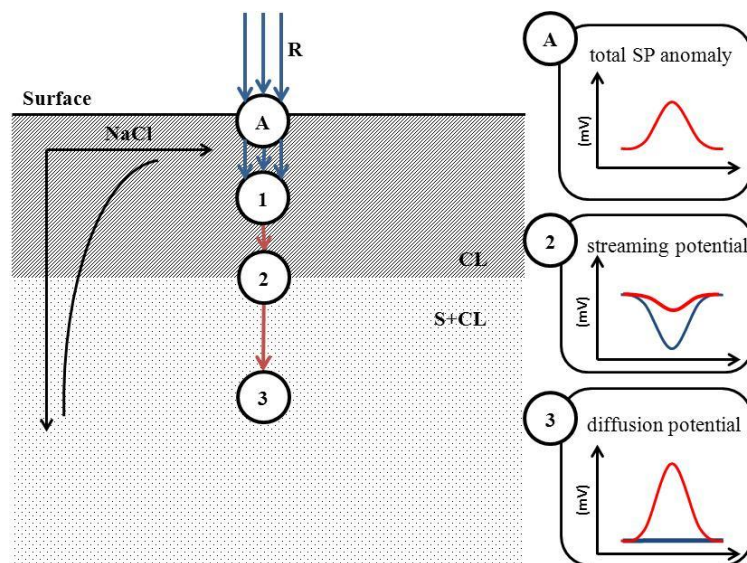
Figure 4: Schematic diagram of the shallow fluid flow, which generates the SP signal; R: rain water; A: SP measurement point (total SP anomaly); (1): rain water mixes with NaCl; (2): SP signal generated from streaming potential; (3): SP signal generated from diffusion potential related to NaCl concentration differences; CL: clay layer; S+CL: clayey sand layer; for (2) and (3): red curve indicates SP signal from salty water flow, blue curve SP signal from normal groundwater flow.

Conclusions

SP measurements in combination with soil temperature data have revealed shallow gravitational water flow paths in an overall saline environment resulting in strong positive SP anomalies, which override any possible signal from geothermal water flow at depth.

References

Friborg, J. (1996). Experimental and theoretical investigations into the streaming potential phenomenon with special reference to applications in glaciated terrain. PhD thesis, Lulea University of Technology, Sweden.

Ikard, S.J. and Ravil, A. (2012). Saline pulse test monitoring with the self-potential method to nonintrusively determine the velocity of the pore water in leaking areas of earth dams and embankments. Water Resources Research, 48, W04201, doi:10.1029/2010WR010247.

Jaafar, M.Z. and Vinogradov, J. (2009). Measurement of streaming potential coupling coefficient in sandstones saturated with high salinity NaCl brine. Geophysical Research Letters., 36, L21306, doi:10.1029/2009GL040549.

Ngansom, W. and Dürrast, H. (2016). Saline hot spring in Krabi, Thailand: a unique geothermal system. SEG International Exposition and 86th Annual Meeting, 5089-5093.

Sill, W.R. (1983), Self-potential modeling from primary flows, Geophysics, 48, 76–86, doi:10.1190/1.1441409.

Vinogradov, J. and Jaafar, M.Z. (2010). Measurement of streaming potential coupling coefficient in sandstones saturated with natural and artificial brines at high salinity. Journal of Geophysical Research., 115, B12204, doi:10.1029/2010JB007593.

VITAE

Name   Miss Maytipa Phalakarn

Student ID   5810220060

Educational Attainment

Degree	Name of Institution	Year of Graduation
Bachelor of Science (Physics)	Princeof Songkla University	2014

Scholarship Awards during Enrolment

2011-Present   Science Achievement Scholarship of Thailand

2015-2018   Teaching Assistant at Department of Physics, Faculty of Science, Prince of Songkla University

List of Publication and Proceeding

Phalakarn, M., Petrit, K., Ngansom, W. and Dürrast, H. (2016). Geoscientific Investigations of Geothermal Systems Case Study Khlongthom, Krabi. Proceeding of the 12th Conference on Energy Network of Thailand, Phitsanulok, Thailand, 1263-1268.

Phalakarn, M. and Dürrast, H. (2018). Near surface flow characteristics from self potential measurements at the Khlongthom Saline Hot Spring in Krabi, Southern Thailand. Proceeding of 5th Conference on Soil & Water Assessment Tool, Selangor, Malaysia.